

2006

## Computational fluid dynamics simulations of jet fuel flow near the freeze point temperature

Rajee Assudani  
*University of Dayton*

Follow this and additional works at: [https://ecommons.udayton.edu/graduate\\_theses](https://ecommons.udayton.edu/graduate_theses)

---

### Recommended Citation

Assudani, Rajee, "Computational fluid dynamics simulations of jet fuel flow near the freeze point temperature" (2006). *Graduate Theses and Dissertations*. 189.  
[https://ecommons.udayton.edu/graduate\\_theses/189](https://ecommons.udayton.edu/graduate_theses/189)

This Dissertation is brought to you for free and open access by the Theses and Dissertations at eCommons. It has been accepted for inclusion in Graduate Theses and Dissertations by an authorized administrator of eCommons. For more information, please contact [mschlange1@udayton.edu](mailto:mschlange1@udayton.edu), [ecommons@udayton.edu](mailto:ecommons@udayton.edu).

**Computational Fluid Dynamics Simulations of Jet Fuel Flow  
Near the Freeze Point Temperature**

**DISSERTATION**

**Submitted to**

**The Department of Mechanical and Aerospace Engineering**

**University of Dayton**

**In Partial Fulfillment of the Requirements for**

**The Degree**

**Doctor of Philosophy in Mechanical Engineering**

**by**

**Rajee Assudani**


**University of Dayton**

**Dayton, Ohio**


**December 2006**

## Computational Fluid Dynamics Simulations of Jet Fuel Flow Near the Freeze Point Temperature


APPROVED BY:




Jamie Ervin, Ph.D.  
Advisory Committee Chair  
Professor, Mechanical and Aerospace  
Engineering Department




Kevin Hallinan, Ph.D.  
Committee Member  
Department Head, Mechanical and Aerospace  
Engineering Department



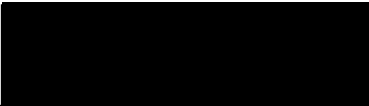
Dilip Ballal, Ph.D.  
Committee Member  
Professor, Mechanical and Aerospace  
Engineering Department



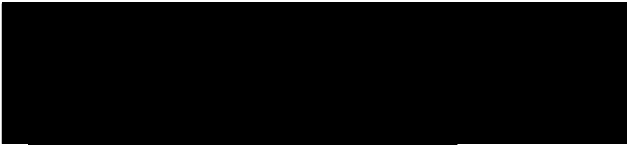
Steven Zabarnick, Ph.D.  
Committee Member  
Professor, Mechanical and Aerospace  
Engineering Department



James Edwards, Ph.D.  
Committee Member  
AFRL, Wright-Patterson AFB



Donald L. Moon, Ph.D.  
Associate Dean  
Graduate Engineering Programs & Research  
School of Engineering



Joseph E. Saliba, Ph.D., P.E.  
Dean, School of Engineering

© Copyright by

Rajee Assudani

All rights reserved

2006

## **Abstract**

### **COMPUTATIONAL FLUID DYNAMICS SIMULATIONS OF JET FUEL FLOW NEAR THE FREEZE POINT TEMPERATURE**

Name: Assudani, Rajee  
University of Dayton, 2006

Advisor: Dr. Jamie S. Ervin

Under low-temperature environmental conditions, the cooling of aircraft fuel results in reduced fluidity with the potential for freezing. Therefore, it is important to study the flow and heat transfer phenomena that occur in an aircraft fuel tank near the freeze point temperature of jet fuels. The purpose of this dissertation is to study the effects of low temperatures on the flow, heat transfer and freezing of commercial and military jet fuels. The research is accomplished with the help of computational models of a thermal simulator tank and a quartz duct.

Experimental results with the thermal simulator tank show that fuel flowability and pumpability decrease substantially as temperature is reduced. Time-dependent temperature and velocity distributions were numerically simulated for static cooling. Measured properties were used in all the computational fluid dynamics simulations. The calculations show that stringers, ribs, and other structures strongly promote fuel cooling. Also, the cooler, denser fuel resides near the bottom surface of the fuel tank simulator. The presence of an ullage space within the tank was found to strongly influence the fuel temperature profile by sometimes reducing cooling from the upper surface. Moreover, since the presence of ullage space is an explosion risk, some military aircraft fuel tanks

are fitted with explosion suppressant polyurethane foam. To study the effect of foam on the flowability and heat transfer inside the simulator tank, the wing tank thermal simulator was filled with military specified polyurethane foam. The tank was simultaneously drained and cooled and the mass flow rate results showed that flowability of the fuel is not affected by the presence of foam. However, the presence of foam certainly affected the heat transfer phenomenon inside the fuel tank when the simulator tank was cooled and drained simultaneously.

To study the freezing behavior of jet fuel under forced flow conditions, a quartz duct was fabricated. The duct walls were cooled below the solidification temperatures of JP-8 and JPTS fuel samples. Freezing was also simulated using computational fluid dynamics, and the validity of the calculations was established by comparing them with experimental measurements. This work demonstrates that computational fluid dynamics techniques can potentially be used to predict fuel hold-up in aircraft fuel tanks. The effect of flow rate on solidification was also simulated, and it was found that lower flow rates result in relatively more solidification of the fuel than do higher flow rates. The simulations of the freezing behaviors of JP-8 and JPTS samples were found to have essentially the same value of morphology constant. However, the crystal structures of these two fuels were studied in experiments and were found to be very different. This shows the inability of the model to capture small-scale details like the crystal microstructure. However, this limitation is not fatal here because the focus is on the overall flow and freezing behavior of jet fuels. The model was successful in predicting the freezing behavior by comparing the calculated frozen area obtained by the model with the measured area.

## **Acknowledgments**

I would like to express my gratitude to my dissertation advisor, Dr. Jamie Ervin for his support, guidance, and encouragement. I am also thankful to my doctoral advisory committee members: Dr. Kevin Hallinan, Dr. Steven Zabarnick, Dr. Tim Edwards and Dr. Dilip Ballal for their help in my research and for reviewing this manuscript. I am grateful to Mr. Mark Laber, Mr. Lee Riehl and Dr. Steven Zabarnick for the experimental work described in this dissertation.

I am obliged to the Mechanical and Aerospace Engineering Department, University of Dayton, who allowed me to use their facilities. I am grateful to the Air Force Research Laboratory (AFRL) and Federal Aviation Administration (FAA) who sponsored my research. I am also thankful to the Dayton Area Graduate Studies Institute (DAGSI) who supported me during my research.

I am especially appreciative of my husband for his love, support, and encouragement throughout my research. I am highly indebted to my parents who have always been my inspiration.

## **Preface**

This material is sponsored by Air Force Research Laboratory under agreement number F33615-03-2-2347 and Dayton Area Graduates Studies Institute (DAGSI). This work was also sponsored by the Federal Aviation Administration, Airport and Aircraft Safety Research and Development Division, AAR-400, located at the William J. Hughes Technical Center, Atlantic City International Airport, New Jersey (Mr. Skip Byrnes, Technical Monitor) under contract DTFA03-01-C-00038. Also,. The U.S. Government is authorized to reproduce and distribute reprints for Governmental purposes notwithstanding any copyright notation thereon. The views and conclusions contained herein are those of the authors and should not be interpreted as necessarily representing the official policies or endorsements, either expressed or implied, of Air Force Research Laboratory or the U.S. Government.



## Table of Contents

Abstract .....	iv
Acknowledgments.....	vi
Preface.....	vii
Table of Contents.....	viii
List of Figures .....	x
List of Tables .....	xiv
List of Symbols and Abbreviations.....	xv
CHAPTER 1 - Introduction .....	1
CHAPTER 2 – Studies of Jet Fuel Flow Near the Freeze Point.....	7
2.1    Introduction.....	7
2.2    Experimental .....	9
2.3    Simulation Methodology .....	13
2.4    Results and Discussion .....	17
2.4.1    Effect of boundary conditions.....	20
2.4.1    Two- and three-dimensional simulations.....	17
2.4.3    Heat transfer and flow during static cooling in a full tank .....	23
2.4.4    Effect of ullage space on tank heat transfer .....	26
2.4.5    Low temperature flowability and pumpability measurements.....	31
2.4.6    Role of viscosity in heat transfer and flowability .....	34
2.4.7    Role of density in heat transfer and flowability.....	43

CHAPTER 3 – Studies of Jet Fuel Flow in Tank Foam .....	46
3.1    Introduction.....	46
3.2    Experimental .....	48
3.2.1    Wing tank simulator.....	48
3.2.2    Measured fuel properties.....	50
3.3    Numerical.....	53
3.4    Results and Discussions .....	57
3.4.1    Effect of foam on fuel flowability .....	57
3.4.2    Effect of foam on heat transfer in the fuel tank .....	59
CHAPTER 4 – Studies of Jet Fuel Freezing in Forced Flow .....	67
4.1    Introduction.....	67
4.2    Experimental .....	70
4.2.1    Flow assembly .....	70
4.2.2    Low temperature properties of jet fuels .....	74
4.3    Simulation Methodology .....	79
4.4    Numerical Modeling .....	84
4.5    Results and Discussion .....	87
4.5.1    Experimental validation and the effect of $C^*$ on freezing.....	88
4.5.2    Effect of fuel flow rate on freezing.....	99
CHAPTER 5 – Conclusions and Recommendations .....	104
Bibliography .....	108

## List of Figures

Figure 1. Frequency of occurrence of fuel freeze points for a sampling of Jet A fuels measured at North American airports <sup>1</sup> .....	3
Figure 2. Drawing of the wing tank simulator .....	11
Figure 3. Wall temperature schedule used for the cooling simulations .....	17
Figure 4. Comparison of temperature color contour plots within the FAA tank simulated by (a) three-dimensional and (b) two-dimensional calculations .....	19
Figure 5. Temperature measurements and two- and three-dimensional simulations at a single location for different times. ....	19
Figure 6. Two-dimensional simulations of cooling in the FAA tank after 15 hours for (a) vertical walls of uniform temperature and (b) insulated vertical walls .....	20
Figure 7. Vector plots showing flow in the FAA tank after 15 hours for (a) vertical walls of uniform temperature and (b) insulated vertical walls .....	22
Figure 8. Measured and simulated temperatures for uniform wall temperature or adiabatic boundary conditions for thermocouples located at (a) 1.2 cm from the sidewall or (b) 1.3 cm above the bottom wall. ....	23
Figure 9. Three-dimensional temperature color contour plots of the Jet A fuel within the tank after (a) 10 minutes, (b) one hour and (c) 2.5 hours .....	25
Figure 10. Vector plot showing three different locations in the tank simulator from a three-dimensional calculation for Jet A fuel after four hours .....	26
Figure 11. Measured and simulated temperatures for Jet A fuel in the tank with an ullage space of (a) 3.8 cm, (b) 25.6 cm and (c) 33.8 cm height for three different thermocouple locations. ....	29

Figure 12. Temperature contours of Jet A fuel for three-dimensional simulations after 2.5 hours of cooling near the center of a tank compartment for (a) full tank and inclusion of air gap heights of (b) 3.8 cm and (c) 26.5 cm.....	31
Figure 13. Plots of flow rate vs. temperature during recirculation in the wing tank simulator using five different fuels. ....	33
Figure 14. Measured viscosities of nine jet fuel samples .....	36
Figure 15. Measured liquid-phase viscosities of nine jet fuel samples.....	38
Figure 16. Plot for increase in dynamic viscosity by either 30% ( $1.3\mu_0$ ) or 200% ( $3\mu_0$ ) relative to the baseline density ( $\mu_0$ ).....	41
Figure 17. Three-dimensional time-varying simulations of the fuel temperature after 4 hours of cooling for (a) viscosity = $\mu_0$ , (b) viscosity = $1.3 \mu_0$ , and (c) viscosity = $3\mu_0$ .....	42
Figure 18. Vertical temperature profile near the center of a tank compartment after four hours of cooling for two different jet fuels .....	43
Figure 19. Density vs. Temperature for changes in density by +5% from the baseline density .....	44
Figure 20. Transient temperature profile above lower surface at the vertical centerline after 60 minutes of cooling for a change of +5% from the baseline density .....	45
Figure 21. Low temperature viscosities of fuel samples of JP-8 (F4751 and F3804) .....	52
Figure 22. Two-dimensional structured grid .....	56
Figure 23. Flow rate of the draining fuel with time .....	58
Figure 24. Comparison of predictions with the measured mass of fuel drained out from the fuel tank in one hour. ....	59

Figure 25. Wall temperature schedule for the cooling tests.....	60
Figure 26. Measured and Simulated temperatures in the tank with foam for two different thermocouple locations. ....	62
Figure 27. Temperature contours for two-dimensional simulations after 20 minutes of cooling and draining (a) with foam and (b) without foam.....	62
Figure 28. Velocity vectors and temperature distribution after 20 minutes of cooling and draining (a) with foam and (b) without foam.....	63
Figure 29. Temperature contours for two-dimensional simulations after 90 minutes of cooling and draining (a) with foam and (b) without foam.....	64
Figure 30. Two-dimensional calculated contour plots showing fuel and air in the simulator tank after 10 minutes and foam with porosity of (a) 0.5 (b) 0.7 and (c) 0.97 .....	66
Figure 31. Image of the quartz duct .....	71
Figure 32. Schematic of the quartz duct .....	72
Figure 33. Measured normal alkane distributions for JPTS (F3775) and JP-8 (F3804)...	75
Figure 34. Measured specific heat for fuel samples (a) F3775 (JPTS) and (b) F3804 (JP-8).....	78
Figure 35. Measured dynamic viscosity of JPTS (F3775) and JP-8 (F3804).....	79
Figure 36. Two-dimensional unstructured grid .....	85
Figure 37. Temperature schedule for the cooled horizontal walls used for freezing simulations .....	86

Figure 38. Predicted liquid fraction and velocity vectors in the quartz duct after two hours of cooling for JP-8 (F3804) at a flow rate of 60 mL/min with $C^* =$ (a) 1, (b) $1 \times 10^5$ , (c) $1 \times 10^{10}$ and (d) visualization image.....	89
Figure 39. (a) Measured and (b) predicted solidified fuel area in the quartz duct after two hours of cooling for JPTS (F3775) at a flow rate of 60 mL/min with $C^* = 1 \times 10^{10}$ .....	91
Figure 40. Crystal structures of fuel samples of (a) JPTS (F3775) and (b) JP-8 (F3804).....	93
Figure 41. Images of JP-8 (F3804) showing (a) measured and (b) calculated liquid fraction after one hour of cooling and a flow rate of 60 mL/min .....	95
Figure 42. Measured and simulated temperatures for the fuel samples of (a) JP-8 (F3804) and (b) JPTS (F3775) at two different thermocouple locations.....	98
Figure 43. Temperature contours and velocity vectors for JP-8 (F3804) in the quartz duct after (a) 10 minutes, and (b) two hours of cooling, and (c) image of frozen fuel after two hours and a flow rate of 60 mL/min.....	99
Figure 44. Predicted liquid fraction of JPTS (F3775) in the duct after two hours of cooling for an inlet velocity of (a) 0.8 cm/sec and (b) 0.08 cm/sec.....	100
Figure 45. Predicted temperature profile of JPTS (F3775) in the duct after two hours of cooling for an inlet velocity of (a) 0.8 cm/sec and (b) 0.08 cm/sec.....	101

## List of Tables

Table 1. Source terms and transport coefficients appearing in Equation 1 .....	13
Table 2. Measured freeze point, total weight percent normal alkanes, and viscosities of jet fuels studied .....	16
Table 3. Measured freeze point, total weight percent normal alkanes, and viscosities of jet fuels studied .....	57
Table 4. Select low temperature freezing experiments .....	73
Table 5. Low temperature jet fuel characteristics .....	75
Table 6. Grid refinement study for the freezing model. The table shows temperatures at three different locations and the fraction of liquid after 1.5 hours of cooling .....	87

## List of Symbols and Abbreviations

$C$	Morphology constant, $m^{-2}$
$C_0$	Kozeny pore geometry constant, dimensionless
$C^*$	Product $C\mu$ , $kg/m^3 \cdot s$
$C_p$	Specific Heat, $J/kg \cdot K$
CFD	Computational Fluid Dynamics
$f_l$	Liquid mass fraction, dimensionless
$f_s$	Solid mass fraction, dimensionless
$g$	Gravity constant, $m/s^2$
GC-MS	Gas Chromatograph - Mass Spectrometer
$H$	Liquid and solid enthalpy, $J/kg$
$h$	Liquid enthalpy, $J/kg$
$k$	Thermal conductivity, $W/m^2 \cdot K$
$K$	Permeability, $m^2$
$P$	Pressure, Pa
$S^\Phi$	Source term
SIMPLE	Semi-Implicit Method for Pressure Linked Equations algorithm
$t$	Time, sec
$T$	Temperature, $^\circ C$
$T_h$	Temperature when solidification starts, $^\circ C$



$T_l$	Temperature when solidification is complete, °C
$u$	Velocity component in x direction, m/s
$\mathbf{u}$	Superficial velocity vector, m/s
$\mathbf{u}_f$	Actual fluid velocity vector, m/s
$v$	Velocity component in y direction, m/s
$w$	Velocity component in z direction, m/s
$x, y, z$	Coordinate directions
$\Delta H$	Heat of fusion, J/kg
$\Delta H_e$	Effective heat of fusion, J/kg
$\lambda$	Porosity, dimensionless
$\mu$	Dynamic viscosity, kg/m-s
$\nu$	Kinematic viscosity, m <sup>2</sup> /s
$\rho$	Density, kg/m <sup>3</sup>
$\Phi$	Assigned variable in equation (1)
$\Gamma^\Phi$	Transport coefficient
$\Sigma$	Interstitial surface area of the pores per unit volume of porous material, m <sup>-1</sup>

# CHAPTER 1

## Introduction

Cooling of jet fuel that takes place during aircraft operation at high altitudes for long flight periods can result in reduced fuel fluidity with the potential for fuel crystallization and gelation. At these low temperatures, fuel viscosity must remain sufficiently low to not impede adequate flow through narrow passageways in fuel lines, filters, screens and valves. In addition, the viscosity must remain sufficiently low to permit proper boost and engine pump operation and provide appropriate fuel atomization and facile ignition in the engine combustor. As the fuel temperature further decreases, fine wax crystals appear and increase in size and concentration on further cooling. With sufficient crystallization, there is potential for catastrophic fuel system failure due to blocked filters, valves, and other flow passages. Low temperature jet fuel specifications are characterized by two physical properties: viscosity and freeze point<sup>\*1</sup>.

Long duration commercial flights are currently limited to operation under conditions where the measured fuel temperature is 3°C above the fuel specification freeze point. The specification freeze points are -40°C for Jet A fuel and -47°C for Jet A-1 fuel (ASTM D1655). As a consequence, aircraft are restricted to operations where fuel temperatures remain above -37°C for Jet A fuel and -44°C for Jet A-1 fuel. When the

---

\* The freeze point (ASTM D2386) is actually a melting point and is determined by measurement of the temperature at which the last visible crystal melts upon heating of solidified fuel.

measured in-tank fuel temperature approaches these low temperature limits, pilots are forced to modify flight path, altitude, and/or airspeed to raise these temperatures. However, many fuel samples exhibit measured freeze points that are significantly lower than the specification freeze point. Figure 1 shows the frequency of occurrence of fuel freeze points for a random sampling of Jet A fuels measured at North American airports.<sup>2</sup> The figure shows that fuels most commonly exhibit freeze points from 2 to 5°C below the specification requirement, but a significant fraction have lower freeze points, with the lowest freezing fuels exhibiting freeze points nearly 18°C below the specification. Thus, for a significant fraction of fuels, use of the measured freeze point would permit aircraft operation at lower fuel temperatures during flight, resulting in more flexibility in flight profiles. Increased flexibility in flight altitude and route can result in significant advantages for airlines and their customers, including lower costs and greater flight availability. However, it is important to assess the safe operability of the fuel system at these lower fuel temperatures.

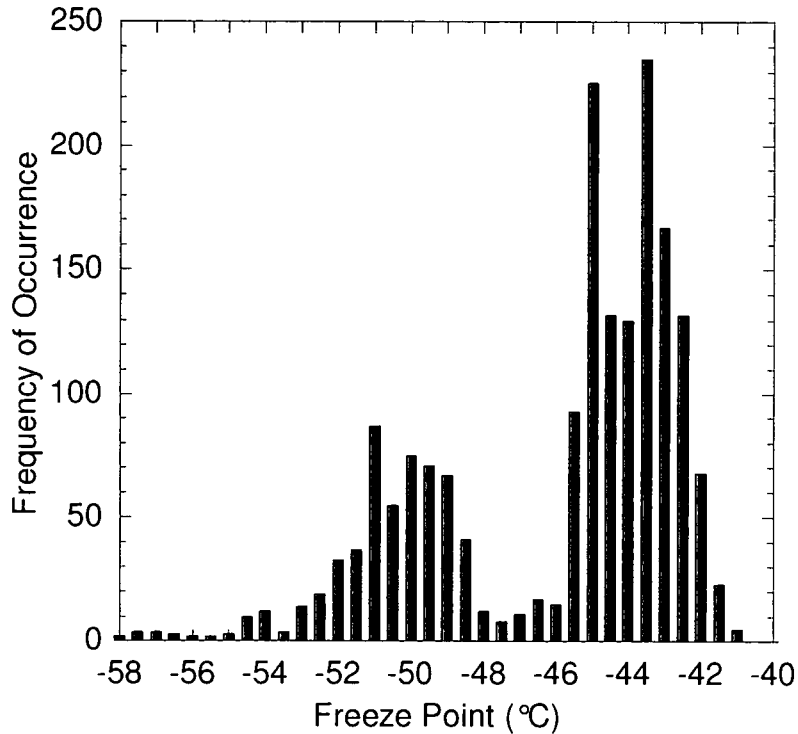


**Figure 1.** Frequency of occurrence of fuel freeze points for a sampling of Jet A fuels measured at North American airports.<sup>1</sup>

Commercial aircraft fuel tanks usually contain temperature sensors that provide the crew with limited information on the fuel temperature within a subset of the aircraft fuel tanks. Such a single sensor within a fuel tank may provide incomplete and misleading temperature information. Thus, it is important to understand better the temperature distribution within aircraft wing tanks so that temperature sensors may be properly located and the temperature which corresponds to a given sensor can be estimated. Also, in wide body aircraft such as the Boeing B747, fuel in the outboard main tanks is subjected to the lowest temperatures because these tanks may not be used until near the end of a long flight. Fuel in these tanks is subjected to the lowest temperatures

for long periods. It is important to simulate the cooling of a buoyancy-driven flow in these wing tanks.

In the Chapter 2, a wing tank simulator is modeled that can be subjected to a variety of temperatures. It is kept inside an environmental chamber to study the effect of low temperatures on jet fuel properties and fuel system operation. A three-dimensional numerical analysis using computational fluid dynamics (CFD) techniques provides the transient thermal behavior of the entire tank. The emphasis is on static cooling, therefore, the flow is buoyancy driven. Because low temperature properties of jet fuel (Jet A) are not readily available, temperature-dependent measured fuel properties are used in all the calculations (In all the chapters, the experiments were performed by others but the data was used in the results presented in this thesis to validate the simulations). Since aircraft fuel tanks are not full near the end of the flight, the gas-filled volume above the liquid fuel (known as ullage space) is unavoidable. The thermal distribution inside the fuel tank may depend on the level of fuel (or, height of ullage space). Therefore, in this study, three different ullage spaces are considered and comparisons are made with respect to flow and temperature distribution.

The presence of air in the fuel tank may be an explosion risk, if the mixture of fuel vapor and air are within the flammable range. For JP-8 and Jet A fuels, the lower and upper flammability limits are 0.6 volume percent vapor in air and 4.7 volume percent vapor in air, respectively.<sup>1</sup> Various military aircraft have been made more safe by using explosion suppressant polyurethane foam (ESF)(MIL-PRF-87260). The foam is formed to nearly fill the entire tank volume which contains the liquid fuel, vapor and air. The foam prevents fuel explosions caused by gunfire, electrical ignition, lightning strikes and

static discharge. It disrupts compression effects that precede an explosion.<sup>3</sup> In the event of an explosion, the foam inhibits the spread of fire by absorbing the explosion. One disadvantage with the use of the foam is that it reduces the available fuel volume and therefore, is not economical for use in commercial aircraft.<sup>3</sup>

Chapter 3 describes how the presence of polyurethane foam in an aircraft fuel tank affects fuel flowability and temperature distribution. Experiments are performed using the fuel tank simulator set-up in the environmental chamber as described in Chapter 2. Here, the simulator is cooled and drained simultaneously for longer periods to study the effect of the presence of foam on temperature distribution and flow behavior. JP-8 is used in the experiments because of its wide military applications, and measured properties of JP-8 fuel sample are used in all the calculations.

In Chapter 4, a quartz duct is used to study the effect of freezing temperatures on the fuel flow and solidification. Due to the complexities of the low-temperature experiments and the involved multiphase transport, no published computational work has been found that incorporates jet fuel solidification in a geometry with one or more internal structures. Therefore, in the present work, a quartz duct with some internal structures is fabricated to study the effect of low temperatures on fuel flow, solidification and hold-up. The duct containing flowing fuel is subjected to temperatures below the freeze point of the jet fuel. Freezing and flow behavior of jet fuel is studied for two different jet fuel samples – JP-8 (F3804) and JPTS (F3775). A two-dimensional numerical grid is used to simulate the solidification of jet fuel in the duct. The frozen areas and temperatures obtained from the calculations are compared with the measurements to validate the simulations.

Jet fuel freezing is a complicated phenomenon because jet fuel is a complex hydrocarbon mixture consisting of thousands of different hydrocarbon species. Jet fuel primarily consists of normal alkanes, branched alkanes, cycloparaffins, olefins, and aromatics. In addition, the composition of individual jet fuel samples varies with the fuel source. Since each hydrocarbon has its own solidification temperature, jet fuel freezes over a range of temperatures, and solidified jet fuel mainly consists of larger normal alkanes.<sup>4</sup> The cloud point temperature (ASTM D2500) is the temperature (few degrees below the freeze point) at which visible crystals first appear in a cooled fuel. As the temperature is reduced, crystals grow in size and adhere to other crystals. The pour point temperature (ASTM D97) is the lowest temperature at which the fuel still flows before entering a semi-rigid state. When the fuel reaches the pour point temperature, it ceases to flow and is unavailable for use. Thus, it is essential to study how fuel system operation will be affected with fuel temperatures below the freeze point.

Chapter 5 presents final conclusions drawn from the research in this dissertation. It is the author's hope that the findings and tools developed here will enable future researchers and engineers to design and create improved fuel systems for future advanced aircraft.

## **CHAPTER 2**

### **Studies of Jet Fuel Flow Near the Freeze Point**

#### **2.1 Introduction**

Jet fuels are subjected to extremely low temperatures in aircraft fuel tanks. Therefore, in the present work, a wing tank simulator is designed and fabricated that can be subjected to a variety of temperatures inside an environmental chamber to study the effect of low temperatures on jet fuel properties and fuel system operation. The simulator, representing the fuel system components of a commercial aircraft was run under conditions similar to those found in the aircraft outer wing tank during long duration flights. The simulator employs actual Boeing B747 fuel hardware, such as flapper valves and a fuel boost pump. Thermocouples in the wing simulator provide temperature measurements within the tank at discrete locations. Computational fluid dynamics (CFD) techniques provide the transient thermal behavior of the entire tank. CFD techniques permit the three-dimensional numerical simulation of the complex flow and heat transfer environment within tank and assist the understanding of laboratory experiments.

Previous experimental and computational studies of fuel tanks at low temperatures have been performed by Boeing and Lockheed.<sup>5,6</sup> These studies concentrated on temperatures significantly below the fuel freeze point where fuel solidification begins to occur. This previous work focused on the implications of fuel solidification on fuel hold-up in aircrafts tanks. In these studies, the transient boundary temperatures for the top and bottom surfaces were controlled via heat exchangers. The



temperatures of the vertical surfaces were not controlled, but were well insulated. It was assumed that the largest changes in temperature would occur in the direction normal to the top and bottom surfaces, and that the vertical surfaces of the tanks were adiabatic. Although this assumption aids the interpretation of the experiments, it is not completely valid due to the imperfections of the actual insulation. Thus, numerical simulation of these experiments is difficult as the true boundary conditions of the vertical walls are unknown. For the present simulator, transient temperatures are measured on all boundary surfaces. Previous thermal simulations of wing tanks have been limited to simple, circular or rectangular, two-dimensional tank geometries.<sup>7,8</sup> The wall temperatures were assumed constant, and temperature-dependent jet fuel properties were not used. In the present calculations, complex tank geometries, transient boundary temperatures, and measured temperature dependent fuel properties are utilized in order to more accurately simulate the flow and heat transfer in these complicated systems.

In the current work, the focus is on the measurements and simulations of the temperature regime near the measured freeze point of the fuel, where the fuel, for the most part, remains a single liquid phase. The simulator is subjected to chilling under controlled conditions and is used to verify three-dimensional predictions of the transient fuel temperature distribution and fuel motion. In the experiments performed, the emphasis was on nearly static cooling. Thus in all simulations, the flow is not pumped, but rather, is driven by buoyancy forces resulting from the transient cooling of the fuel tank. In addition, temperature-dependent fuel properties are used. The viscosity of jet fuel is not readily available for temperatures below -40°C. Here, the viscosity is obtained from low temperature scanning Brookfield dynamic viscosity measurements, as it may vary

significantly at temperatures near the freeze point. (The term viscosity in this dissertation represents the dynamic viscosity unless otherwise specified.) The objective of the work described in chapter 2 is to understand better the effects of temperature on the fuel flowability and pumpability near the freeze point, as well as to elucidate the primary heat transfer and buoyancy-driven flow effects in fuel tanks at low temperatures. During static cooling of the tank, the fuel temperatures are measured. In addition, the fuel temperatures are measured while the fuel is recirculated using a boost pump. CFD techniques are used to calculate the time-dependent temperature distribution in the fuel tank and to analyze the effects of low-temperature properties on the fuel flow. The computations are used to advance the understanding of the influence of the ullage space on the heat transfer in the tank and the resulting fuel temperature profile.

## **2.2 Experimental**

A commonly used aircraft for long duration flights include the various varieties of the Boeing B747. Therefore, all of the experimental and most of the simulation work reported here is directed towards the tank design of this aircraft. In order to understand better the effect of low temperature on aircraft fuel systems, a wing tank simulator, which uses actual B747 components, was fabricated. Figure 2 shows the simulator, which is made of aluminum (internal dimensions 77.5 cm x 50.8 cm x 50.8 cm) and includes a baffle rib in the center with three “flapper” check valves (4.7 cm diameter). In addition, there are two aluminum Z-stringers (7.6 cm high) positioned at the bottom of the tank that run the length of the simulator. These Z-stringers are supporting structures in an actual fuel tank and have elliptical 1.25 in. (3.18 cm) “limber” holes to allow fuel flow

between the stringer divided sections. A single boost pump (Hydro-Aire, Model 60-98976-2), used for each engine in the Boeing 747-400, is powered by a Hobart/AXA 2200, 400 Hz, 115/200V, 7.5 kVA frequency converter/power supply. Also a 16-mesh screen has been installed in the boost pump inlet. This screen is significantly finer which results in a more conservative flow test than the 4-mesh screen used in the inlet of the B747 aircraft. The top of the tank is closed with a plexiglass plate. The simulator is designed so that the fuel can be gravity drained, pumped out via the boost pump, or recirculated through the boost pump back to the tank through a "piccolo" return tube. The entire tank is contained within an environmental chamber (Tenney Environmental, Model T64C15SPL), which can provide a minimum temperature of -73°C. The chamber is sufficient to produce a low temperature environment similar to that expected for aircraft flying at high altitudes for long periods. For safety concerns, the environmental chamber is purged with nitrogen, and nitrogen resides in the fuel tank ullage space. The pressure within the fuel tank is maintained at normal atmospheric pressure.

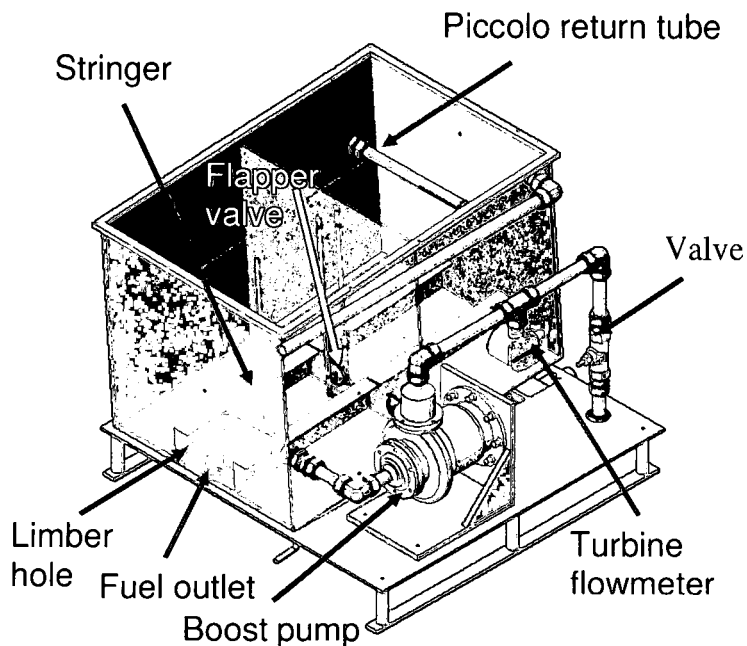


**Figure 2.** Drawing of the wing tank simulator.

The wing tank simulator was instrumented with a series of 48 thermocouples, a flow meter, and pressure gauges. Vertical temperature profiles were obtained at three locations in the tank. A post was located near the center of each of the two internal chambers (created by the single baffle rib) for the mounting of thermocouples. A third post was installed near a side wall to obtain boundary temperatures. Thermocouples were also mounted internally on the side walls and the inside bottom surface of the tank. A thermocouple was located on the boost pump housing to measure the pump temperature. Thermocouples were also located in the pump inlet and outlet to measure the fuel temperature rise due to pump operation. A calibrated turbine flow meter was located downstream of the pump. Pump power measurements could be obtained from current and voltage measurements of the three-phase power supplied to the pump. Thermocouple,

flow, and pressure measurements were obtained at ten minute intervals during cool down from ambient conditions and at one second intervals during pump operation.

Two types of tests using the wing tank simulator are reported here: static cool down and recirculation. In static cool down tests, the fuel was cooled from ambient temperature down to a given target temperature near the fuel freeze point while monitoring fuel and tank temperatures without flow. In recirculation tests, the fuel was cooled down (typically overnight) to a target temperature (usually a temperature slightly below the measured freeze point of the fuel). When the target temperature was reached, the pump was started and the fuel recirculated back to the tank through the piccolo tube. The fuel temperature would slowly increase due to heat input from the pump. Recirculation continued until the fuel temperature reached the high temperature target, usually -37°C. The fuel recirculation typically lasted one to two hours.

Viscosity is one of the most important fuel properties to consider when studying the effect of temperature on fuel flowability and pumpability. Viscosity measurements were performed using a scanning Brookfield Viscometer (Tannas, Plus two). As the fuel sample (30 mL) is cooled from -40 to -65°C at 5°C/hour, the viscosity is measured continuously by the increasing torque generated by a spindle rotating in the fluid at constant speed (12 rpm). The viscosity measurements are anchored at -40°C by calibrating to measurements obtained at the same temperature using ASTM D445, which measures the time for a volume of liquid to flow under gravity through a calibrated glass capillary viscometer.<sup>9</sup> Freeze point data were acquired using a Phase Technology PSA-70V Petroleum Analyzer via ASTM D5773.

## 2.3 Simulation Methodology

The commercially available CFD code (CFD-ACE, ESI Group) is used to simulate the laminar, time-varying flow and heat transfer by finite volume solution of the unsteady, two- and three-dimensional Navier-Stokes and energy (enthalpy) equations.<sup>10</sup> Equation 1 represents the momentum or energy equation depending on the variable represented by  $\Phi$  (velocity component or enthalpy, respectively).

$$\frac{\partial(\rho\Phi)}{\partial t} + \text{div}(\rho\vec{u}\Phi) = \text{div}(\Gamma_{\Phi} \text{grad}\Phi) + S^{\Phi} \quad (1)$$

For a given  $\Phi$ ,  $\Gamma_{\Phi}$  is the appropriate transport coefficient, and  $S^{\Phi}$  is the source term. With respect to the momentum equation, buoyancy forces induced by temperature differences within the tank are included in  $S^{\Phi}$ . In addition, the viscous dissipation was neglected. Table 1 lists the transport coefficients,  $\Gamma^{\Phi}$ , and the source terms,  $S^{\Phi}$ , of the governing equations.

**Table 1.** Source Terms and Transport Coefficients Appearing in Equation 1

$\Phi$	$\Gamma^{\Phi}$	$S^{\Phi}$
$u$	$\mu$	$-\frac{\partial p}{\partial x} + \frac{\partial}{\partial x}\left(\mu \frac{\partial u}{\partial x}\right) + \frac{\partial}{\partial y}\left(\mu \frac{\partial v}{\partial x}\right) + \frac{\partial}{\partial z}\left(\mu \frac{\partial w}{\partial x}\right)$
$v$	$\mu$	$-\frac{\partial p}{\partial y} + \frac{\partial}{\partial x}\left(\mu \frac{\partial u}{\partial y}\right) + \frac{\partial}{\partial y}\left(\mu \frac{\partial v}{\partial y}\right) + \frac{\partial}{\partial z}\left(\mu \frac{\partial w}{\partial y}\right) + \rho g$
$w$	$\mu$	$-\frac{\partial p}{\partial z} + \frac{\partial}{\partial x}\left(\mu \frac{\partial u}{\partial z}\right) + \frac{\partial}{\partial y}\left(\mu \frac{\partial v}{\partial z}\right) + \frac{\partial}{\partial z}\left(\mu \frac{\partial w}{\partial z}\right)$
$h$	$k$	0

The convective terms are represented by a third-order accurate upwind scheme, and a version of the SIMPLEC (Semi-Implicit Method for Pressure-Linked Equations Consistent) algorithm is used in the solution procedure.<sup>10</sup> To study the effect of an ullage space on heat transfer and flow within the tank, the interface between the liquid fuel and air can be tracked by techniques, such as the volume-of-fluid (VOF) method.<sup>11,12</sup> Unfortunately, the VOF method requires excessive computation time for the long time periods considered in the present simulations. For simplicity, only the behavior of the bulk liquid fuel is simulated and flow and thermal boundary conditions at the liquid-air interface are imposed. The calculations were simplified by assuming an adiabatic fuel-air interface. This assumption is reasonable since the convective heat transfer coefficient on the air side of the interface is small ( $\sim 1 \text{ W/m}^2 \text{ }^\circ\text{C}$ ) for natural convection. In addition, since the bulk behavior of the media was the focus, surface tension was neglected. Hence, the fuel-air interface was assumed to be planar. The viscosity of the air is orders of magnitude smaller than that of the fuel. Thus, it was assumed that the shear stresses on the fuel at the interface were negligible.

A three-dimensional unstructured grid representing the fuel tank simulator was employed. The three-dimensional geometry of the simulator involves two compartments, separated by a baffle plate that has three circular passages available for flow. In the simulations, the actual “flapper” valves are represented by holes for simplicity, as the actual valves offer little flow resistance. Also, two Z-stringers, 7.6 cm high located at the bottom of the tank, are included in the calculations. Since only the static flow was simulated, the piccolo tube was not included in the calculations. For the ullage case,

structured grids were used instead of unstructured grids as the structured grids required less computation time.

When the global error residuals were reduced below four orders of magnitude from their maximum values, the solution was considered to be converged. A coarse grid was first made with fewer cells and was further refined by increasing the number of grid points until grid independence was achieved. Three-dimensional structured grids representing the fuel tank simulator, with different ullage spaces (3.8 cm, 25.6 cm and 33.8 cm), were studied for grid independence of the solution. Results from a grid with 64,824 cells were found to be grid independent for ullage height of 3.8 cm, and are described in this work. Results with 56,010 and 47,736 cells were found to be grid independent for ullage heights of 25.6 cm and 33.8 cm, respectively. Also, using an unstructured grid for the full tank, calculations obtained from a grid of 159,862 cells were grid independent. Further grid refinement resulted in negligible changes in the solutions.

For the current simulations, the temperature-dependent viscosity of fuel sample 3166 (Jet A) is used as this fuel was used in the experiments. Viscometer measurements (described above) provided the temperature dependent fuel viscosity for the simulations. Table 2 shows properties of twelve jet fuels which were selected for their relatively wide range of freeze points. In addition, the temperature dependent values of the density, thermal conductivity and specific heat of Jet A fuel compiled by the Coordinating Research Council were used in all simulations.<sup>13</sup> As they vary slowly and linearly in the region below  $-40^{\circ}\text{C}$ , values of density, thermal conductivity and specific heat were linearly extrapolated from higher temperatures.



**Table 2.** Measured freeze point, total weight percent normal alkanes, and viscosities of jet fuels studied

Fuel Sample ID	Fuel Type	Freeze Point (°C)	Viscosity (cP) at freeze point	Total weight percent normal alkanes
3688	Jet A	-41.6	10	20.7
3686	Jet A	-41.9	8	14.6
2827	Jet A	-42.9	10	20.6
3166	Jet A	-43.7	15	21.6
3219	Jet A	-46.4	19	18.3
4336	JP-8	-47.2	19	15.2
3804	JP-8	-47.6	15	23.6
4339	JP-8	-48.6	13	23.4
3658	Jet A	-53.1	25	7.1
3633	Jet A	-55.1	18	19.1
4177	JP-8	-57.2	25	12.3
2976	JPTS	-58.5	18	17.2

The temperature boundary conditions for the simulations come from a spatial average of the thermocouples embedded in the walls. These spatial averages are represented as a function of time and used as the transient temperature boundary condition in the calculations. The initial air and fuel temperature is assumed to be uniform. Figure 3 shows the temperature boundary conditions employed in the static cool down simulations. With the set point of the environmental chamber fixed, the chamber was allowed to reach a low temperature of its own accord. The fuel is initially at 20°C, and the top and bottom walls decrease uniformly in time from 21°C to -61.2°C, while the sidewalls decrease to -53.3°C, after 15 hours.

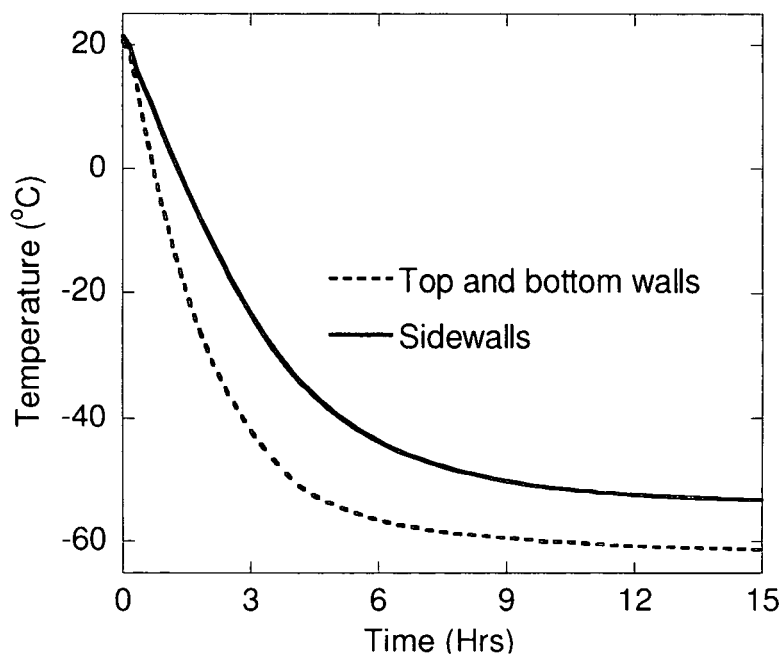


**Figure 3.** Wall temperature schedule used for the cooling simulations.

## **2.4 Results and Discussion**

Here, the effect of ullage on heat transfer and fuel temperature is described using computational and experimental data. In addition, simulations of heat transfer and flow during static cooling are validated with the experimental measurements. The effects of low temperature and viscosity on heat transfer, pumpability and flowability are presented. (Jet A is the fuel used in all numerical simulations.)

### **2.4.1 Two- and three-dimensional simulations**

Two-dimensional simulations require much less computer memory and fewer computations than do the three-dimensional simulations of the experimental vessels. However, the two-dimensional simulations may offer less fidelity with respect to velocity

and temperature than the three-dimensional solutions. In order to study if three-dimensional calculations can be reasonably replaced by two-dimensional calculations for simplicity, both two- and three-dimensional calculations were performed.

Three-dimensional CFD calculations were used to study the temperature profile in the FAA tank during static cooling. Figure 4 shows temperature contours for three- and two-dimensional simulations (two-dimensional plane near the center of the tank) after 4 hours. The boundary conditions are the same as the previous simulations, and the skin temperatures follow the schedule of Figure 3. The heat transfer with the center aluminum plate is significant which results in lower fuel temperature near the center in the three-dimensional simulation (Figure 4a). As the wall effects are not considered, the profile from two-dimensional calculation (Figure 4b) does not represent the fuel temperature of all the locations in the tank. Moreover, Figure 4b shows two large vortical cells while Figure 4a shows a more complex flow pattern, which changes with the location of the two-dimensional viewing plane in the tank. If we consider the thermal plot of the three-dimensional simulation at a location near the center of a tank section, the profile is similar to the two-dimensional result. Figure 5 compares both two- and three-dimensional time-varying simulations of the temperature with measurements for the thermocouple located at 0.25 inches from the bottom near the tank center. Figure 5 shows that for this location in the tank, the measured temperatures agree much better with the three-dimensional simulations. The conduction particularly from the baffle plate located at the center of the tank is not taken into account in the two-dimensional calculations.

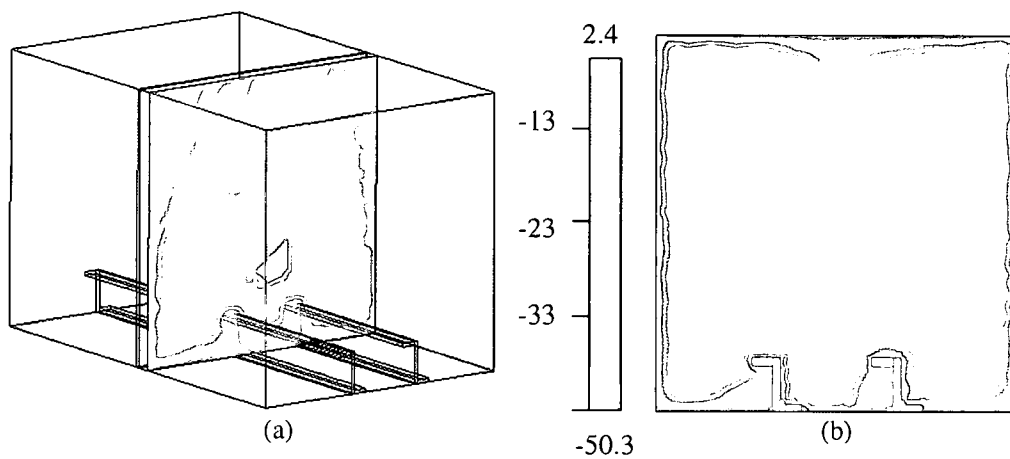


**Figure 4.** Comparison of temperature color contour plots within the FAA tank simulated by (a) three-dimensional and (b) two-dimensional calculations.

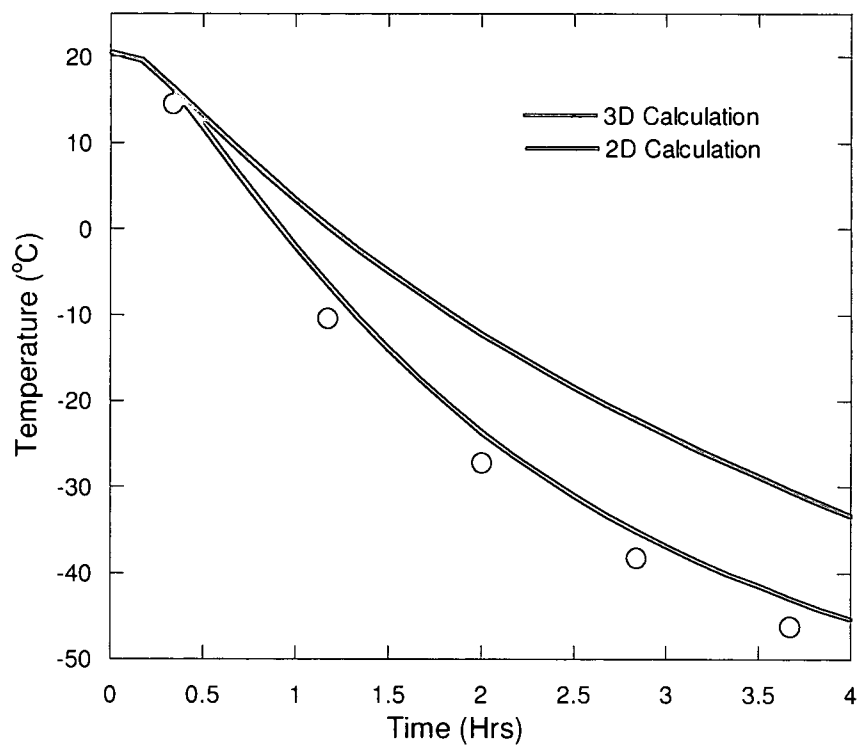


**Figure 5.** Temperature measurements and two- and three-dimensional simulations at a single location for different times. The symbols represent measured temperatures.

#### 2.4.2 Effect of boundary conditions

Simulations were performed to study the differences in the calculated temperature profiles within the FAA tank for conditions of adiabatic vertical walls or vertical walls in which the temperature uniformly decreased. The horizontal walls followed the temperature schedule shown in Figure 3. The vertical walls were either insulated or followed the schedule of Figure 3.

Both Figures 6(a) and 6(b) show that near the tank center, the fuel is relatively warm and that cooler fuel tends to reside near the stringers on the tank bottom. However, as indicated by the fuel temperature contours, the flow is very different for the two sets of imposed wall conditions. In Figure 6(a), as the vertical walls are also cooled with the horizontal walls, a thermal boundary layer can be observed adjacent to the vertical walls. In Figure 6(b), the adiabatic sidewalls result in uneven fuel motion and temperature distribution. As might be expected, Figure 6 shows that overall the fuel is cooler when the sidewalls are also cooled with the horizontal surfaces.

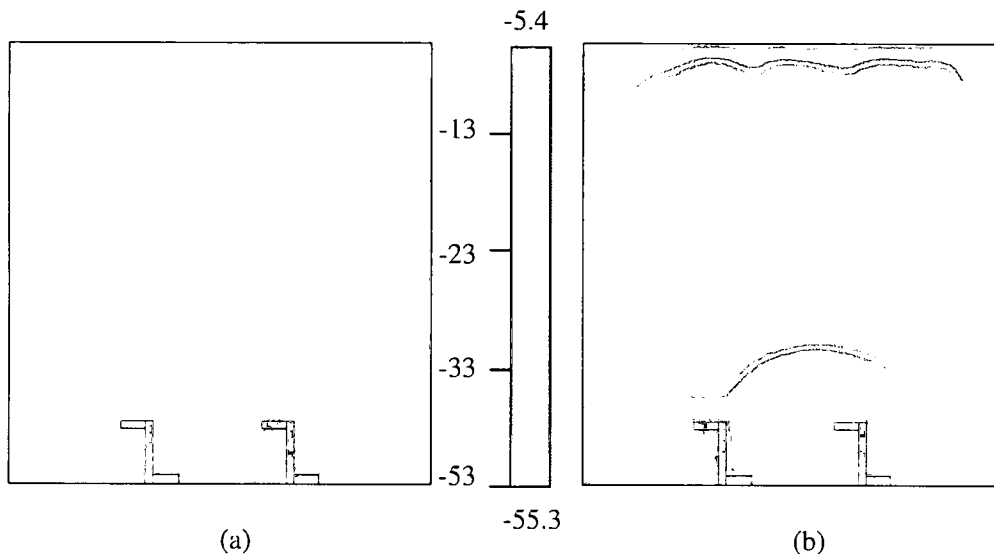


**Figure 6.** Two-dimensional simulations of cooling in the FAA tank after 15 hours for (a) vertical walls of uniform temperature and (b) insulated vertical walls.

Figures 7(a) and (b) show the vector plots describing the fuel flow behavior in the tank for these two different vertical wall conditions. In Figure 7(a), there are two nearly symmetrical vortices. On the other hand, the flow in Figure 7(b) is more complex with several smaller vortical cells. Figures 8(a) and (b) show the thermal profiles for the two vertical wall boundary conditions at two different thermocouple locations. Figure 8(a) represents the thermocouple location at 1.2 cm from the sidewall, while Figure 8(b) represents the thermocouple location at 1.3 cm above the bottom wall. There is a large temperature difference for the thermocouple located at about 1.2 cm from the sidewall as shown in Figure 8(a). The sidewalls with uniform temperature profile are in better agreement with the measured values relative to the adiabatic sidewalls. In Figure 8(b), for the thermocouple located at 1.3 cm from the bottom wall, the measured and calculated temperatures are in good agreement for both vertical wall cases as they are near the lower surface boundary where there is less influence from the vertical surfaces. Thus, the choice of transient uniform temperature or heat flux boundary conditions imposed on a computational grid has a large influence on the resulting computations. An important advantage of using the newly fabricated FAA tank is that it provides numerous thermocouple readings about all tank surfaces. Thus, the necessity of assuming boundary conditions for the vertical surfaces for purposes of comparison with experimental measurements as in the previously performed Boeing and Lockheed experiments is eliminated with use of the FAA tank.

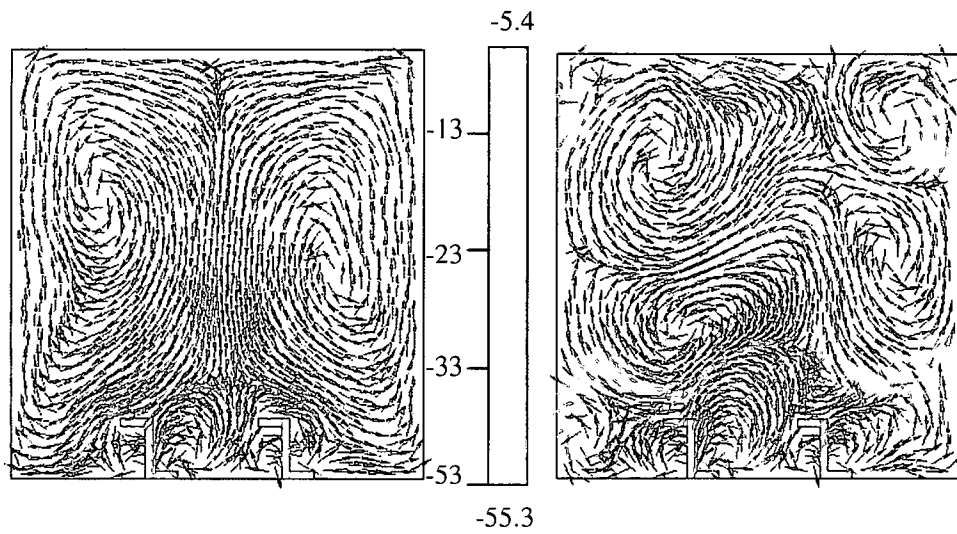
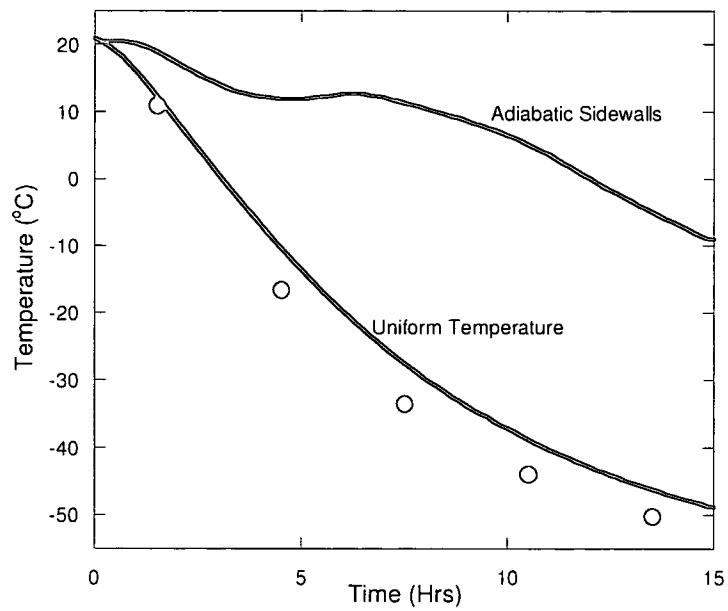


**Figure 7.** Vector plots showing flow in the FAA tank after 15 hours for (a) vertical walls of uniform temperature and (b) insulated vertical walls.



(a)

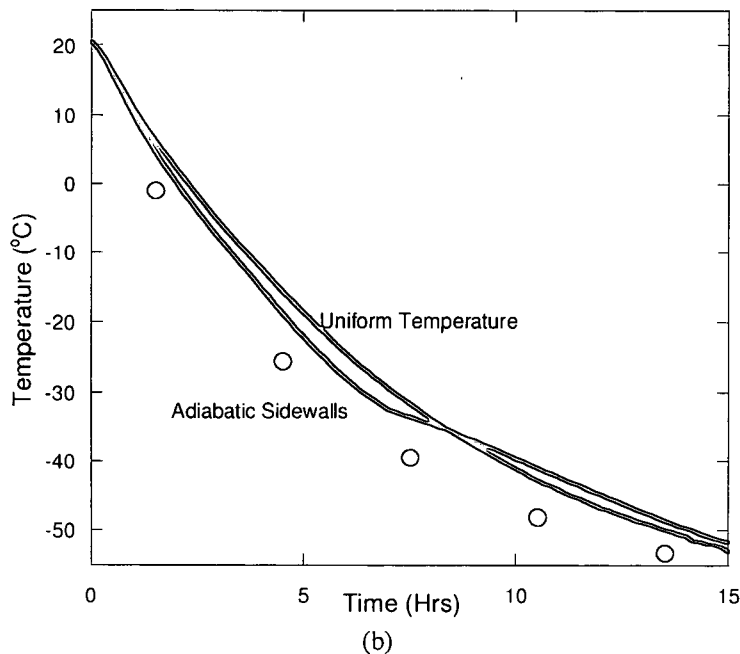


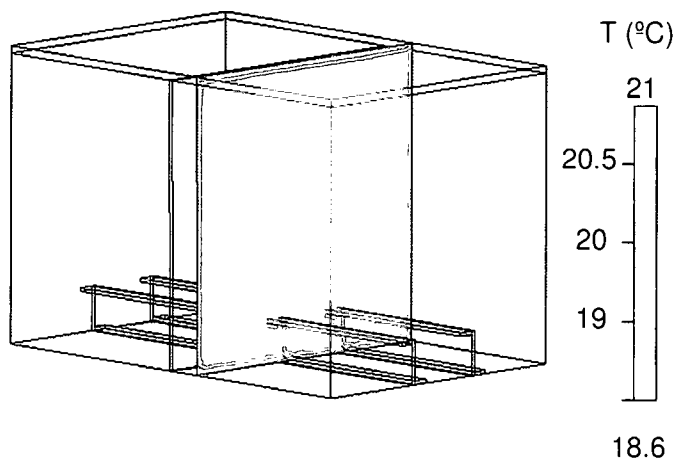
**Figure 8.** Measured and simulated temperatures for uniform wall temperature or adiabatic boundary conditions for thermocouples located at (a) 1.2 cm from the sidewall or (b) 1.3 cm above the bottom wall. The symbols represent measured temperatures.

#### 2.4.3 Heat transfer and flow during static cooling in a full tank

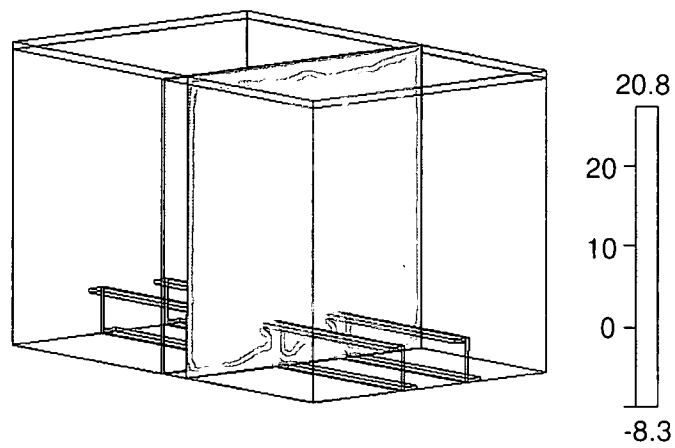
Figures 9(a) through 9(c) show the results of three-dimensional temperature calculations (via two-dimensional viewing planes near the center of the tank) at times up to 2.5 hours of cooling. Figure 9(a) shows that after 10 minutes, a thermal boundary layer develops and fuel temperatures near the baffle plate reduce to nearly 18°C. As the cooling proceeds, stratification in the tank increases. Figures 9(b) and 9(c) show an increase in the thermal boundary layer after one hour and 2.5 hours, respectively. Flow of cold fuel flowing from the top surface can be observed. Most of the fuel near the baffle plate reduces to nearly -3°C and -23°C after two hours and four hours of cooling, respectively. Figure 10 shows the velocity vector plot demonstrating the development of a complex flow pattern in the three-dimensional calculation at four hours. The velocity vectors



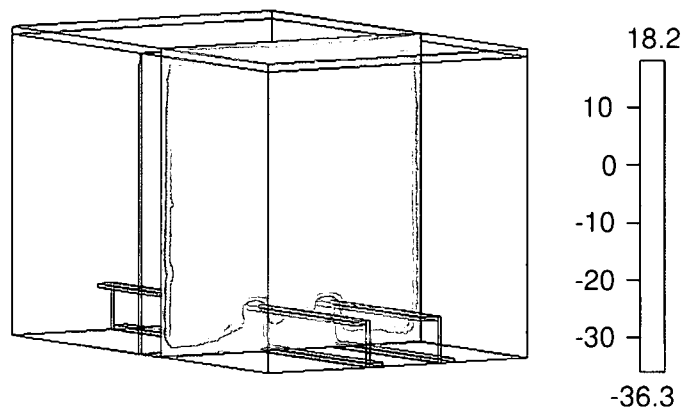
shown are proportional to the velocity magnitude, which vary over the range 0 to 0.048 cm/s. The vector plots show that the flow pattern is similar but opposite in direction for the two fuel compartments. Also, for a location near the baffle rib, the flow is more complex and the temperature there is much lower than elsewhere in the tank, due to the increased heat transfer caused by the baffle rib. Also, the thermal boundary layer around the stringers causes increased convective motion and stratification. The results demonstrate that much of the heat conduction occurs through the stringers and the colder, more dense fuel tends to be located near the bottom of the tank. Since the focus here is to find a suitable location for thermocouple sensors that can give the lowest temperature in a fuel tank, and because more dense fuel tends to be located near the tank bottom, it is much preferred to locate the thermal sensors near the tank bottom.



(a)



(b)



(c)

**Figure 9.** Three-dimensional temperature color contour plots of the Jet A fuel within the tank after (a) 10 minutes, (b) one hour and (c) 2.5 hours.

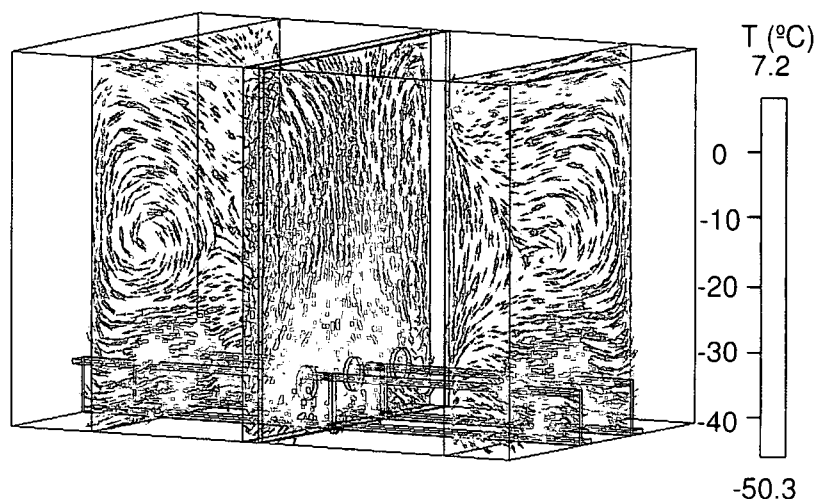


**Figure 10.** Vector plot showing three different locations in the tank simulator from a three-dimensional calculation for Jet A fuel after four hours.

#### **2.4.4 Effect of ullage space on tank heat transfer**

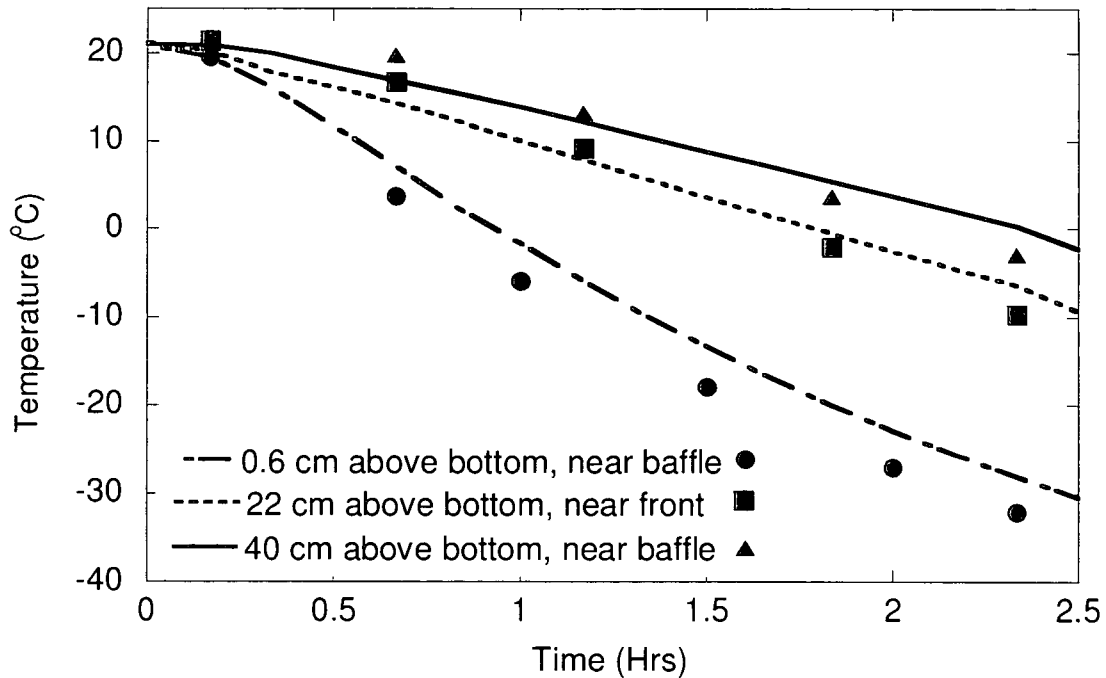
To better understand the implication of the location of fuel tank temperature sensors and the distribution of fuel temperatures within fuel tanks during cooling, experimental measurements and CFD simulations of fuel cooling in the wing tank simulator were performed. These studies simulate the fuel cooling which occurs in aircraft wing tanks upon exposure to the low temperature environment at altitude. The previous sections described the heat transfer and flow for conditions in which the tank was entirely filled with fuel. However, aircraft fuel tanks are almost never entirely full and thus, usually have ullage spaces above the fuel. Even when a flight starts with a completely full tank, fuel use during the flight results in ullage formation during the flight. Thus, the effect of varying levels of ullage space on the resulting heat transfer and fuel temperature distribution are studied. Ullage heights of 3.8, 25.6 and 33.8 cm were

studied. The volume of these three ullage spaces is 15000, 100,000 and 130,000 cm<sup>3</sup>, respectively. These simulations follow the wall temperature schedule of Figure 3.

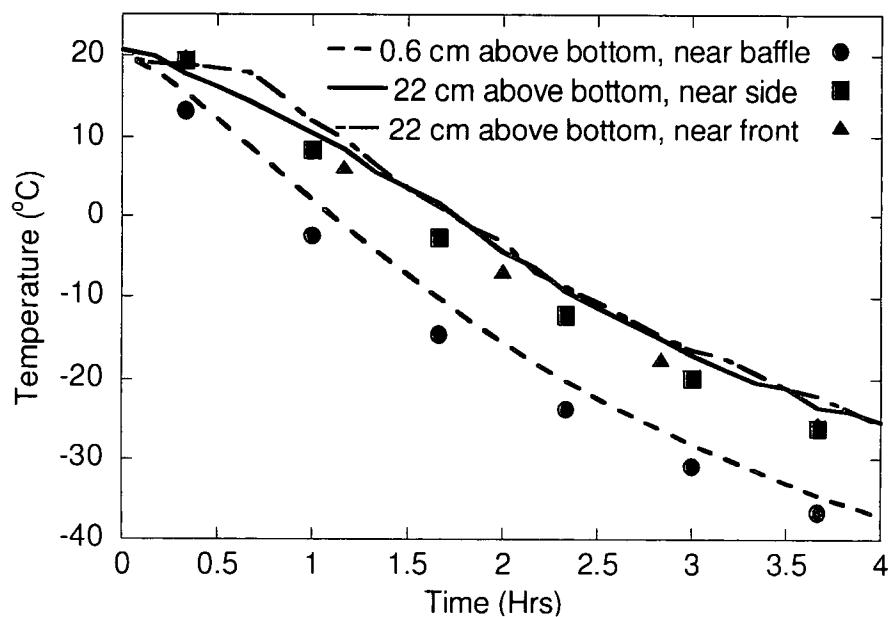
Figures 11(a) through 11(c) show that the three-dimensional calculations agree reasonably well (within 3°C) with the temperature measurements for different ullage spaces at three different thermocouple locations. Simulations with an air gap of 3.8 cm were performed for 2.5 hours, while all the other simulations were performed for four hours. The calculations show that the model can be used successfully to predict the temperature profiles in an aircraft fuel tank. Figure 12(a) shows a calculated temperature contour plot representing 2.5 hours of cooling for the full tank relative to Figures 12(b) and 12(c), which represent the calculations with an air gap. Much of the fuel near the center of the tank remains at a relatively warm temperature. Figure 12(b) shows that when a small ullage space is present (3.8 cm in height), the fuel temperature is significantly higher (about 5°C) than the full tank case. This difference demonstrates that the heat transfer from the top surface has a significant effect on the fuel temperature. Thus in the full tank case, this increased heat transfer from fuel contact results in lower fuel temperatures. In contrast, in the small ullage space case, the presence of air limits the heat transfer with the top surface and results in higher fuel temperatures. Interestingly, when the ullage height is increased to 25.6 cm (Figure 12c), the fuel temperatures are even lower than in the full tank case.

These lower temperatures are a result of the significantly lower fuel volume and increased surface area to volume ratio, which results in faster cooling. These results show that a relatively small ullage space results in increased fuel stratification and higher fuel temperatures relative to a full tank or a large ullage space. Aircraft fuel tanks are rarely

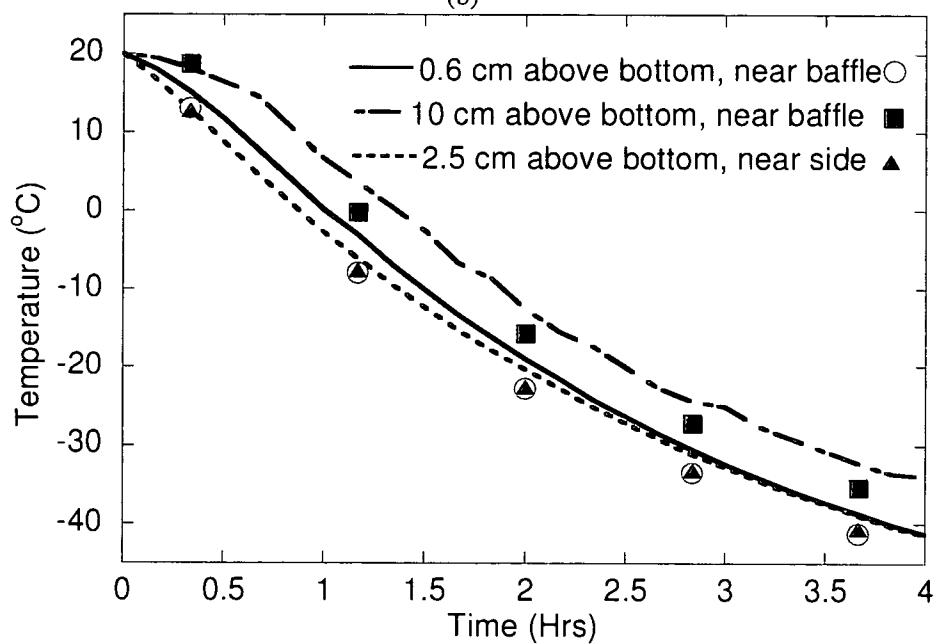
completely filled with fuel, but the varying dihedral wing angle during flight results in portions of the tank having a wetted top surface, while other portions will have varying amounts of ullage space. In addition, the relative amount of these two regions will vary as fuel is consumed during flight. Thus, the implications of the presence or absence of ullage space in fuel tanks on heat transfer and fuel temperature is extremely complex and dependent on numerous flight conditions.



(a)

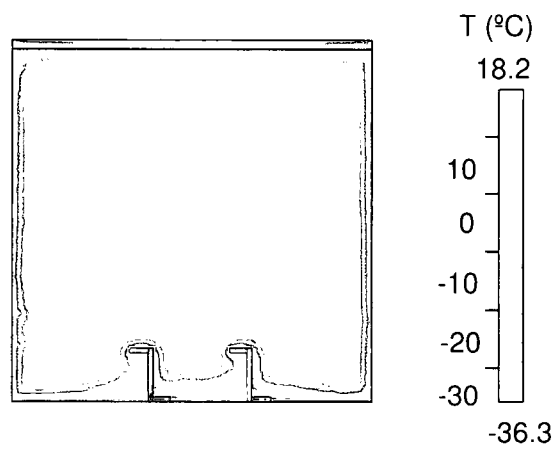


(b)

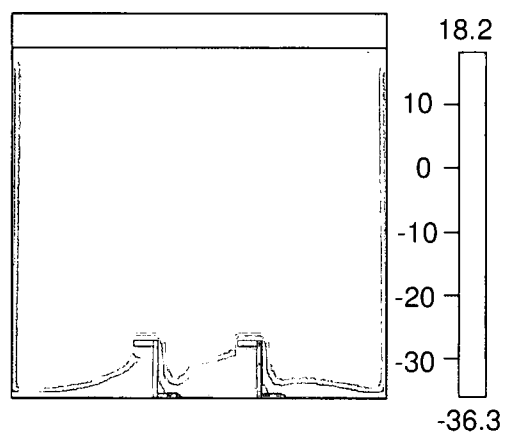


(c)

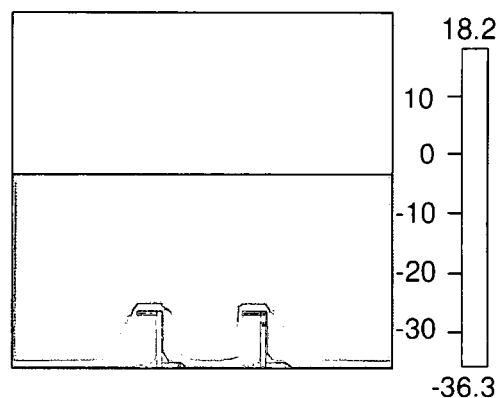
**Figure 11.** Measured and simulated temperatures for Jet A fuel in the tank with an ullage space of (a) 3.8 cm, (b) 25.6 cm and (c) 33.8 cm height for three different thermocouple locations. The symbols represent measured temperatures.



(a)



(b)



(c)

**Figure 12.** Temperature contours of Jet A fuel for three-dimensional simulations after 2.5 hours of cooling near the center of a tank compartment for (a) full tank and inclusion of air gap heights of (b) 3.8 cm and (c) 26.5 cm.

#### 2.4.5 Low temperature flowability and pumpability measurements

Experiments using the wing tank simulator were conducted to assess the effect of low temperatures on fuel flowability and pumpability. These tests examined a series of fuels (JP-8, Jet A, Jet A fuel with a low temperature flow improving additive, and JPTS - fuel properties shown in Table 2) in which cool down and recirculation runs were performed. JPTS (Freeze point specification  $-53^{\circ}\text{C}$ ) and JP-8 (Freeze point specification  $-47^{\circ}\text{C}$ ) fuels are refined to provide improved low temperature capability beyond Jet A fuels. They were chosen to provide a comparison of the flowability of these improved low temperature fuels with that of Jet A. During the recirculation tests, fuel was cooled down to a target temperature near the freeze point and subsequently pumped via the boost pump out the fuel inlet and back into the tank via the piccolo return tube. The pump



operation results in heat being added to the fuel. This added heat resulted in a slow fuel temperature rise (approximately 20°C per hour) during recirculation. Fuel recirculation was continued until the fuel reached the target temperature of -37°C, which is 3°C above the Jet A specification maximum freeze point and an operational limit for commercial flights. In this way, this fuel recirculation method is used to evaluate the fuel flowability and pumpability over a range of temperatures in a single experimental run.

Figure 13 shows that, for each fuel, as the temperature increases, the flow rate increases. This observation results primarily from the decrease in viscosity with increasing temperature shown later in viscometer measurements. The flow rates at 3°C above the measured freeze point temperature (shown as vertical arrows for each fuel in the figure) can be compared with the flow rates at -37°C for each fuel. Over this temperature range, flow reductions of 2.2 %, 4.1 %, 9.2 %, and 10.2% are observed for fuels 3166, 3804, 4177, and 2976, respectively. These data show that the low freeze point fuels exhibit greater flow reduction relative to the -37°C temperature than do high freeze point fuels. This important result shows that operating fuels near their measured freeze point rather than near the specification freeze point can result in reduced fuel flowability, in agreement with the viscometry measurements. The important question is how such a reduction in fuel flowability will affect aircraft and engine operation. The answer to this question is likely fuel system dependent. Each aircraft fuel system would need to be evaluated individually to evaluate the flow rate requirements of the engine. In addition, it is also important to take into account the effect of the engine main pump on fuel flow. For example in the B747 aircraft, suction from engine main pump operation may lessen the observed effect.

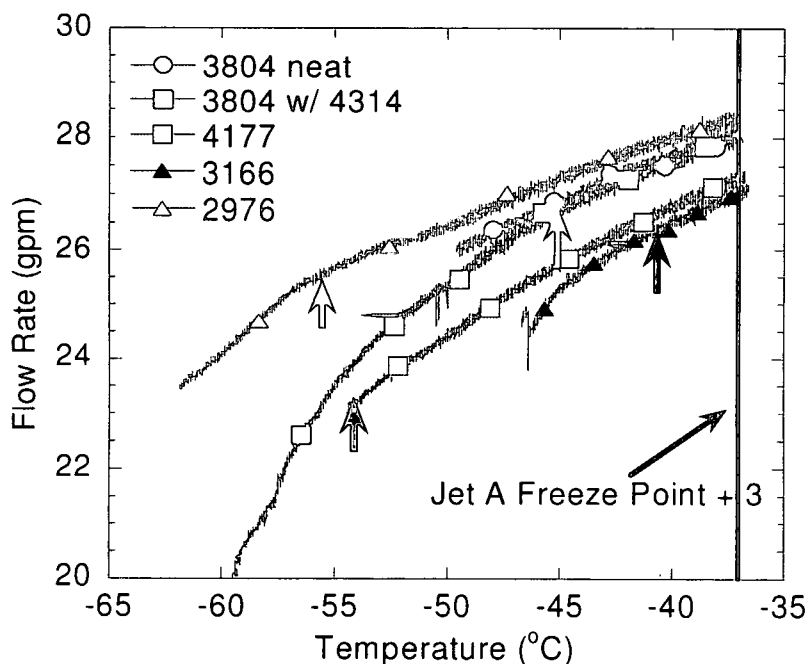


**Figure 13.** Plots of flow rate vs. temperature during recirculation in the wing tank simulator using five different fuels. The vertical arrows represent the measured freeze point plus 3°C for each fuel. The vertical black line shows the Jet A specification plus 3°C (-37°C).

Figure 13 also shows a comparison of the flowability of a fuel containing a candidate cold flow-improving additive (referred to here as additive 4314) with that of the unadditized fuel. The figure shows that the additized fuel remained flowable to temperatures almost 15 degrees below the fuel freeze point. In the temperature range where the two fuels overlap, their flow rates remained nearly identical. It is hypothesized that the additives modify crystal morphology to attain improved low-temperature fluidity.<sup>9</sup> At very low temperatures and long residence times, crystals continue to nucleate and grow and ultimately increase the effective viscosity of the liquid-solid mixture,

regardless of crystal morphology. Nevertheless, the current results indicate that flow-improving additives hold promise for providing jet fuels with improved reduced temperature capabilities.

#### **2.4.6 Role of viscosity in heat transfer and flowability**

Viscosity is one of the most important fuel properties to consider when studying the effect of temperature on fuel flowability and pumpability. Viscosity is a measure of the resistance to flow of a fluid. The specification for Jet A and Jet A-1 fuels, ASTM D1655, as well as the specification for JP-8 fuel, MIL-DTL-83133E, require a maximum kinematic viscosity of 8.0 cSt measured at -20°C. Since the temperature of the fuel is much higher at the engine (above -40°C) than in the fuel tanks, specifications for fuel viscosity are not given below -40°C. The viscosity specification was designed to assure adequate fuel flow through fuel lines, valves, and pumps at reduced temperature. In addition, the viscosity specification also assures proper fuel atomization in engine combustors. The performance of combustor nozzle atomizers, as well as subsequent proper fuel evaporation and mixing with air, are strongly dependent on the fuel viscosity. Engine manufacturers usually specify a maximum fuel kinematic viscosity of 12 cSt at the nozzle to assure reliable engine starting performance. The standard viscometry technique used for specification measures kinematic viscosity by measuring the time required for a fixed volume of fuel to flow through a calibrated capillary tube. This test is performed at the desired fixed temperature. In the present studies, the dynamic viscosity is measured via a Scanning Brookfield Viscometer. This technique offers the advantage of being able to rapidly measure viscosity as a function of temperature. Such

measurements would be extremely time consuming and/or impractical using the capillary tube technique.

Figure 14 shows plots of dynamic viscosity vs. temperature using the scanning Brookfield technique for nine fuel samples. This technique measures dynamic viscosity rather than kinematic viscosity as in the ASTM D445 method. The dynamic viscosity ( $\mu$ ) can be related to the kinematic viscosity ( $\nu$ ) via the density ( $\rho$ ) by,  $\mu = \nu\rho$ . The figure shows that the fuels display a very slow rise in viscosity as they are cooled below  $-40^{\circ}\text{C}$ . Upon further cooling, the fuels display a relatively sudden, rapid increase in viscosity. Previous work has shown that this sudden, rapid rise in viscosity occurs very close to the measured cloud point (ASTM D5773-95), and that microscopic crystal formation begins at this temperature.<sup>9</sup> These observations support the conclusion that this increase in viscosity is due to the occurrence of solid crystal formation in the fuel, as the cloud point is the temperature at which visible solids are first observed upon cooling. For the current study, the interest is in how the liquid phase viscosity varies with temperature. To show this variation better, the portions of the viscosity in the crystallization regime (i.e., the high viscosity regime) have been deleted. The rescaled and re-plotted liquid-phase only data is shown in Figure 15 for the nine jet fuel samples.

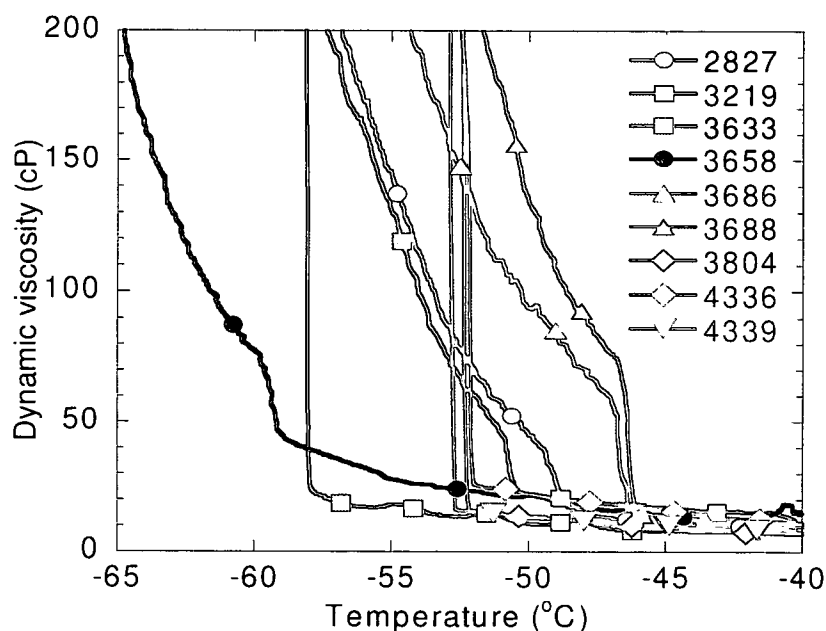


**Figure 14.** Measured viscosities of nine jet fuel samples.

Figure 15 shows how the liquid-only dynamic viscosity changes with temperature over a range of jet fuel samples. The figure shows that, in general, there is a gradual rise in viscosity over this temperature range. More interestingly, it is apparent that fuels with relatively high cloud/freeze points have relatively low viscosities at their cloud/freeze point, while fuels with low cloud/freeze points have relatively high viscosities at their cloud/freeze point (the cloud point is near the lowest viscosity measurement for each fuel). These results have important implications for fuel system operation. The results show that there may be issues in using the fuel freeze point (which is usually 2 to 6°C above the cloud point) to evaluate fuel flowability. For example, the low temperature freezing fuel 3658, which has a freeze point of -53.1°C and a cloud point of -59.2°C, displays a viscosity of 46.4 cP at its cloud point, while fuel 3688, which has a freeze point of -41.6°C and a cloud point of -46.1°C, has a viscosity of 11.7 cP at its cloud

point. This factor of four difference in viscosity may have a significant effect on fuel flowability and pumpability at these temperatures. Despite these differences near their cloud point temperatures, these two fuels display very similar viscosities in the temperature range -40 to -45°C. The significance of this factor of four difference in viscosity will depend on the specific fuel system requirements, such as required flow rate for the engines, ability of the fuel system pumps to handle higher viscosity fuel and the efficiency of combustor nozzle to atomize higher viscosity fuel. This observation of increased viscosity near the freeze point of lower freeze point fuels relative to high freeze point fuels is an important issue to consider when deciding whether to use low freeze point fuels at temperatures below the specification freeze point. These data show that it is important to consider the effect that this increase in viscosity will have on fuel flow to the engine and on fuel atomization in the combustor. Studies in the wing tank simulator reported above further elucidate how low temperatures affect viscosity and the resulting fuel flowability and pumpability in actual fuel system components.

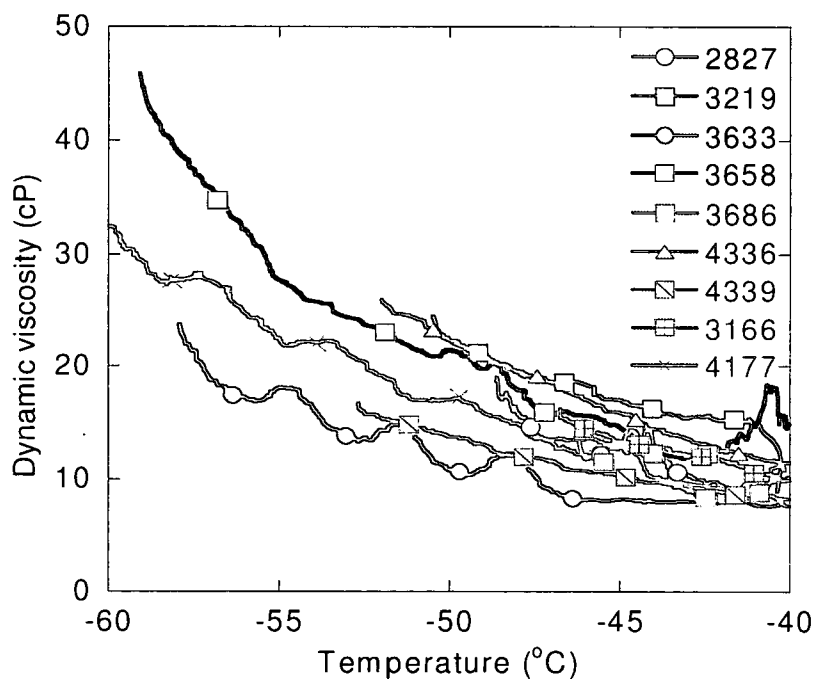


**Figure 15.** Measured liquid-phase viscosities of nine jet fuel samples.

It is interesting to consider why lower freeze point fuels have higher viscosities near their freeze point than do high freeze point fuels. One possible explanation relates to the ideality of the jet fuel mixture in the liquid phase versus the solid phase. It is known, in the temperature region in which crystallization begins, that the incipient solid crystals consist of highly non-ideal solid solutions of the larger normal alkanes (such as  $C_{16}$ - $C_{19}$ ) present in the fuel.<sup>14</sup> These large normal alkanes make up only a small fraction of the total normal alkane concentration. In contrast, the remaining liquid fuel displays mixture properties that are very close to ideal. Thus, the crystallization of normal alkanes from the fuel, and therefore the freeze point, is highly dependent on the concentration and identity of these species. The liquid mixture should display ideal mixture viscosity behavior, with the resulting viscosity being a function of the bulk of the species present. Numerous

components within jet fuel contribute to the overall viscosity of the fuel mixture, and the contribution of each species also depends upon its concentration within the fuel.<sup>15</sup> The freeze point is more dependent on the distribution of the largest normal alkane species.<sup>15</sup> Thus the viscosity is a function of the overall distribution of contributing species within the fuel, while the freeze point is more dependent on the distribution of the largest normal alkane species. Therefore, if two fuels differ only in the concentration of the larger normal alkanes, the one with the higher level of large normal alkanes will exhibit a higher temperature freeze point (Table 2). Since the distribution of the remaining species remains the same, these fuels should have similar viscosities. However, the lower freeze point fuel will crystallize at lower temperatures, where the liquid viscosity will be higher than that of the higher freeze point fuel at its freeze point. Thus, the observation that lower freeze point fuels display higher viscosities near their freeze points likely results from the fact that the viscosity is mostly a function of the bulk species present, while freeze point is more sensitive to the concentration of the larger normal alkanes present.

Figure 15 shows that fuel samples that meet a particular fuel specification can have very different viscosities at the same temperature. Thus, it is important to understand how changes in viscosity can influence the flow and temperature within a cooled fuel tank. The simulation methodology employs a three-dimensional grid for the present calculations. The dynamic viscosity used in the calculation was increased by either 30% ( $1.3\mu_0$ ) or 200% ( $3\mu_0$ ) above that of the measured baseline fuel ( $\mu_0$ ) as shown in Figure 16. These relatively large changes in viscosity are studied because large changes in viscosity do occur upon cooling jet fuels, as shown in Figure 15. Figure 17 shows the calculated temperature contours obtained after four hours of cooling using each



of the three viscosity vs. temperature curves from Figure 16. The temperature contours represent a two-dimensional viewing plane near the center of a tank compartment. The figures indicate that there is increased mixing and fluid motion when the fuel viscosity is low. The figures also show that less convective motion and an increase in temperature throughout the tank can be observed when the viscosity is increased. The result is an increase in fuel stratification with increasing viscosity. The calculation predicts the temperature at the center of a tank compartment to be  $-13.7^{\circ}\text{C}$  for  $\mu_0$ ,  $-11.2^{\circ}\text{C}$  for  $1.3\mu_0$ , and  $-4^{\circ}\text{C}$  for  $3\mu_0$ , after four hours. Thus, a 30% viscosity increase has little effect on the bulk fuel temperature, while a 200% increase can alter fuel temperatures by  $10^{\circ}\text{C}$ . These calculations show that it is important to know the range of typical fuel viscosities as a function of temperature that are encountered during aircraft operation and use these typical viscosity ranges when locating tank temperature sensors and evaluating fuel tank designs.

Three-dimensional calculations were also performed to understand the effect of change in viscosity on the temperature profile in the simulator tank using the measured temperature-dependent viscosities of two Jet A fuel samples. As shown earlier in Figure 15, viscosities of nine different jet fuel samples were measured at temperatures below  $-40^{\circ}\text{C}$ . Among these samples, fuels 3219 and 3633 exhibit a maximum viscosity difference (15 cP) between each other. Therefore, viscosities of these two samples were used in the calculations. Figure 18 shows a plot of height vs. temperature after four hours. The plot shows that near the bottom surface, lowest fuel temperatures can be observed. The fuel temperature increases as the tank height increases upto 0.075 m above the bottom surface. Above that, the temperature is nearly constant for rest of the tank till it

approaches the top surface. The temperature starts to decrease at approximately 0.075 m below the top surface. The plot also shows that the profile remains the same for both the fuel samples - 3219 and 3633. The identical profiles of the results from these two fuels indicate that a viscosity difference up to 15 cP does not significantly affect the temperature profile in the tank.

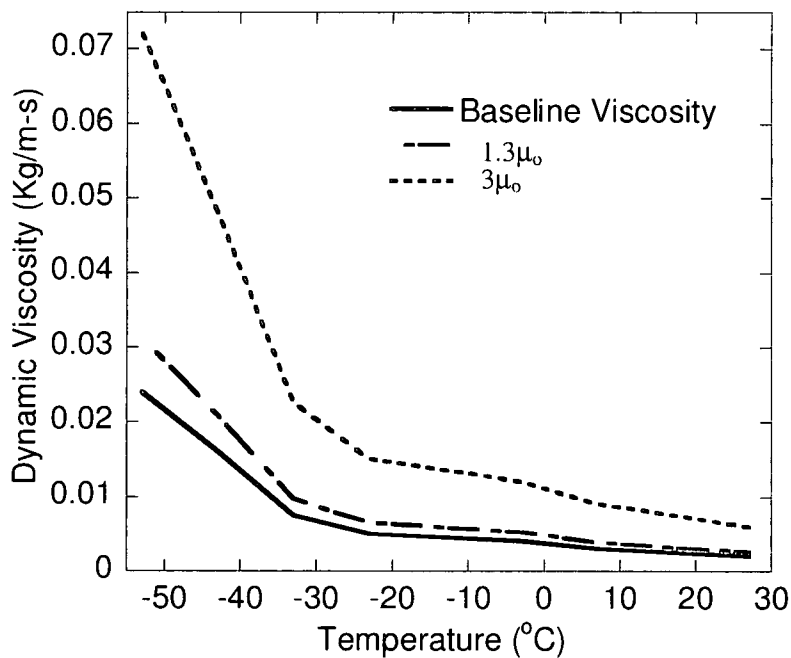


**Figure 16.** Plot for increase in dynamic viscosity by either 30% ( $1.3\mu_0$ ) or 200% ( $3\mu_0$ ) relative to the baseline density ( $\mu_0$ ).

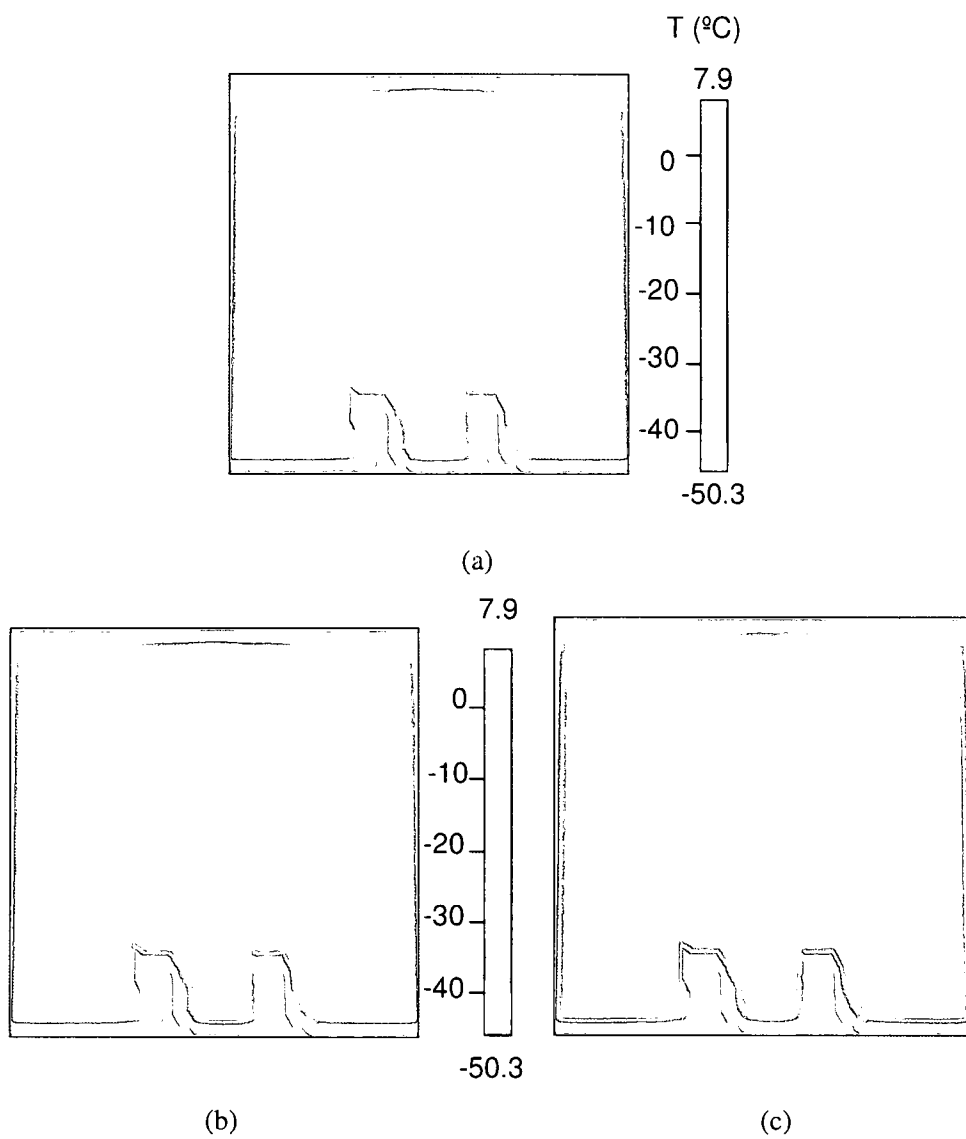


**Figure 17.** Three-dimensional time-varying simulations of the fuel temperature after 4 hours of cooling for (a) viscosity =  $\mu_0$ , (b) viscosity =  $1.3 \mu_0$ , and (c) viscosity =  $3 \mu_0$ .

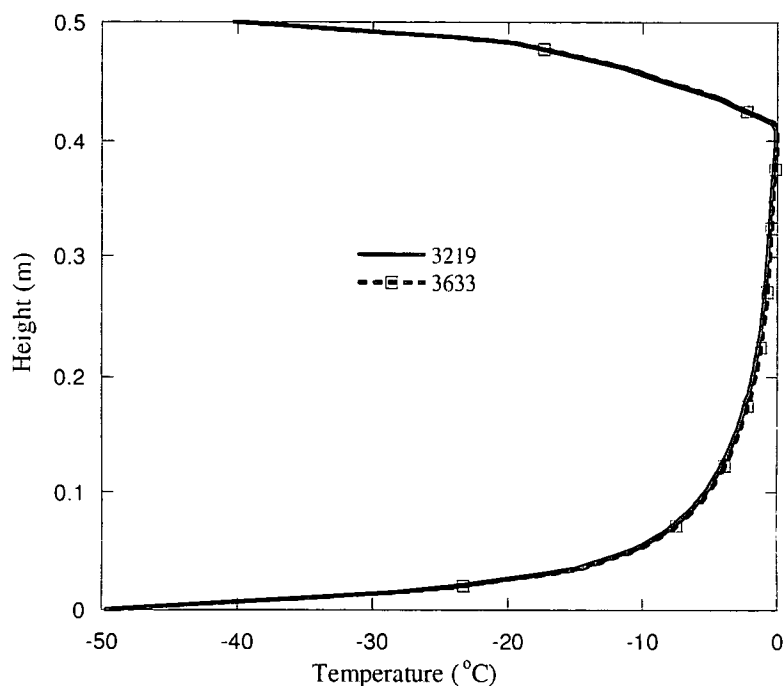


**Figure 18.** Vertical temperature profile near the center of a tank compartment after four hours of cooling for two different jet fuels.

#### **2.4.7 Role of density in heat transfer and flowability**

One of the important jet fuel properties is density. It was observed that large density variations may affect the fuel temperature distribution inside the fuel tank. Therefore, it was of interest to study how variations in fuel density change the resulting temperature distribution in the FAA tank given otherwise identical conditions. According to specifications (ASTM D1298), density of the jet fuel can vary by not more than  $\pm 5\%$  ( $775 \text{ kg/m}^3$  to  $840 \text{ kg/m}^3$ ) at  $15^\circ\text{C}$ . In performing three-dimensional CFD simulations, the density was varied by  $\pm 5\%$  from the baseline fuel density, as shown in Figure 19. The skin temperature follows the schedule of Figure 3. The temperature contours (not shown here) are nearly identical in both cases with the lower density fuel having a slightly lower average bulk temperature of  $-14.9^\circ\text{C}$  as compared to  $-13.6^\circ\text{C}$  for the higher density fuel

(calculated along the tank vertical centerline). It is not surprising that these relatively small changes in density result in little change in the simulated tank temperatures. Figure 20 shows a plot of temperature as a function of distance above the lower surface after 4 hours of cooling at the center of the tank. The figure shows a similar profile as observed in Figure 18 above. The lowest temperature observed is near the bottom surface. For all the three cases, the temperature increases as the tank height increases, up to 0.075 m. The temperature remains constant for the remaining height of the tank and then again starts to decrease as the top wall approaches. The temperature profile is similar for all 3 cases with small differences in temperature (about 1 to 2°C) near the center of the tank.

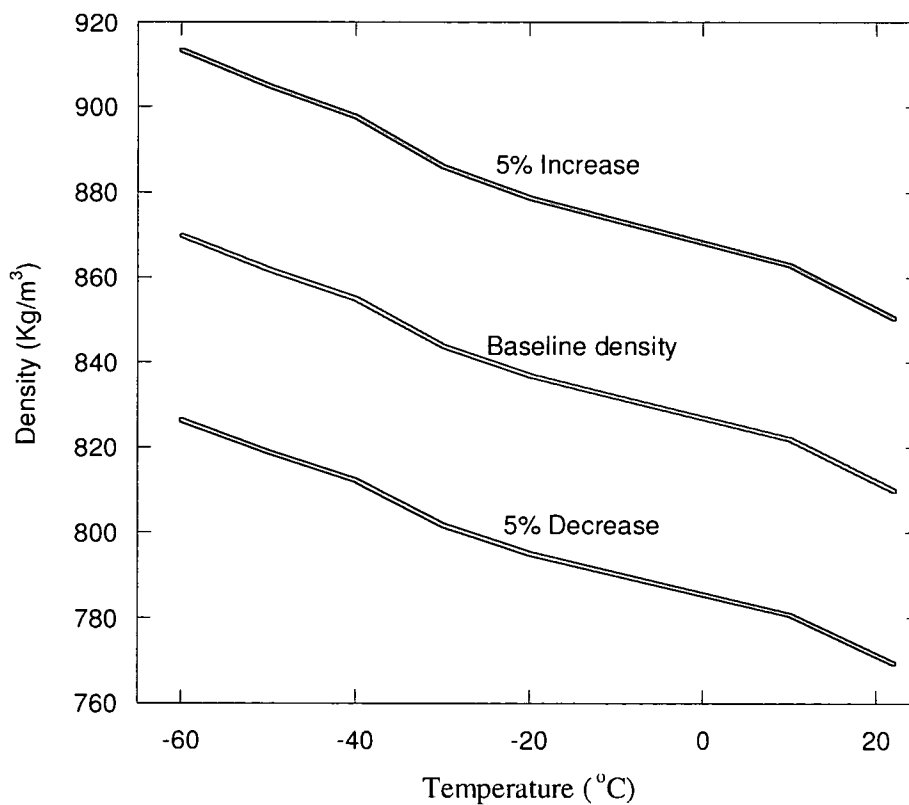


**Figure 19.** Density vs. Temperature for changes in density by  $\pm 5\%$  from the baseline density.

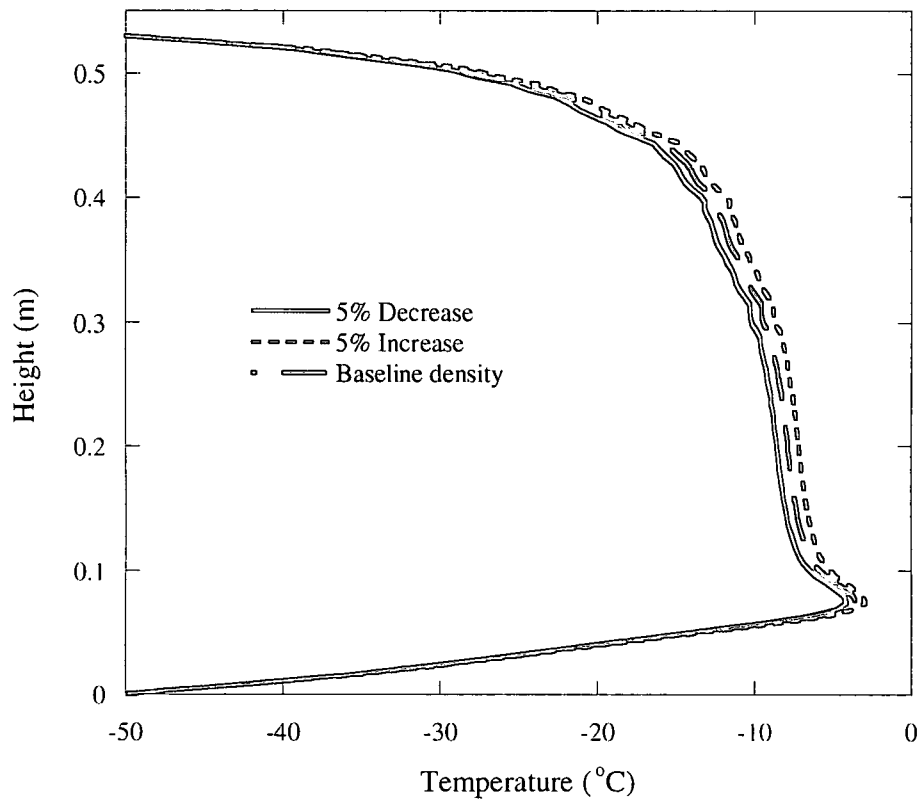


**Figure 20.** Transient temperature profile above lower surface at the vertical centerline after 60 minutes of cooling for a change of  $\pm 5\%$  from the baseline density.

## **CHAPTER 3**

### **Simulations of Jet Fuel Flow in Tank Foam**

#### **3.1 Introduction**

In Chapter 2, it is stated that aircraft fuel tanks during a long duration flight are not completely full near the end of the flight. As fuel is consumed, the volume (ullage space) above the remaining fuel is occupied by mixture of fuel vapor and air. The presence of air and fuel vapor is an explosion risk.<sup>1</sup> Therefore, various military aircraft are made safe by filling the fuel tanks entirely with explosion suppressant foam (ESF) (MIL-B-83054B). The foam prevents fuel explosions caused by gunfire, electrical ignition, lightning strikes and static discharge. Aircraft also experience low temperatures at high altitudes and polar routes, which results into higher fuel viscosity and hence, reduced fluidity. The foam may also potentially act as a flow restrictor and thermal insulator, and these characteristics are particularly important at low temperatures. Therefore, it is desirable to study the effect of the foam on the flow and heat transfer of the fuel and air in the fuel tank at low temperatures.

Flow and thermal fuel tank studies have been both experimental and numerical. Past experimental work by Boeing and Lockheed focused on the low temperature behavior of jet fuel in wing tank simulators.<sup>5,6</sup> These studies concentrated on temperatures significantly below the fuel freeze point to understand the solidification and melting of the jet fuel. They did not study the effect of ullage space on the temperature distribution

or the effect of the presence of foam on the flow and thermal performance. In recent experimental work (described in Chapter 2), the flow and heat transfer behavior of jet fuel in an aircraft fuel tank simulator were studied.<sup>16</sup> Although this work considered the effects of different ullage volumes on the temperature and flow behavior, the effects of foam were not considered. In addition, the flow was buoyancy-driven and did not involve the draining of the fuel tank simulator as done here. Moreover, the focus was on commercial aircraft and therefore, the fuel used was Jet A. The study of aircraft fuel tanks that include foam has been limited due to experimental and computational challenges.

Computational Fluid Dynamics (CFD) methods can be used to simulate the presence of foam in a fuel tank. Porosity and permeability are two characteristics that define a porous medium like foam. Porosity represents the presence of numerous cavities within the foam, while permeability is defined as the rate at which liquid or gas can penetrate into or through a foam material. Numerous researchers have studied multiphase flow and heat transfer within porous media.<sup>17</sup> Much research has been published with materials like sand or clay as porous media and water and air as the two-phase flow components, but there is very limited research in which polyurethane foam and jet fuel are used. Jet fuel is a complex hydrocarbon mixture and jet fuel properties are not readily available at low temperatures. Also, jet fuel properties vary significantly with the fuel sample. These challenges make the numerical simulations of jet fuel more difficult. Moreover, numerical simulations of jet fuel and polyurethane foam in the aircraft fuel tanks have not been explored thus far. In short, no published work has been found that



investigates the influence of polyurethane foam on the flow and heat transfer in an aircraft fuel tank.

Therefore, a simulator is designed and fabricated to represent a section of an aircraft fuel tank. The objective of this work is to experimentally and numerically simulate the effects of polyurethane foam in an aircraft fuel tank simulator. Experiments are performed where the simulator tank is drained under different thermal conditions. Fuel temperatures at various locations inside the fuel tank are measured. The flow rate of the fuel draining from the simulator tank is also measured. Aircraft experience low temperatures at high altitudes and therefore the simulator is subjected to chilling under controlled conditions and is used to verify predictions obtained from CFD calculations. Computations are used to advance the understanding of the influence of the polyurethane foam on the heat transfer and flow distribution in the draining fuel tank. CFD simulations are used to predict the two-dimensional transient fuel temperature distribution and fuel motion. In addition, temperature-dependent properties of JP-8 (F4751) are measured and are used in the current simulations.

## **3.2 Experimental**

### **3.2.1 Wing tank simulator**

The first explosive suppressant foam was placed in the fuel tanks of Lockheed Martin's C-130J aircraft in mid 1960s. Since then, most of the military aircraft have been made safer by the use of polyurethane foam. In order to better understand the effect of foam on temperature and flow distribution in an aircraft fuel system, a wing tank simulator was fabricated (described in Chapter 2). Coarse polyurethane foam is fitted in

the entire tank according to military specifications (MIL-PRF-87260A). The top of the tank is closed with a plexiglass plate. The tank is contained within an environmental chamber (Tenney Environmental, Model T64C15SPL), which can provide a minimum temperature of  $-73^{\circ}\text{C}$ . The simulator is designed so that the fuel can be gravity drained, pumped out via a boost pump, or recirculated via a boost pump back to the tank through a piccolo return tube. For all the experiments in this study, the fuel was gravity drained from the simulator tank to a collection tank located outside the environmental chamber. For safety concerns, the environmental chamber is purged with nitrogen, and nitrogen resides in the fuel tank ullage space. The pressure within the fuel tank is maintained at normal atmospheric pressure.

The wing tank simulator was instrumented with a series of 48 thermocouples, a flow meter, and pressure gauges. Vertical temperature profiles were obtained at three locations in the tank. A post was located near the center of each of the two internal chambers (created by the single baffle rib) for the mounting of thermocouples. A third post was installed near a side wall to obtain boundary temperatures. Thermocouples were also mounted internally on the side walls and the inside bottom surface of the tank. A flow meter was located near the outlet to measure the flow rate of the fuel draining out of the tank. The collection tank was positioned on a measuring scale and measured the total mass of the fuel drained out of the simulator tank. Thermocouple, flow, mass and pressure measurements were obtained at one minute intervals during draining and cool down from initial conditions.

The experiments presented here can be classified into two categories: with foam and without foam. While most of the results presented in this paper are with the presence

of foam, a few experiments were performed without foam to study the difference in heat transfer and flow behavior. All the experiments were either cool down tests or isothermal (static temperature) tests. In the cool down tests, the fuel was cooled from ambient room temperature down to a given target temperature while monitoring the fuel draining rate. In isothermal tests, the chamber was cooled down (typically overnight) to a desired temperature, and then held constant while the fuel drained out. The fuel draining typically lasted from one to two hours.

### **3.2.2 Measured fuel properties**

One of the objectives of this study is to use temperature dependent jet fuel properties in the numerical simulations. The accuracy of calculations depends on accurate values of transport properties. The properties of jet fuel vary with the refinery source. Thus, different samples of JP-8 may exhibit differences in density, viscosity, thermal conductivity, and specific heat. In a previous study, the thermal properties of JP-8 fuel sample F3804 were measured.<sup>18</sup> But, the JP-8 fuel sample which is used in the experiments here is F4751. Using properties of other JP-8 fuel sample like F3804 might not be appropriate and may result in inaccurate computational results. Hence, it is important to measure the properties of fuel sample F4751. Moreover, the properties of JP-8 (F4751) are unavailable for temperatures below -40°C. Although the experiments and simulations in this work do not include temperatures below -40°C, it is still beneficial to present low temperature properties here, for any future studies, which might incorporate fuel temperatures below -40°C.

One of the important transport properties of jet fuels is viscosity. Figure 21 shows the measured viscosity of fuel samples of F4751. As mentioned earlier, F4751 may exhibit significantly different viscosity when compared with other JP-8 fuel samples. Hence, it is compared with the measured viscosity of another JP-8 fuel sample (F3804), obtained from a previous study.<sup>18</sup> As seen in Figure 21, the two fuel samples (F4751 and F3804) show significant variation in the viscosity at lower temperatures. For example, at -48°C, F4751 has a viscosity of 12.2 cP, whereas F3804 shows a viscosity of 9.6 cP (approximately 27% lower than F4751). However, Figure 16 in Chapter 2 showed that a viscosity variation of 30% does not affect the temperature distribution significantly. But, in that case, the flow was buoyancy driven and foam was not present. Here, the fuel is draining and the tank is filled with polyurethane foam. These two factors can significantly contribute towards effect of viscosity variations less than 30%. Therefore, for accurate numerical results, it is important to use the measured viscosities of the individual jet fuel samples that are used in the experiments.

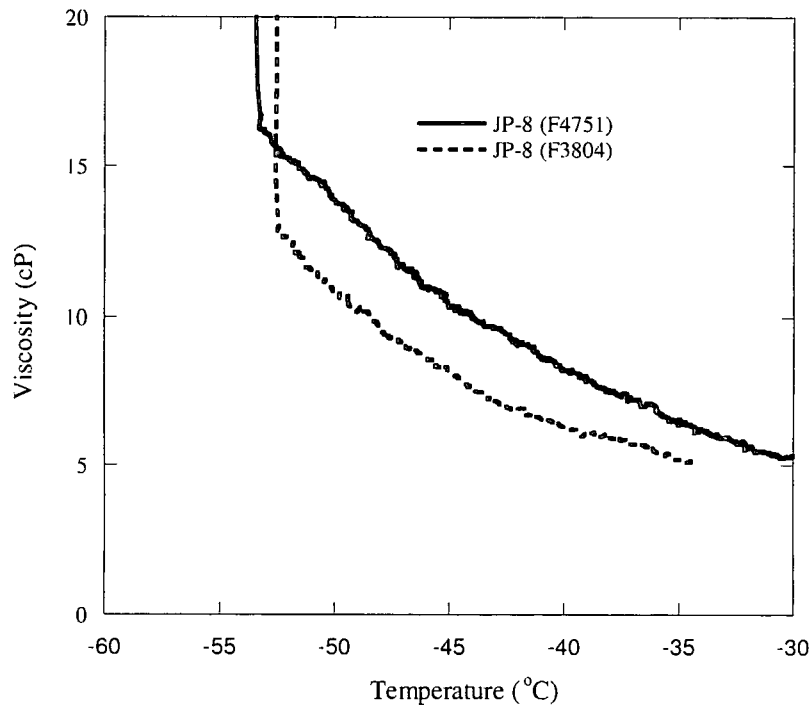


**Figure 21.** Low temperature viscosities of fuel samples of JP-8 (F4751 and F3804).

Other thermal properties of F4751 like density, thermal conductivity and specific heat were also measured (not shown here). It was observed that these properties do not vary significantly between different fuel samples of JP-8. For example, the measured density of F4751 at 20°C is 814 kg/m<sup>3</sup> and the density of F3804 at 20°C is 810 kg/m<sup>3</sup>. This difference of 4 kg/m<sup>3</sup> (0.5%) between the two fuel samples is very small to make any significant effect on the fuel flow or temperature profile. This was also confirmed in Chapter 2 by means of CFD calculations. Similar observations were made for thermal conductivity and specific heat. Moreover, as they vary slowly and linearly in the region below -40°C, values of density, thermal conductivity and specific heat can be linearly extrapolated from higher temperatures.

### 3.3 Numerical

The flow through the polyurethane foam can be numerically represented by treating the foam as a solid matrix with interconnected voids (pores) which allow the flow of one or more fluids through them. Transport through porous media is governed by the conservation equations of mass, momentum, and energy. Mass conservation is given by the equation:<sup>19</sup>

$$\frac{\partial}{\partial t}(\varepsilon \rho) + \nabla \cdot (\varepsilon \rho U) = 0 \quad (2)$$

where  $\varepsilon$  is the porosity of the medium, and represents the ratio of volume occupied by the pores to the total volume of the porous solid. The momentum equation within the porous region may be written as:<sup>19</sup>

$$\frac{\partial}{\partial t}(\varepsilon \rho U) + \nabla \cdot (\varepsilon \rho U U) = -\varepsilon \nabla p + \nabla \cdot (\varepsilon \tau) + \varepsilon B - \frac{\varepsilon^2 \mu}{\kappa} U \quad (3)$$

where,  $\rho$  is the fluid density,  $p$  is the pressure,  $\mu$  is the viscosity of the fluid,  $\tau$  is the shear stress tensor,  $B$  is the body force vector, and  $U$  is the fluid velocity. The permeability,  $\kappa$ , is a quantity representing the surface area to volume ratio of the porous matrix. The flow governed by Equation (3) is also characterized by the non-dimensional parameters – Reynolds number (Re) and Darcy number (Da).

$$\text{Re} = \frac{LU}{\mu} \quad \text{Da} = \frac{\kappa}{L^2} \quad (4)$$

For a given medium, the ratio between the linear and non-linear drag can be approximately expressed as  $\sqrt{\text{Da} \cdot \text{Re}}$ . Therefore, for the cases in which the Reynolds number or Darcy number is small, the non-linear drag can be neglected. In a region of only the fluid,  $\varepsilon \rightarrow 1$  and  $\kappa \rightarrow \infty$ , and the standard Navier-Stokes equation is recovered.

The energy equation within the porous region may be written as:

$$\frac{\partial}{\partial t}(\varepsilon \rho h) + \nabla \cdot (\varepsilon \rho U h) = \nabla \cdot q + \varepsilon \tau \cdot \nabla U + \varepsilon \frac{dp}{dt} \quad (5)$$

where,  $h$  is the enthalpy of the fluid and  $q$  is the Fourier heat flux, which depends, mostly on the effective thermal conductivity of the porous medium. The effective thermal conductivity,  $k$ , of the porous medium is the volume average of the thermal conductivities of the pores and solid regions, and can be written as:

$$k = \varepsilon k_f + (1 - \varepsilon) k_s \quad (6)$$

where,  $k_s$  and  $k_f$  are the thermal conductivities of the solid (matrix) and fluid regions (pores), respectively.

In addition to the presence of the foam, our study must also include an approach to represent the presence of ullage space as the fuel drains from the simulator tank. The volume-of-fluid (VOF) method is a frequently used method, which is used to treat the presence of the interface between the liquid and air (free surface).<sup>11, 12</sup> With the VOF

method, the distribution of the liquid fuel is represented by the scalar,  $F$ , which specifies the fraction of the volume of each computational cell occupied by liquid fuel.  $F$  is 1 in cells that contain only fuel and 0 in cells having only air. Thus, a cell containing the interface has a value of  $F$  between 0 and 1.  $F$  is found by solving:

$$\frac{\partial F}{\partial t} + \nabla \cdot (\vec{u}F) = 0 \quad (7)$$

where,  $F$  is the liquid volume fraction,  $t$  is time and  $u$  is the velocity vector. Equation (7) must be solved together with the above-mentioned equations of conservation of momentum and energy. Here, the bulk behavior of the two fluids (air and fuel) is of interest rather than details of the interface shape and, thus, surface tension was not used in the calculations. Using the VOF model with the porous media can be a challenge due to the presence of foam (represented by a drag term) in addition to the liquid fuel and air. However, it also depends on the porosity of the medium. Here, polyurethane foam is highly porous ( $\epsilon = 0.97$ ), which is very close to the porosity value of 1. As already mentioned above, as the porosity approaches unity, the standard Navier-stokes equation can be used. Therefore, it is appropriate to use porous medium along with the VOF model.

A commercially available CFD code (FLUENT) was used to simulate the laminar, time-varying flow and heat transfer by finite volume solution of the unsteady momentum and energy equations. The temporal differencing was represented by a second order Crank-Nicolson scheme, and an upwind spatial differencing scheme was used.

A two-dimensional structured grid (Figure 22) was employed for transient solution of the flow, heat transfer and VOF in the simulator tank. When the global error residuals were reduced below four orders of magnitude from their maximum values, the



solution was considered to be converged. Table 3 shows the grid refinement study conducted to ensure the grid independence of the solution. A course grid was first made with fewer cells and was further refined by increasing the number of grid points until grid independence was achieved. Results from a grid with 1036 cells were found to be grid independent and are described in this work. A grid with less than 1036 cells was not run because of the convergence limitations of the model. Further grid refinement resulted in negligible changes in the solutions.

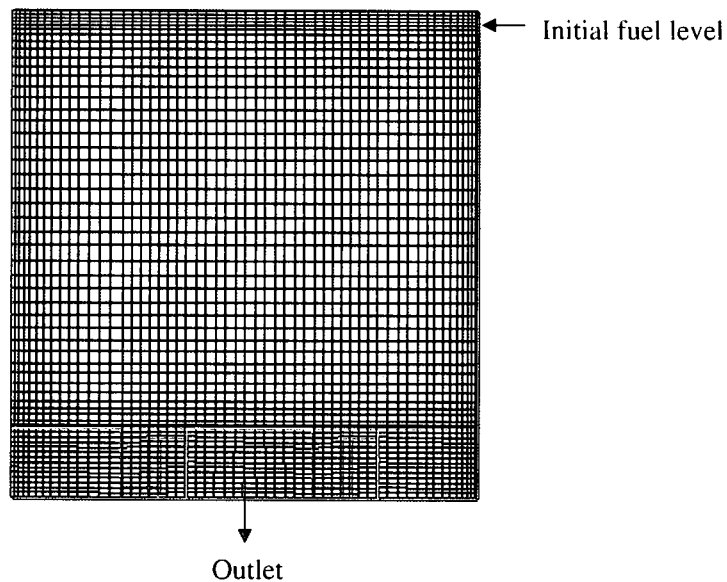


**Figure 22.** Two-dimensional structured grid.

**Table 3.** Grid refinement study

Number of cells	Temperature (°C) Center	% change	Temperature (°C) x=25.5 cm, y=47 cm	% change	Temperature (°C) x=5 cm, y=25.5 cm	% change	Remaining mass of fuel (Kg)	% change
1036	22	-	17.7	-	22	-	168.3	-
2045	22	0	17.2	0.17	22	0	168.3	0
3080	22	0	16.8	0.14	22	0	168.3	0

### 3.4 Results and Discussions

#### 3.4.1 Effect of foam on fuel flowability

To better understand the effect of polyurethane foam on fuel flowability within a fuel tank, experimental measurements and CFD simulations of fuel draining in the wing tank simulator were performed. As already mentioned, fuel tanks are not entirely full near the end of the flight, hence, it is desired to study how the fuel flow inside the tank changes as the fuel level changes. These studies simulate the fuel draining at flow rates changing in time, which occurs in aircraft wing tanks. In the experiments, the fuel was drained by gravity out of the fuel outlet and flow rate was measured with the help of a flow meter. The simulations discussed here follow the draining flow rates as shown in Figure 23. Figure 23 shows that the flow rate is approximately 1.3 gpm when the fuel starts draining and then reduces gradually thereafter for one hour. Moreover, the temperature remains constant (isothermal test) at -37°C.

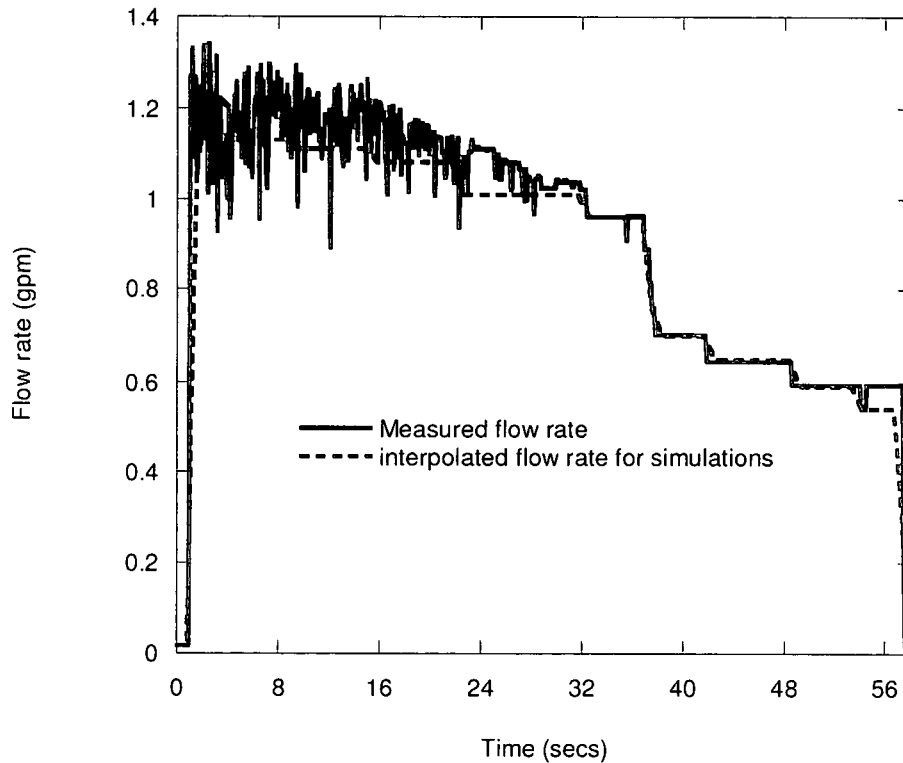


**Figure 23.** Flow rate of the draining fuel with time.

Figure 24 shows the profile of the fuel draining out of the tank with time. The figure shows the results obtained from the simulations performed with and without foam in the simulator tank. Since experiments were performed with foam in the simulator tank, simulations are compared with the experiments. In the experiments, the collection tank was positioned on a measuring scale and measured the mass of the fuel draining out of the simulator tank. The figure shows that the simulations agree well with the measurements. Although the experiments were not performed without foam, the simulations were still performed to compare the results with those obtained with the presence of foam. Figure 24 shows that the mass of the fuel draining out does not vary

much ( $< 3$  Kg) when the foam is removed relative to when the foam is present in the tank. This indicates that the presence of foam does not affect the fuel flow inside the tank for the temperature studied here.

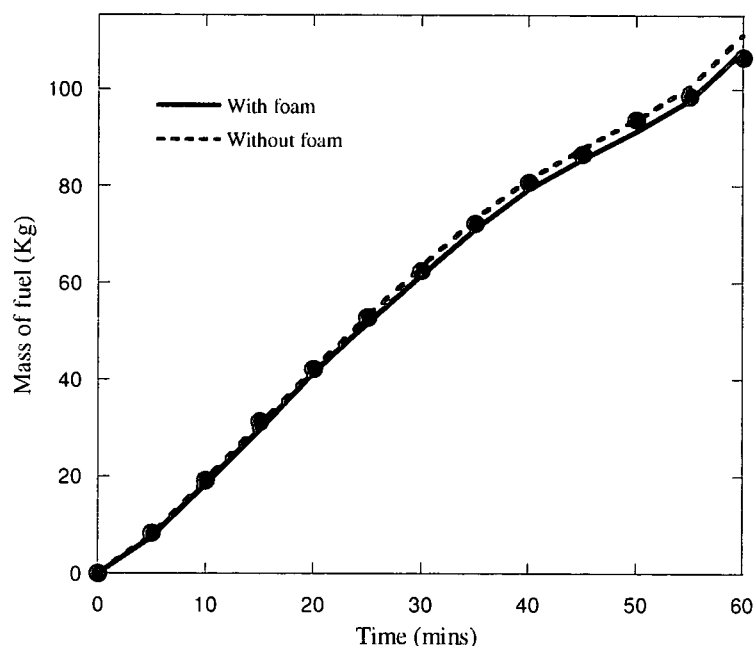


**Figure 24.** Comparison of predictions with the measured mass of fuel drained out from the fuel tank in one hour. The symbols represent measured mass of fuel with foam.

### 3.4.2 Effect of foam on heat transfer in the fuel tank

In the above section, isothermal tests were discussed where the fuel temperature does not change as the fuel drains out of the fuel tank. However, aircraft at high altitudes experience extremely low temperatures, which may affect the fuel temperature distribution inside the fuel tank. It is important to know the temperature distribution inside the fuel tank in order to predict the suitable locations for the temperature sensors. In previous works, it was observed that fuel temperature distribution inside the fuel tank

changes significantly at low temperatures.<sup>5,6</sup> Nevertheless, these studies did not consider dynamic cooling and also did not have foam placed in the simulator tank. Therefore, in the present section, the focus is on dynamic cooling of the simulator tank with polyurethane foam. The wall temperature schedule as obtained from the cool-down experiments is shown in the Figure 25. The temperatures decrease from 22°C to -1.4°C for the horizontal walls and to -17.6°C for the vertical walls in 90 minutes. The draining of the simulator tank follows the flow rate schedule of Figure 23.

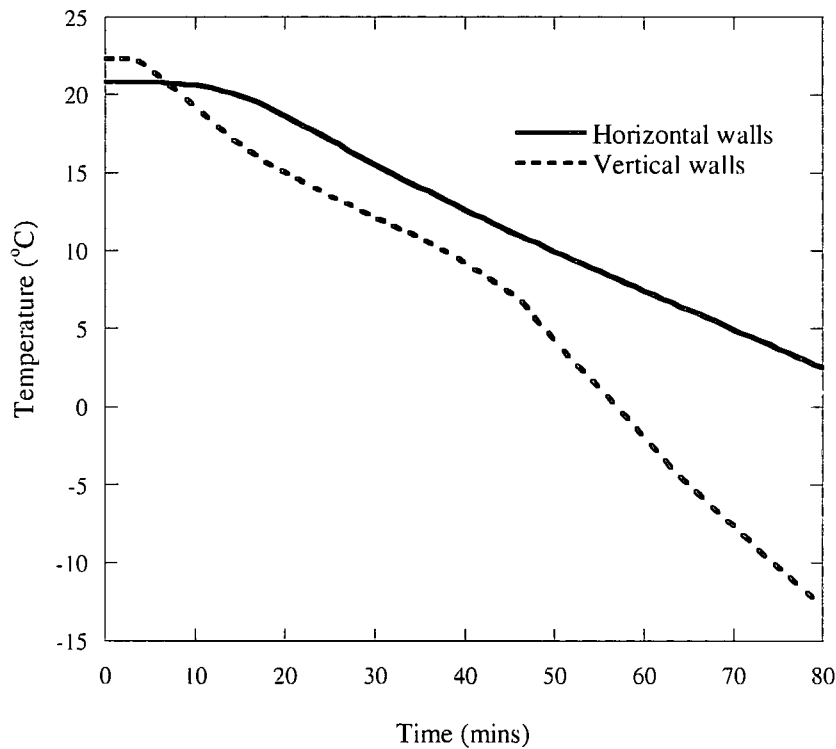


**Figure 25.** Wall temperature schedule for the cooling tests.

Figure 26 shows that the calculations agree reasonably well (within 3°C) with the temperature measurements at two different thermocouple locations. For both the locations, the fuel temperature decreases in time. As expected, Figure 26 shows that for the location near the vertical wall, the fuel temperature follows the schedule of the vertical wall temperature as shown earlier in Figure 25. However, the other thermocouple which represents a location near the tank center does not necessarily follow the wall temperature schedule because the influence of wall temperature is not very strong near the center of the tank. The calculations show that the model can be used successfully to predict the temperature profiles in an aircraft fuel tank. Figure 27(a) shows the temperature contour plot representing 20 minutes of cooling and draining with foam relative to Figure 27(b), which represents the calculations without foam. Figure 27(a) shows that due to the presence of foam, the fuel and air, and in effect the entire tank shows a nearly uniform temperature distribution. The air and fuel regions are not easily distinguishable, while in Figure 27(b), the air and fuel regions can be distinctively observed. Figure 27(b) shows that the tank volume consisting of air cools down faster than the volume that contains jet fuel. Here, it is observed that air acts as an insulation and therefore, the rest of the tank is at a higher temperature. Similar observations were made in earlier research (described in chapter 2) with fuel tanks that have a small ullage space where air acts as an insulating medium and results in an overall higher fuel temperature.<sup>16</sup> However, in both the cases, as expected, the stringers cool down faster than rest of the tank due to conduction.

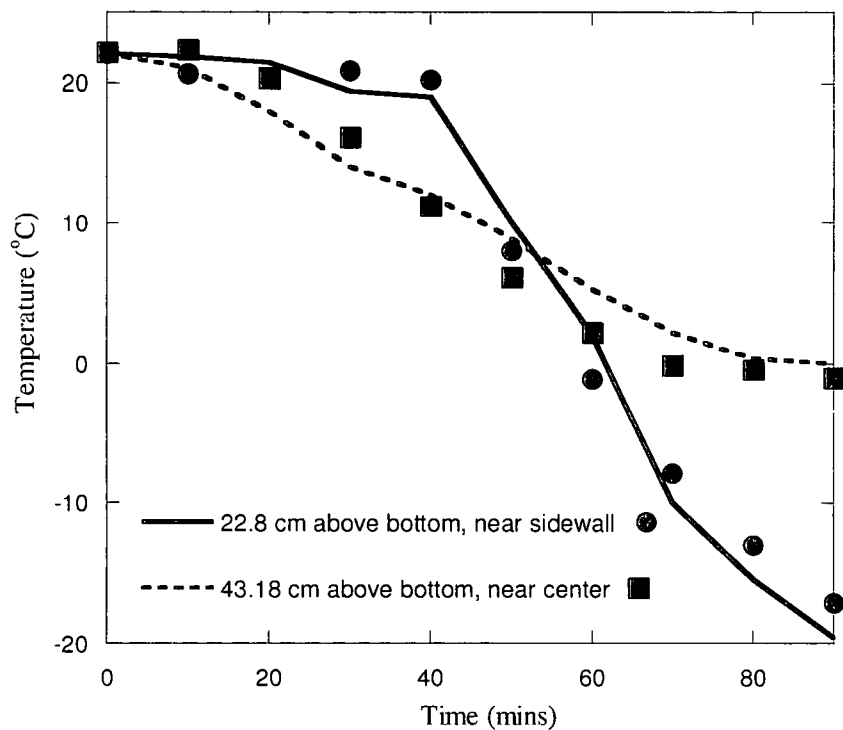


**Figure 26.** Measured and Simulated temperatures in the tank with foam for two different thermocouple locations. The symbols represent measured temperatures.

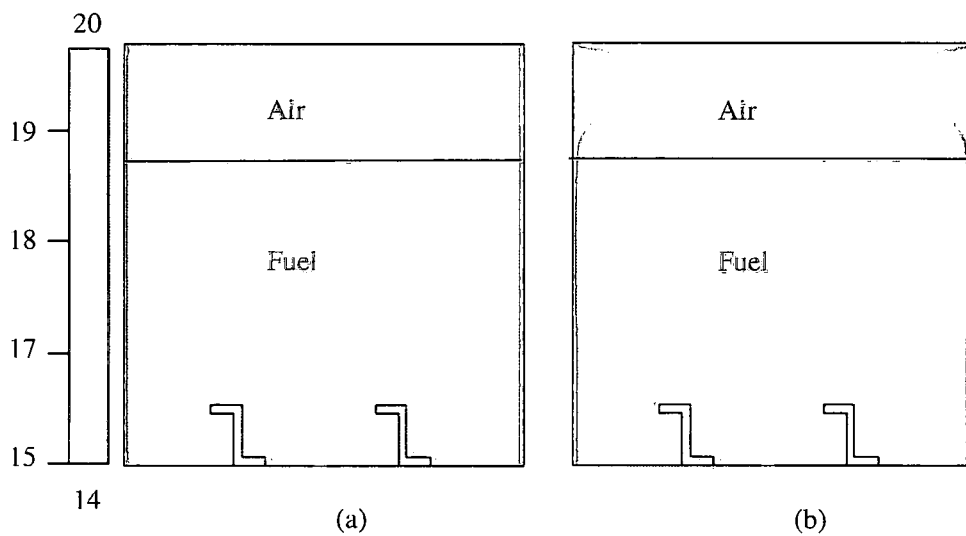


**Figure 27.** Temperature contours for two-dimensional simulations after 20 minutes of cooling and draining (a) with foam and (b) without foam.

Figures 28(a) and (b) show the velocity vector plots demonstrating the development of a complex flow pattern in the heat transfer calculation after 20 minutes. The velocity vectors shown are proportional to the velocity magnitude, which vary over the range 0 to 0.62 cm/s. The velocity vectors in Figure 28(b) are larger than those in Figure 28(a) due to increased convective motion and stratification. Again, this is due to the presence of foam represented by Figure 28(a), which restricts the fuel and air motion.

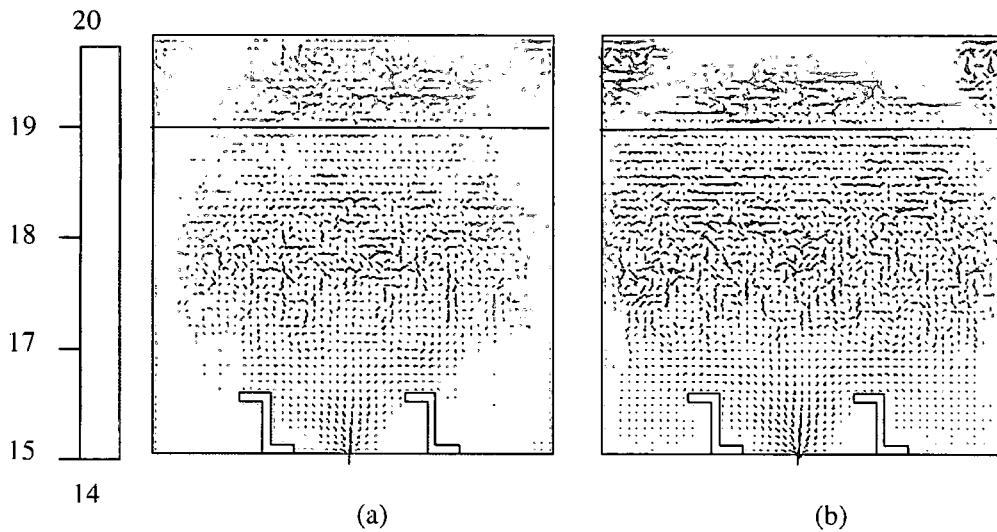


**Figure 28.** Velocity vectors and temperature distribution after 20 minutes of cooling and draining (a) with foam and (b) without foam.

Figure 29 shows the calculated temperature contour plots after 90 minutes of cooling and draining. At this time, the tank is nearly completely drained and most of the volume in the tank is occupied by air. Figure 29(b) represents the calculations without foam, and therefore, shows more stratification of air and a much lower temperature than Figure 29(a). Figure 29(a) shows the calculations with foam and as observed earlier, foam restricts the air motion in the tank and hence, the overall temperature in the tank remains higher. The higher temperature in the tank with foam is also due to the thermal



inertia and thermal conductivity of the foam. These observations imply that the presence of foam does not adversely affect the fuel temperature distribution in the fuel tank for the temperature range studied here. However, there is still need to study the low temperature issues like fuel freezing or restricted fuel flow due to high viscosity which may pose a concern due to the presence of foam in aircraft fuel tanks. Also, the issues concerning the heating of an already cold fuel tank with the presence of foam need to be further explored.

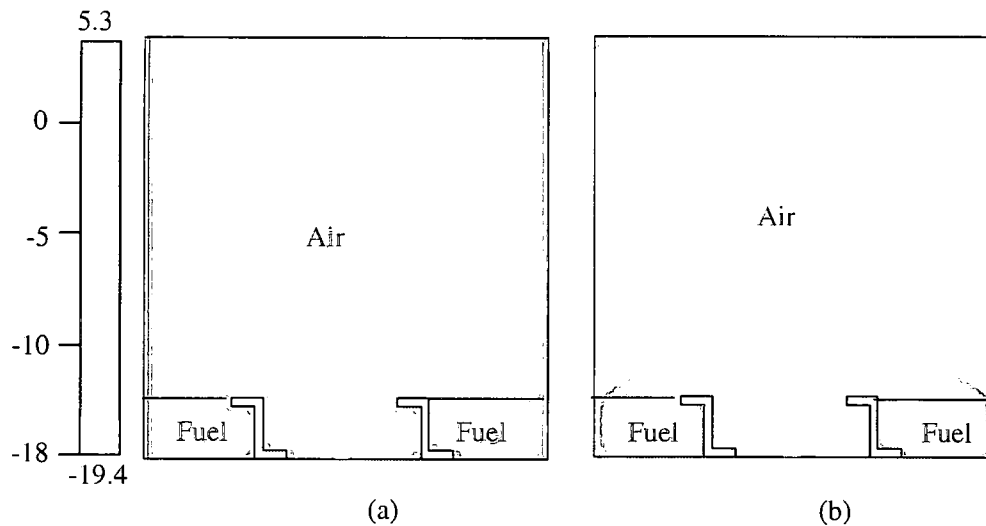
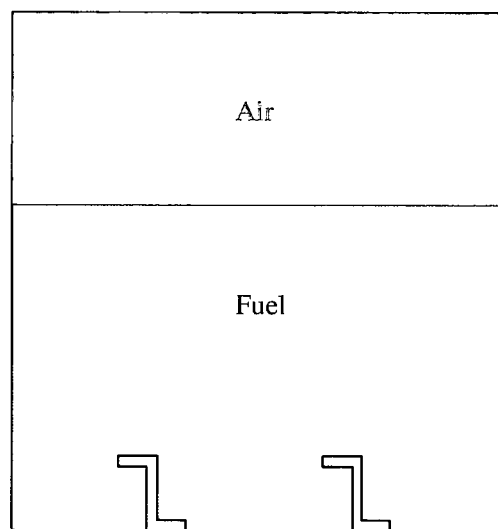


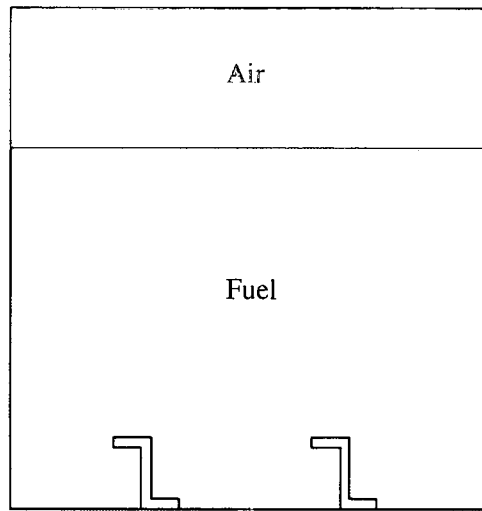
**Figure 29.** Temperature contours for two-dimensional simulations after 90 minutes of cooling and draining (a) with foam and (b) without foam.

All the calculations discussed so far in this chapter have used polyurethane foam (porosity = 0.97) as the porous medium. To study how the porosity may affect the fuel flow in a fuel tank, the porosity of the foam was varied in the numerical simulations. Three different values of porosities are studied here, 0.5, 0.7, and 0.97. Figures 30(a) through (c) show the color contour plots of the simulator tank representing these three

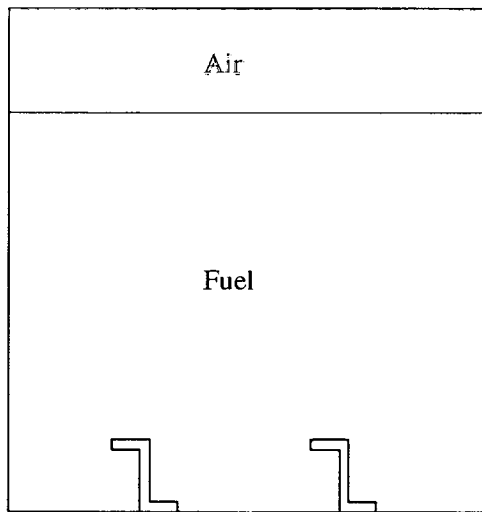
different porosities, respectively after 10 minutes of draining. It can be observed that the porosity is a very important factor in draining of the fuel tank. Figure 30(a) shows that when a porosity of 0.97 is used, the draining is more rapid than when a lower porosity is used. Draining of the tank slows down with a porosity of 0.7 and further reduces when a porosity of 0.5 is used. It can be observed that the mass of fuel drained out with porosity of 0.97 is twice as much as when a porosity of 0.5 is used.



(a)



(b)



(c)

**Figure 30.** Two-dimensional calculated contour plots showing fuel and air in the simulator tank after 10 minutes and foam with porosity of (a) 0.97 (b) 0.7 and (c) 0.5.

## CHAPTER 4

### Studies of Jet Fuel Freezing in Forced Flow

#### 4.1 Introduction

In Chapters 2 and 3, the focus was on the temperatures above the freeze point, where the jet fuel is always in liquid state. However, with extended flight duration and the prevalence of cold air masses along polar routes or at high altitudes, the potential exists for fuel freezing. As the fuel temperature decreases, fine wax crystals appear and increase in size and concentration on further cooling. With sufficient crystallization, there is potential for catastrophic fuel system failure due to blocked filters, valves, and other flow passages. Hence, it is desirable to simulate jet fuel freezing by computational fluid dynamics (CFD) in order to study fuel system design and performance at low temperatures.

The simulation of jet fuel freezing by CFD is complicated because jet fuel is a mixture of thousands of different hydrocarbon species. In past work, researchers simulated the solidification of mixtures involving two or three compounds with known phase composition relationships.<sup>20</sup> Although those mixtures are much simpler in composition than jet fuel, there were several challenges in the simulations such as calculating heat transfer during molecular rearrangement due to solidification.<sup>20</sup> The problem of simulating jet fuel flow is more difficult for several reasons such as the lack of published thermo-physical properties at low temperatures.<sup>18</sup> Another complexity in the

simulation of jet fuel flow behavior at low temperatures is that phase composition relationships for jet fuel are unavailable. Moreover, jet fuel forms a liquid-solid matrix during solidification, which is challenging to simulate. Thermodynamic models for solid-liquid phase equilibria for jet fuel are being developed.<sup>4</sup> Although these thermodynamic models have been employed to study the solid-liquid phase behavior of jet fuels, they have not been convenient for the prediction of the flow and heat transfer conditions involving jet fuel solidification.

There have been limited attempts using numerical methods to simulate the freezing of jet fuel. A previous one-dimensional heat transfer analysis of an external wing tank did not predict the heat transfer satisfactorily because the tank height was neglected.<sup>21</sup> Results from that study showed that tank height was important in the heat transfer and flow analysis and that a multi-dimensional analysis was required. An early work involving low temperatures and two-dimensional CFD simulations of the fuel tanks did not use real jet fuel properties.<sup>7,8</sup> A mixture of glycerin and water was used to represent jet fuel. Although the viscosity of the mixture was varied to characterize the effect of freezing, the use of glycerin and water to represent jet fuel is likely not appropriate. Moreover, actual phase change itself was not simulated.

A recent study used two-dimensional CFD calculations to represent the actual solidification of fuel in an optical cell.<sup>18</sup> Real jet fuel properties were used, and the optical cell model involved a simple rectangular geometry. A momentum resistance source term was used to represent the flow resistance caused by crystal structures that were found to exist in liquid-solid regions. In addition, the flow was buoyancy driven due to temperature differences between the vertical cell walls. Although buoyancy driven

flow is dominant in some fuel tanks, forced flow is important in others. The fuel temperature and interaction between the solid particles and liquid are influenced by the flow rate. However, freezing behavior under forced flow has gone unstudied. Thus, it is important to numerically simulate the freezing of jet fuel under forced flow conditions. The enthalpy method has been used to simulate solidification in other work concerning simple mixtures in buoyancy driven flow and is used in the present computations.<sup>22</sup> This method solves the energy equation that governs the heat transfer and phase change. It is also essential to study fuel solidification in a more intricate geometry because aircraft fuel tanks include internal structures (e.g., baffle plates, ribs, stringers) that may affect the overall heat transfer during the solidification process. An objective of the present work is to use a two-dimensional CFD model and temperature dependent fuel properties to simulate the solidification behavior of jet fuel in a forced flow.

In another previous work, the low temperature behavior of jet fuels was studied in experiments where the fuel was chilled slowly for hours to maintain low temperatures within a fuel tank simulator.<sup>5,6</sup> The liquid fuel was discharged from the tank to determine the fraction of fuel hold-up. (The mass of solidified and partially solidified fuel that cannot flow from the tank is referred to as the hold-up.) However, CFD simulations concerning jet fuel solidification under forced flow conditions, which also have experimental validation, are not available. In addition, no published computational work has been found that incorporates jet fuel solidification in a geometry with one or more internal structures. This is due to the complexities of the low-temperature experiments and the involved multiphase transport. Therefore, in the present work, a quartz duct is fabricated to study the effect of low temperatures on fuel flow, solidification and hold-up.

The duct containing flowing fuel was subjected to temperatures below the freeze point of the jet fuel. The second objective of the present work is to use flow visualization and temperature measurements within the quartz duct to develop a better fundamental understanding of the freezing of jet fuel and to validate the numerical simulations.

## **4.2 Experimental**

### **4.2.1 Flow assembly**

The accuracy of the computational results can be evaluated by comparing them with experimental measurements. Therefore, to validate the numerical simulations and to study the behavior of flowing jet fuel at low temperatures, a quartz duct (Figures 31 and 32) was fabricated. The rectangular duct (39.4 cm x 8.9 cm x 8.9 cm) was fabricated from quartz because of its high optical quality and strength. Figure 31 shows an image of the duct that is separated into two compartments by a dividing plate similar to what might be encountered in flow passages within a fuel tank. The dividing plate has two openings available for flow. One opening is circular (2.5 cm diameter) and located at the dividing plate center, while the other is rectangular (3.8 cm x 1.3 cm) at the plate bottom. The jet fuel flows into the duct through an inlet (1.3 cm diameter) located on one of the sidewalls. A deflector near the inlet redirects the inlet flow. In the absence of the deflector, much of the fuel entering through the inlet would essentially pass straightway through the circular opening on the dividing plate. It is presumed that this would result in inadequate mixing of the fuel. In addition, an outlet (1.3 cm diameter) is located at the opposite end of the chamber. Hollow aluminum plates are attached to both top and bottom surfaces. The plates are sealed on both the ends and allowed for threaded pipe

fittings and mountings. By passing cooled methanol through these plates, the horizontal surfaces were cooled to the desired temperatures. Thermally conductive grease was applied to ensure good thermal contact between the quartz duct and plates.

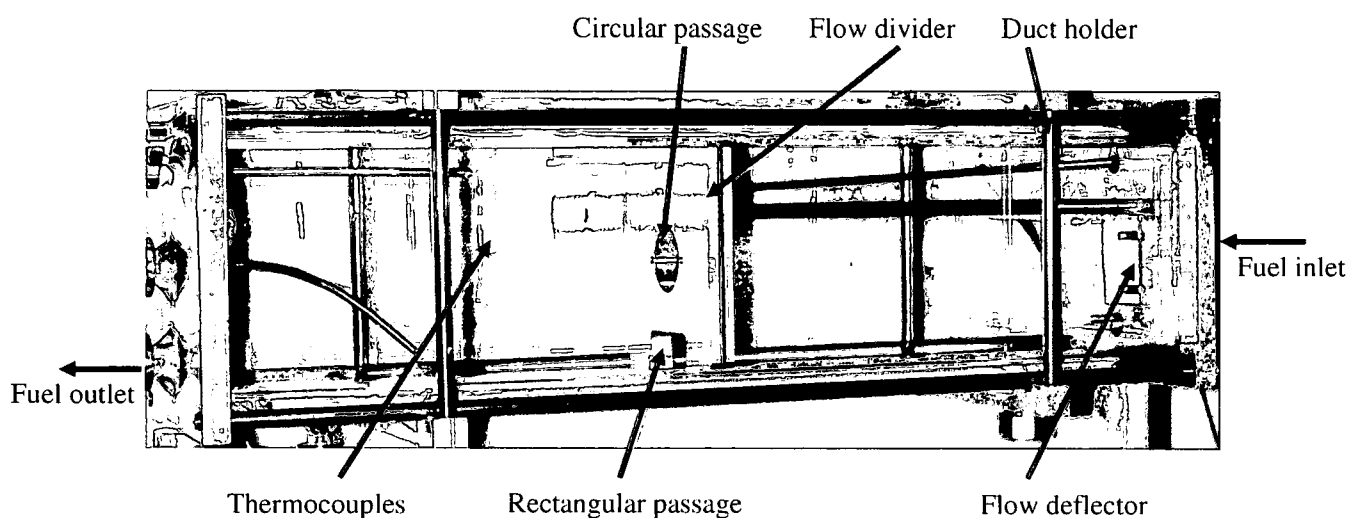


**Figure 31.** Image of the quartz duct.



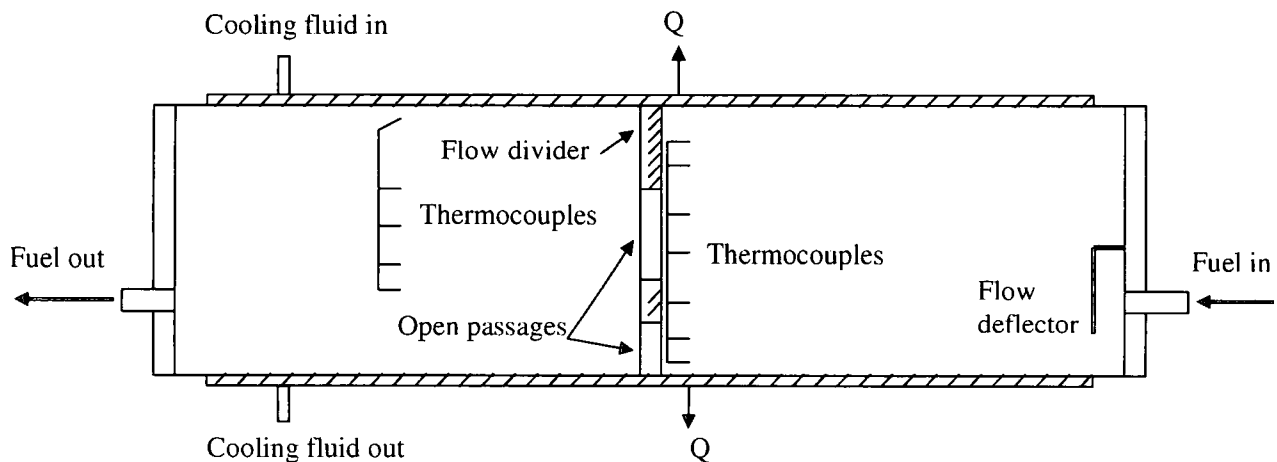


**Figure 32.** Schematic of the quartz duct.

The entire quartz duct was placed in an environmental chamber to simulate the low temperature conditions existing in a high altitude flight. A positive displacement pump forced fuel from an insulated reservoir (5 liter capacity) through the duct. A flow meter installed at the pump outlet monitored the fuel flow rate. A coil-type heat exchanger was used to cool the fuel before entering the duct. Fuel exited the duct through the outlet and passed through insulated tubing back to the reservoir. Two different neat jet fuel samples F3804 (JP-8) and F3775 (JPTS) were used in these experiments. JP-8 is widely used by the United States Air Force, and JPTS is a special purpose jet fuel and is known for high thermal stability and excellent low temperature properties. Here, the alphanumeric designations (F3804 and F3775) refer to particular fuel samples used in the experiments and do not have any other meaning. The characteristics of these fuel samples are described in the subsequent sections.

Calibrated (Type T) thermocouples were located inside the duct. Figure 31 shows a rake of seven thermocouples near the flow divider and another rake of five

thermocouples near the center of the other compartment within the duct. Thus, temperature measurements on both sides of the flow divider were recorded. Thermocouples were installed in the fuel lines entering and exiting the duct, and the temperature of the methanol entering and leaving the chiller plates was also measured. The temperatures of the top and the bottom walls were recorded and later used as the boundary conditions for the CFD calculations. A pressure transducer measured the pressure drop between the inlet and outlet of the duct. All data was recorded using the data acquisition system (Personal DaqView PlusXL Version 1.9) once every minute. Table 4 shows the select experiments that were performed and are discussed later in the results.

**Table 4. Select low temperature freezing experiments**

Experiment No.	Fuel sample ID	Flow rate mL/min	Chamber temperature (C)	Chiller plates temperature (C)
1	JP-8 (3804)	60	-48	-65
2	JPTS (3775)	60	-48	-65
3	JP-8 (3804)	120	-62	-60
4	JPTS (3775)	120	-62	-60

Lighting for the quartz duct consisted of an optical fiber panel that uniformly illuminated the cell. Polarizing filters on the front and back of the duct maximized the contrast between the solid and liquid fuel as cross polarization eliminated light transmittance through the liquid fuel. A high-resolution digital camera (Sony DKC- ST5, 4 Mega-Pixel) equipped with a zoom lens (Sony VCL1205B) was used to capture several images every 30 minutes. These images were used for area measurements of the frozen fuel for purposes of comparison with CFD calculations.

#### 4.2.2 Low temperature properties of jet fuels

To simulate jet fuel solidification, it is also important to study the effect of jet fuel properties and temperature on freezing. Although used for jet fuel specification, the fuel freeze point temperature is not what limits fuel flow to the boost pumps. Pumpability, or flowability, is limited by the fuel viscosity, which in turn, is related to the cloud point and pour point temperatures of the fuel. The cloud point temperature ( $T_h$ ) (ASTM D2500) is known as the temperature at which visible crystals first appear in a cooled fuel. The pour point temperature ( $T_l$ ) (ASTM D97) is defined as the lowest temperature at which the fuel still flows before entering a semi-rigid state. When the fuel is lower than the pour point temperature, it ceases to flow and is unavailable for use. The freeze point, cloud point and the pour point temperatures were measured using a Phase Technology Series 70V Petroleum Analyzer and are listed in Table 5. Although the crystallization dynamics of jet fuels is not well understood, it is known that the solidifying crystals essentially consist of larger normal alkanes. The crystallizing normal alkanes entrap other fuel species that remain in the liquid phase. The normal alkane distributions for two fuel samples, JPTS (F3775) and JP-8 (F3804), were measured by gas chromatography with mass spectroscopy (GC-MS) and are shown in Figure 33.<sup>15</sup> The individual normal alkane constituents in Figure 33 add up to give the total normal alkane mass fraction of 0.274 for JPTS (F3775) and 0.238 for JP-8 (F3804).

**Table 5. Low temperature jet fuel characteristics**

Fuel	Freeze Point (K)	Pour Point (K)	Cloud Point (K)	Heat of fusion, $\Delta H$ (J/kg)	Solid fraction, $f_s$	Effective heat of fusion, $\Delta H_e$ (J/kg)
JPTS (F3775)	218.7	210	214	4410	0.07	63000
JP-8 (F3804)	224.9	215.2	221.2	4968	0.08	62100
Jet A (F3219)	227.2	217.2	222.2	3487	0.06	58117

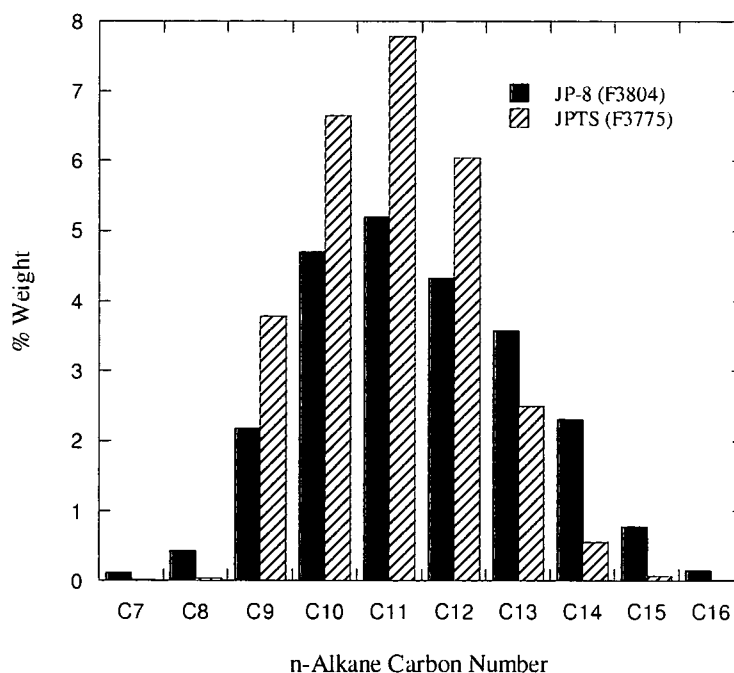


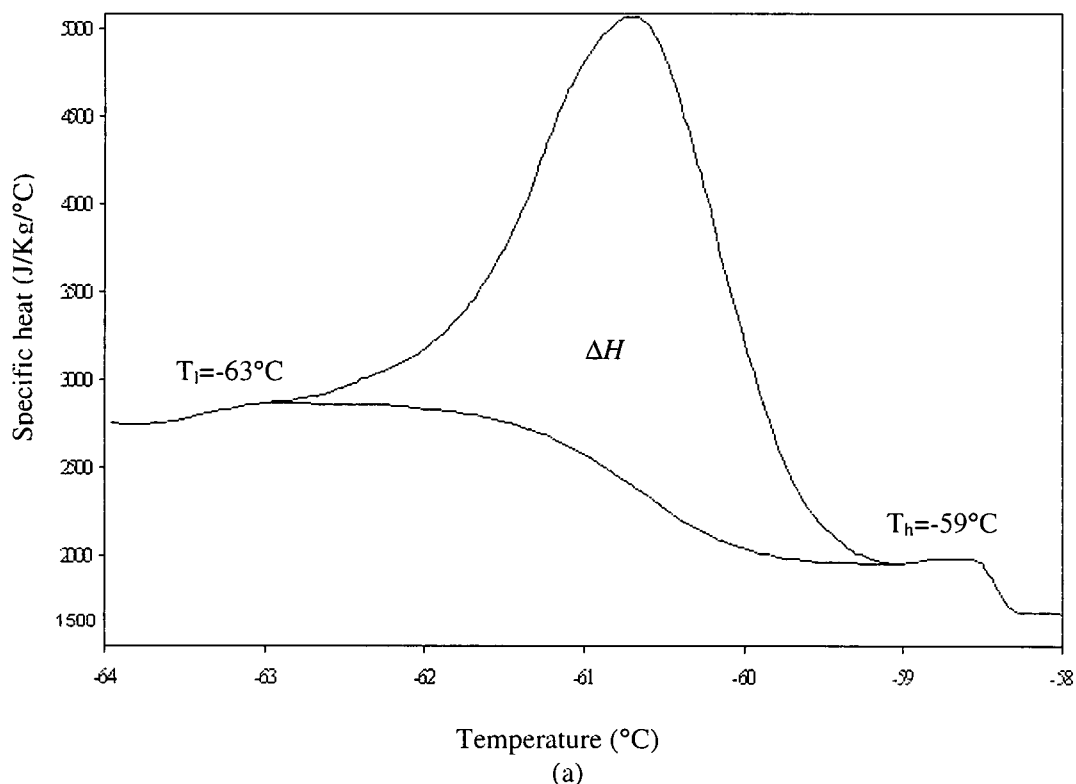
**Figure 33.** Measured normal alkane distributions for JPTS (F3775) and JP-8 (F3804).

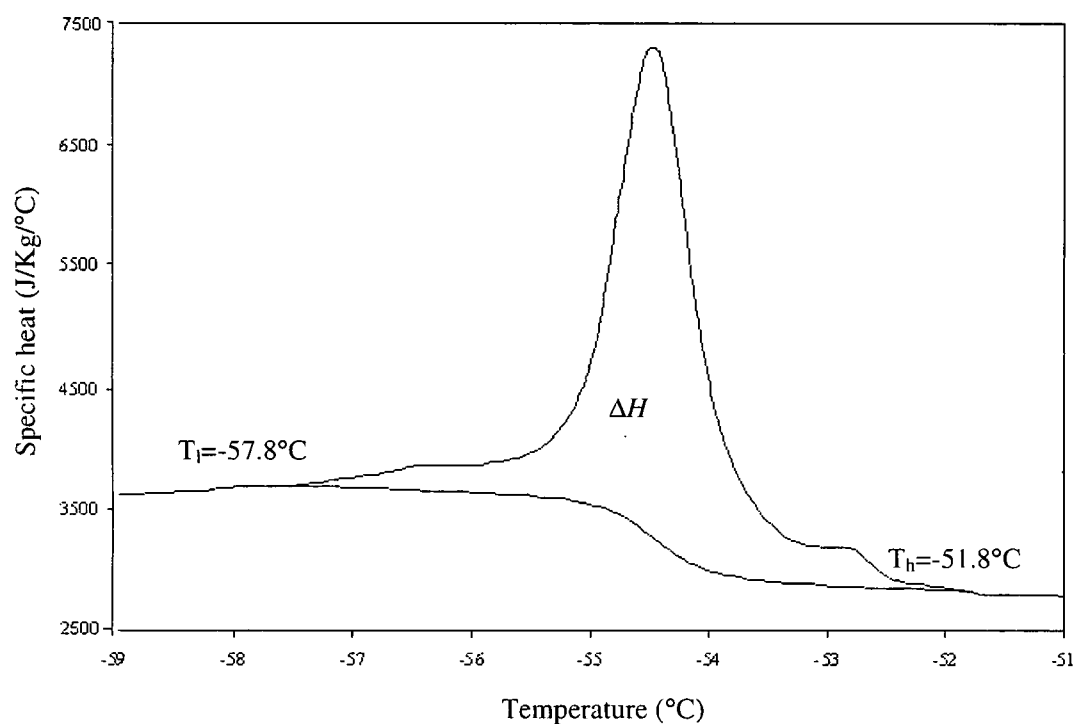
CFD calculations involve the solution of governing equations that require low temperature properties (density, viscosity, thermal conductivity and specific heat) of jet fuels. Low temperature properties of JP-8 (F3804) have been reported in previous work

and are used in the current simulations.<sup>18</sup> However, since the published properties of JPTS (F3775) are not available for temperatures below -40°C, measured values of specific heat and viscosity were obtained in the current work. In addition, temperature dependent values of density and thermal conductivity compiled by the Coordinating Research Council were used in all simulations.<sup>13</sup> Since the density and thermal conductivity vary linearly between 22°C and -40°C, they were linearly extrapolated for temperatures below -40°C. During solidification, large normal alkanes increase in density by only 6% and since normal alkanes represent only a fraction of the total fuel mass, large variations in density are unexpected. Moreover, the extrapolated values of jet fuel thermal conductivity were compared with the thermal conductivities of individual normal alkane constituents. The extrapolated values of thermal conductivity agree well with the thermal conductivity of individual normal alkane constituents at their solidification temperatures.<sup>18</sup> Therefore, it is reasonable to accept the extrapolated values of thermal conductivity for temperatures below -40°C. The specific heat and viscosity were measured as a function of temperature and are described in the following paragraphs.

A differential scanning calorimeter (DSC) (TA instruments, Model 2920, cooling rate 1°C/min) was used to determine the effective specific heat below -40°C for the fuel sample of JPTS (F3775). Figure 34(a) shows the measured specific heat for JPTS (F3775) for temperatures below -58°C. From Figure 34(a), it can be observed that the specific heat varies by less than 5% before solidification begins at  $T_h = -59^\circ\text{C}$ . In contrast, it increases significantly after solidification is initiated. The specific heat is approximately 1700 J/kg·°C at -59°C and increases to 5200 J/kg·°C at -61°C due to continued cooling of the solidifying fuel. After the solidification is complete at -63°C

( $T_i$ ), the specific heat is essentially constant again. Hence, it is reasonable to treat the specific heat as a constant (1700 J/kg·°C) before the onset of freezing and as another constant (2750 J/kg·°C) after the freezing is complete. Figure 34(b) shows the measured specific heat of JP-8 (F3804) for temperatures below -51°C.<sup>18</sup> The overall specific heat behavior of JP-8 is similar to that of JPTS, but the curve for JP-8 lies within a higher temperature range than that of JPTS.





(b)

**Figure 34.** Measured specific heat for fuel samples (a) F3775 (JPTS) and (b) F3804 (JP-8).

Figure 35 shows the measured dynamic viscosity of JPTS between  $-40^{\circ}\text{C}$  and  $-60^{\circ}\text{C}$ , which is  $3^{\circ}\text{C}$  above the pour point,  $T_l = -63^{\circ}\text{C}$  of F3775. For temperatures between  $-60^{\circ}\text{C}$  and  $-63^{\circ}\text{C}$ , the viscosity values were linearly extrapolated for simplicity. Similarly, for JP-8, the viscosity measurements are shown for temperatures in the range between  $-40^{\circ}\text{C}$  and  $-53^{\circ}\text{C}$ , which is approximately  $5^{\circ}\text{C}$  above the  $T_l = -57.8^{\circ}\text{C}$  of F3804.<sup>18</sup> Figure 35 shows that both fuels display a gradual increase in viscosity with decreasing temperatures. As the fuels approach their cloud point temperatures ( $T_h$ ), the viscosity increases rapidly. This sudden increase in viscosity is due to the onset of crystal formation at the cloud point temperature.<sup>15</sup> The rise in viscosity also agrees with the rapid

increase in specific heat at the cloud point temperature and that the jet fuels solidify over a narrow temperature range. The viscosity measurements were calibrated with measurements obtained at  $-40^{\circ}\text{C}$  using a glass capillary viscometer (ASTM D445).<sup>9</sup>

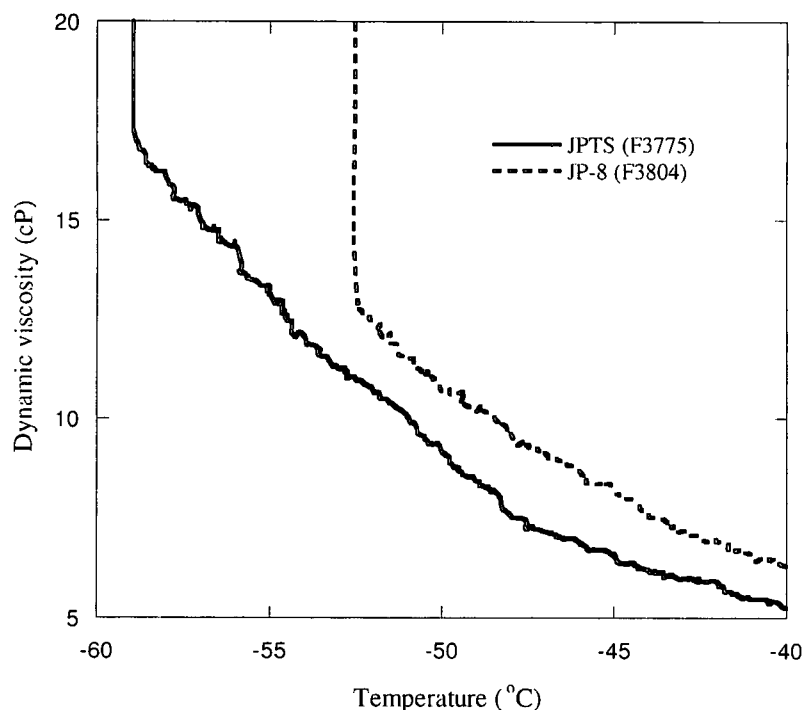


**Figure 35.** Measured dynamic viscosity of JPTS (F3775) and JP-8 (F3804).

### 4.3 Simulation Methodology

Here, the enthalpy method is used to simulate solidification which follows the work of Voller and Prakash, and is outlined below.<sup>22</sup> With the enthalpy method, the solid-liquid mixture is characterized by the solid mass fraction,  $f_s$ . The enthalpy within the solid-liquid region,  $H$ , is expressed as



$$H = h + \Delta H \quad (8)$$

where  $h$  is the sensible heat and  $h - h_0 = \int_{T_0}^T C_p dT$ . Here,  $C_p$  is the specific heat and  $h_0$  is a reference enthalpy. In Equation (8),  $\Delta H$  is the heat of fusion and is written as a function of temperature

$$\Delta H = f(T) = \begin{cases} L & T > T_h \\ L(1 - f_s) & T_h \geq T \geq T_l \\ 0 & T < T_l \end{cases} \quad (9)$$

where,  $T_h$  is the temperature at which the solid formation begins,  $T_l$  is the temperature at which freezing is complete and  $L$  is the heat of fusion in solid-liquid co-existence region (also known as mushy region).

The entire domain is treated as a porous medium, where the porosity,  $\lambda$ , has the following values

$$\lambda = (1 - f_s) = \begin{cases} 0 & \text{Solid} \\ 0 < \lambda < 1 & \text{Solid \& Liquid} \\ 1 & \text{Liquid} \end{cases} \quad (10)$$

The governing equations are written in terms of the superficial velocity (i.e., the ensemble-average velocity) defined as

$$u = \lambda u_f \quad (11)$$

where,  $u_f$  is the actual fluid velocity vector.

In the solid-liquid co-existence region, solidifying structures form that may resist fuel flow. The flow in the solid-liquid region is represented by the Darcy relation<sup>23</sup>

$$u = -(K / \mu) \nabla P \quad (12)$$

In Equation (12),  $K$  is the permeability that characterizes the ease with which a fluid flows under a pressure gradient through a porous material.  $K$  is determined by pore geometry and has a statistical distribution of sizes. Many empirical and semi-empirical representations for  $K$  exist, and the Kozeny relation<sup>24</sup> is often used

$$K = C_0 \lambda^3 / \Sigma^2 \quad (13)$$

where,  $C_0$  is a dimensionless constant that depends on the pore geometry and  $\Sigma$  is the interstitial surface area of the pores per unit volume of porous material. It is impractical to measure  $\lambda$  and  $\Sigma$  and a simpler expression can be written as<sup>22</sup>:

$$K = \lambda^3 / C (1-\lambda)^2 \quad (14)$$

where,  $C$  is a constant and includes the effects of  $\Sigma$ , pore shape, size and orientation. During the phase-change process, the value of  $C$  is assumed to depend on the morphology of the porous media and is referred to as the morphology constant. Equation (14) can be combined with Equation (12) to give the superficial velocity in the solid-

liquid phase region (For simplicity, here, the product,  $C\mu$  will be written as  $C^*$  using appropriate units)<sup>22</sup>:

$$u = - \lambda^3 \nabla P / [C^* (1-\lambda)^2] \quad (15)$$

Equation (15) shows that for the liquid phase, as the porosity ( $\lambda$ ) approaches unity, pressure losses due to flow through the porous medium decrease to zero. Similarly, for the solid region, as the porosity approaches zero, the velocity decreases to zero. Moreover, as  $C^*$  is increased for a fixed  $\mu$ ,  $\lambda$ , and  $\nabla P$ , Equation (15) shows that the velocity decreases or the flow resistance increases. Thus for jet fuel, crystallization behaviors that inhibit flow would tend to have larger values of  $C^*$ .

Figure 34 shows that  $T_h$  and  $T_l$  are the measured cloud and pour point temperatures, respectively. The prediction of the solidified fuel mass which is unavailable for use is important, and by the definition of the pour point, the fuel does not flow at  $T_l$ . Hence,  $f_l$  between  $T_h$  and  $T_l$  can be estimated as

$$f_l = (T - T_l) / (T_h - T_l) \quad (16)$$

Therefore,  $f_l$  is one (all liquid) at temperatures above  $T_h$ , and, zero (all solid) at temperatures below  $T_l$ .

As normal alkanes precipitate from the solution,  $f_s$  increases while  $f_l$ ,  $K$ , and  $\lambda$  decrease. Since it is difficult to measure  $\lambda$  within freezing jet fuel,  $\lambda$  has been assumed to be proportional to  $f_l$ , which is a function of temperature. The cloud point and pour point temperatures can be accurately measured as described earlier and hence,  $f_l$  can replace  $\lambda$

in Equation (14).<sup>18</sup> For convenience,  $f_i$  is normalized to vary between 0 and 1. Since there is large uncertainty in  $C$  of Equation (17), it is acceptable to use the normalized value of  $f_i$ .

$$K = f_i^3 / [C (1-f_i)^2] \quad (17)$$

The fuel enthalpy can be calculated by integrating the specific heat with respect to temperature. Thus, for the jet fuel sample JPTS (F3775), the confined area between  $T_h$  (-59°C) and  $T_l$  (-63°C) in Figure 34(a) is an integrated value and represents the heat of fusion ( $\Delta H$ ) of precipitating normal alkanes. For the present JPTS sample, the measured heat of fusion,  $\Delta H$  is 4410 J/kg (enclosed area, Figure 34a). Analytical phase-separation techniques<sup>15</sup> have shown that approximately 7% (mass) of the JPTS (F3775) sample actually solidifies at -63°C ( $T_l$ ). Thus, for the JPTS (F3775) fuel sample, the maximum value of the solid fraction,  $f_s$  is 0.07, which is approximately one-fourth of the total normal alkane distribution (0.274). The solid fraction of 0.07 corresponds to a minimum liquid fraction of 0.93. The measured heat of fusion is divided by  $f_s$  to calculate an effective heat of fusion,  $\Delta H_e$ .

$$\Delta H_e = \Delta H / f_s \quad (18)$$

Hence,  $\Delta H_e = 63000$  J/kg. Similar DSC and gas chromatography-mass spectrometer (GC-MS) measurements of JP-8 (F3804) and Jet A (F3219) are listed in

Table 5.<sup>18</sup> It is observed that the specific heat behavior during phase change varies by  $\pm 5\%$  among the fuel samples.

#### 4.4 Numerical Modeling

This section describes the numerical techniques used in all the simulations. The commercial CFD code, CFD-ACE (ESI Group) that was discussed in Chapter 2, is also used in this work to simulate the laminar, time-varying flow and heat transfer. In a previous work, the code was modified to treat solidification.<sup>18</sup> The unsteady Navier-Stokes and energy (enthalpy) equations were solved by a finite volume method. The temporal differencing was represented by a second order Crank-Nicolson scheme, and an upwind spatial differencing scheme was used.<sup>10</sup> A source-term based, fixed grid enthalpy method is used to implement the calculations.<sup>18,22</sup>

A two-dimensional unstructured grid (Figure 36) was employed for transient solution of the flow and heat transfer in the quartz duct. The boundary conditions for temperature come from a spatial average of the thermocouples located at discrete locations. These spatial averages are represented as functions of time and are used as transient temperature boundary conditions for the horizontal walls, while the vertical walls are assumed to be insulated. The initial measured fuel temperature is uniform. Figure 37 shows the temperature profile of the horizontal walls employed in the simulations of fuel cooling. The temperature profiles of the horizontal walls are different for both the jet fuel samples of JP-8 and JPTS due to differences in the temperature ranges of solidification for these fuel samples. The top and bottom walls decrease

uniformly in time from 8°C to -58°C for JP-8 (F3804) and from 24°C to -63°C for JPTS (F3775) after 3 hours.

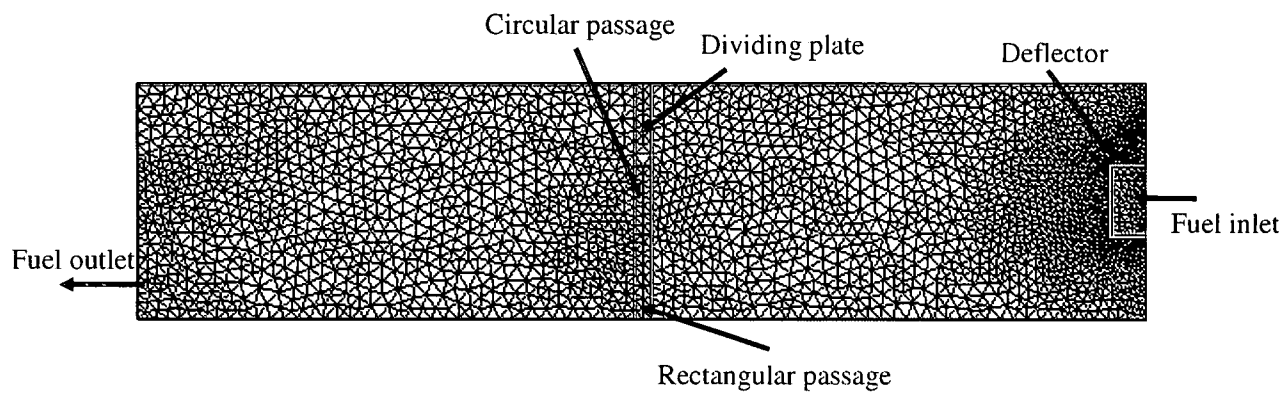


**Figure 36.** Two-dimensional unstructured grid.

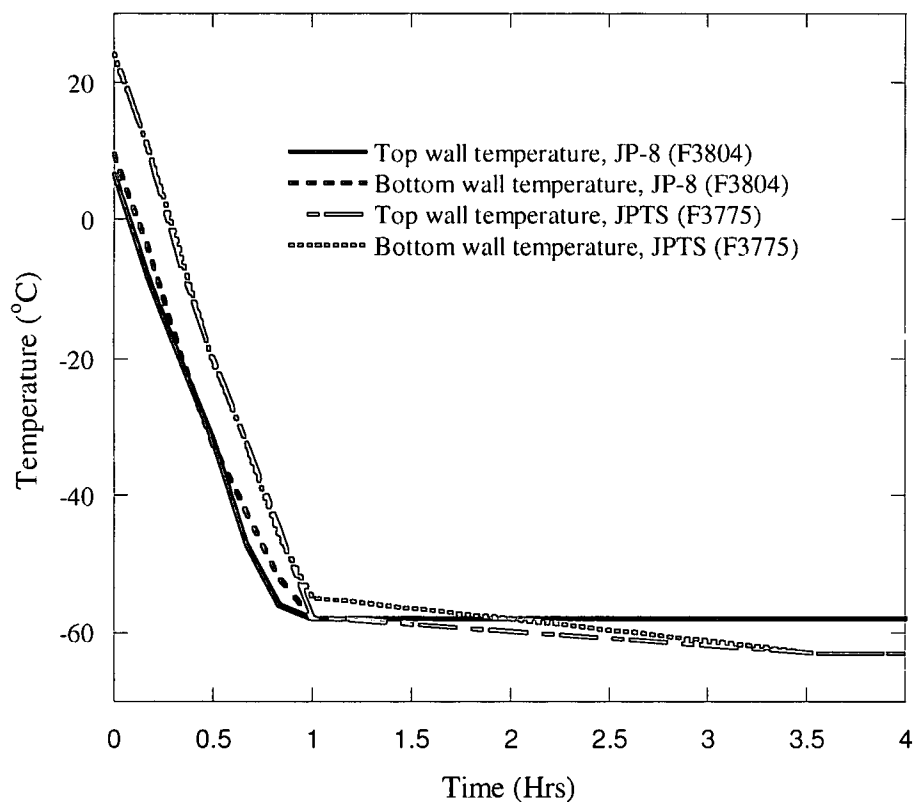


**Figure 37.** Temperature schedule for the cooled horizontal walls used for freezing simulations.

As described earlier, temperature dependent properties of JP-8 (F3804) and JPTS (F3775) were used in the simulations as these fuels were used in the experiments. The internal structures of the duct are made of aluminum, and the properties of aluminum do not significantly change between the temperatures of interest here. Thus, constant properties of aluminum were used in all the simulations.

When the global error residuals were reduced below four orders of magnitude from their maximum values, the solution was considered to be converged. Table 6

describes the grid refinement study conducted to ensure the grid independence of the solution. The table shows temperatures and liquid fraction at three different locations in the duct after the fuel was cooled for 1.5 hours. Results from a grid with 6932 cells were found to be grid independent and are described in this work. Further grid refinement resulted in negligible changes in the solutions.

**Table 6. Grid refinement study for the freezing model. The table shows temperatures at three different locations and the fraction of liquid after 1.5 hours of cooling**

Number of cells	Temperature (°C) (center)	% change	Temperature (°C) (x=28 cm, y=1.5 cm)	% change	Temperature (°C) (x = 10 cm, y = 7.5 cm)	% change	Normalized liquid fraction	% change
2679	-48.3	-	-51.2	-	-48.7	-	0.9374	-
4786	-48.2	0.05	-50.9	0.14	-48.5	0.09	0.9237	1.46
6932	-48.1	0.05	-50.7	0.09	-48.4	0.05	0.9207	0.33
10369	-48.1	0	-50.7	0	-48.3	0.05	0.9196	0.12

## 4.5 Results and Discussion

Here, the computational and experimental results of jet fuel freezing in the quartz duct are reported. The effect of the morphology constant is studied and an optimum value of  $C^*$  is determined by numerical calculations. The simulations are validated with the help of temperatures and images recorded during the experiments. The images show the solidified area and the resulting crystal structures of jet fuels at different times. The effect of the freezing temperature and the influence of forced flow on phase change are described.



#### 4.5.1 Experimental validation and the effect of $C^*$ on freezing

It was explained in earlier sections that flow resistance and the crystallization behavior of jet fuel are characterized in the current model by the value of  $C^*$ . Equation (7) elucidates the significance of  $C^*$  and that larger values of  $C^*$  reduce the liquid fuel flow through the two-phase region. Because  $C^*$  for the freezing of jet fuels cannot be directly measured, it is obtained by adjustment until agreement between the measured and calculated area of the solidified fuel is observed. The calculations were performed for three different values of  $C^*$ , which varied by several orders of magnitude.

Figures 38(a), (b), and (c) compare the effects of three different values of  $C^*$  ( $1 \text{ kg/m}^3$ ,  $1 \times 10^5 \text{ kg/m}^3$ , and  $1 \times 10^{10} \text{ kg/m}^3$ , respectively) on the calculated solidified fuel area and the velocity profile. These figures show contour plots of the normalized liquid fraction and velocity vectors for JP-8 (F3804) in the glass duct after two hours of cooling. The figures show that as the horizontal walls are cooled, a thick layer of solidified fuel develops at the top and bottom surfaces. (The length of a velocity vector is proportional to its magnitude, which varies over the range 0 and 0.12 cm/sec.) A black contour line in Figures 38(a) through 38(c) distinguishes the liquid from the solidified fuel. The contour line represents the liquid fraction,  $f_l = 0.93$  occurring at an average temperature of  $-52.2^\circ\text{C}$  which is  $0.4^\circ\text{C}$  below the cloud point temperature of F3804 ( $-51.8^\circ\text{C}$ ). Considering a difference of  $0.4^\circ\text{C}$  (an error of 0.18%) negligible, it can be said that the contour line represents the cloud point temperature. As stated earlier, the cloud point temperature is the temperature at which solidified fuel is visible in the liquid fuel. Hence, the black contour line representing the cloud point temperature demonstrates the capability of the model to calculate the correct profile of the solidifying structure.

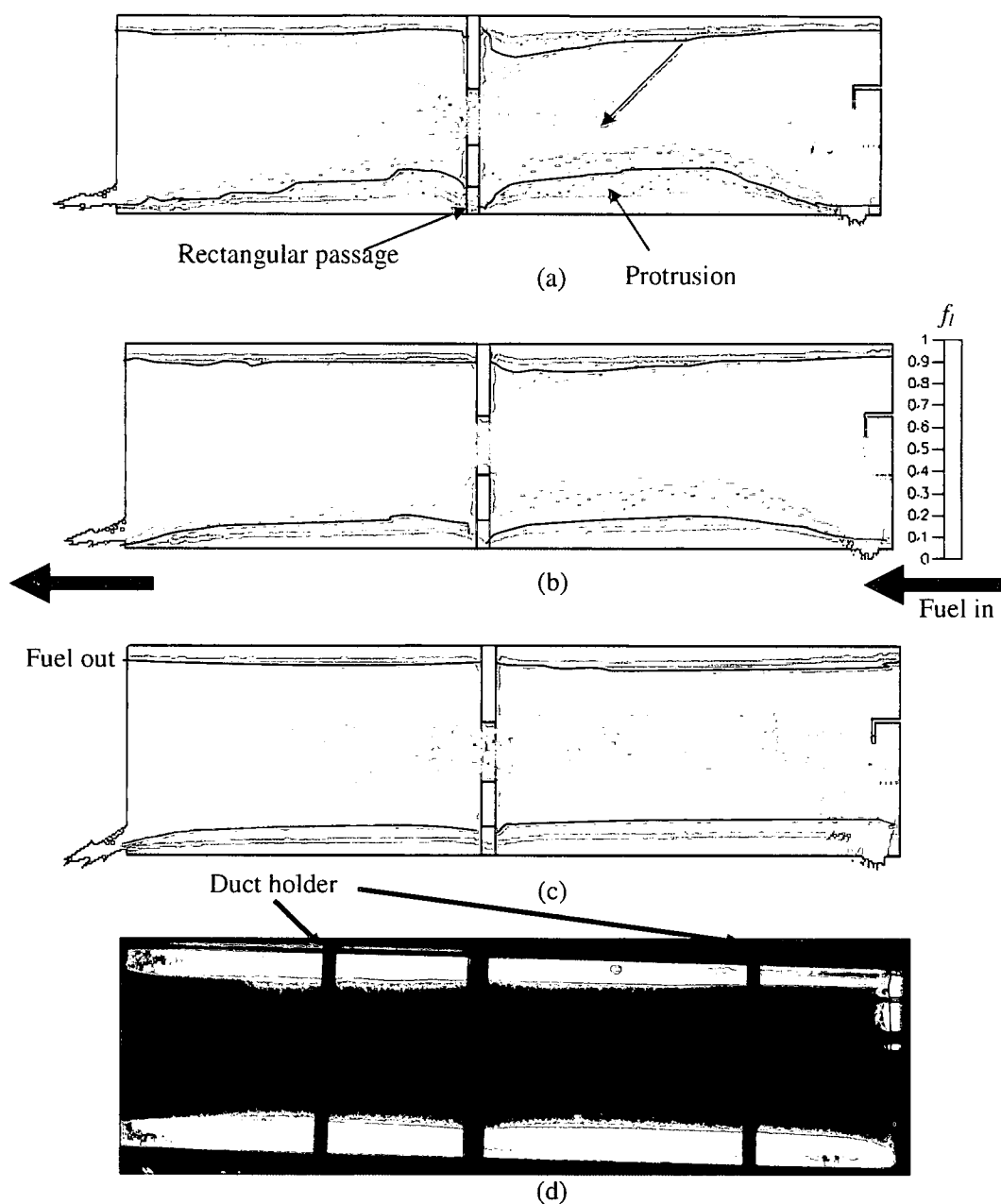


**Figure 38.** Predicted liquid fraction and velocity vectors in the quartz duct after two hours of cooling for JP-8 (F3804) at a flow rate of 60 mL/min with  $C^*$  = (a) 1, (b)  $1 \times 10^5$ , (c)  $1 \times 10^{10}$  and (d) visualization image.

Figure 38(a) represents a  $C^*$  value of  $1 \text{ kg/m}^3$  and shows an uneven and abrupt (protruded) solidified area. It also shows the maximum area occupied by frozen fuel, relative to Figures 38(b) and (c). The protruded area in Figure 38(a) is caused by the flowing fuel in the liquid-solid region. It is evident that the velocity vectors in the region within the black contour line are larger in Figure 38(a). The protrusion decreases near the top and bottom walls when  $C^*$  is increased to  $1 \times 10^5 \text{ kg/m}^3$  (Figure 38b). Also, smaller velocity vectors can be observed in Figure 38(b) indicating less flow relative to Figure 38(a). This means that a lower value of  $C^*$  causes higher velocity in the liquid-solid region. A further increase in the value of  $C^*$  to  $1 \times 10^{10} \text{ kg/m}^3$  (Figure 38c) shows that the solidified fuel area decreases, relative to Figures 38(a) and 38(b) and the protrusion nearly vanishes. The area of solidified fuel confined within the black contour line in Figure 38(c) is  $12.9 \text{ cm}^2$ , which is in agreement with the measured area ( $13.4 \text{ cm}^2$ ). (The uncertainty in the measured solidified area due to measurement using an image is  $\pm 0.5 \text{ cm}^2$ .) Thus, the calculated area represented by Figure 38(c) best approximates the visualization image (Figure 38d). Further increases in  $C^*$  did not yield improved predictions. Previous study with buoyancy driven flow also established the value of  $C^*$  as  $1 \times 10^{10} \text{ kg/m}^3$  for the JP-8 fuel sample.<sup>18</sup>

Similar calculations were performed for the JPTS (F3775) fuel and comparisons were made with the visual images.  $C^*$  was varied from  $1 \times 10^5 \text{ kg/m}^3$  to  $1 \times 10^{12} \text{ kg/m}^3$  to find an optimal value. As observed with JP-8 fuel sample, calculations with a  $C^*$  value of  $1 \times 10^{10} \text{ kg/m}^3$  showed the greatest similarity with the images. Figures 39(a) and (b) show the solidified fuel area in the duct by means of an image and a simulation, respectively. Figure 39(b) shows the contour plot of JPTS (F3775) for a  $C^*$  value of  $1 \times 10^{10} \text{ kg/m}^3$

which gives a calculated solidified fuel area of  $15.4 \text{ cm}^2$  and is in agreement with the measured area of  $14.9 \text{ cm}^2 (\pm 0.5 \text{ cm}^2)$  of Figure 39(a). Both the figures show that the solidified fuel accumulates near the top and bottom surfaces (The black patch on the top surface in Figure 39a is due to visual artifact). The mass of solidified fuel increases in time due to the low temperatures of the horizontal walls.

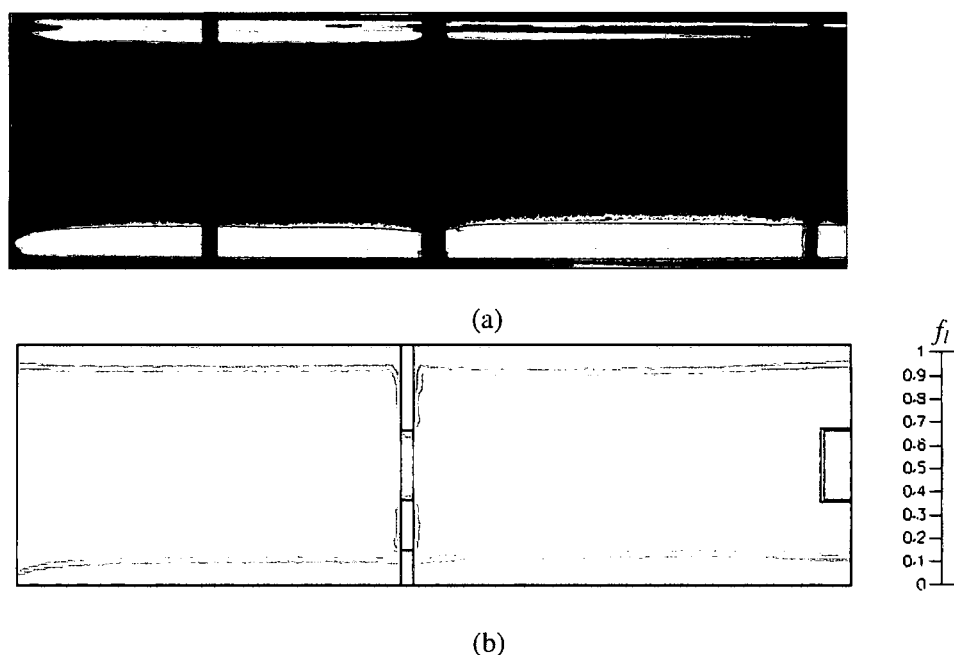
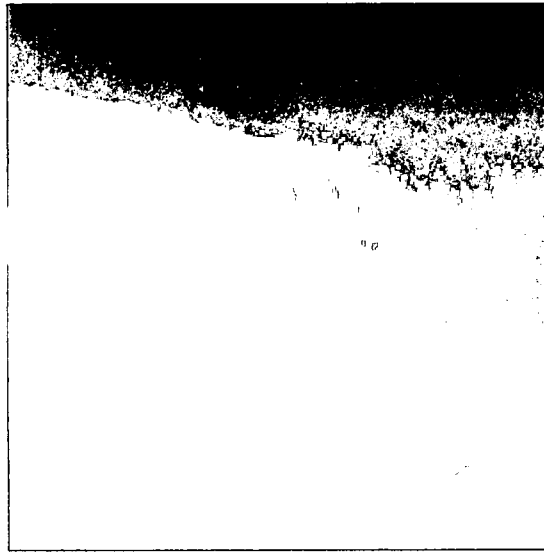


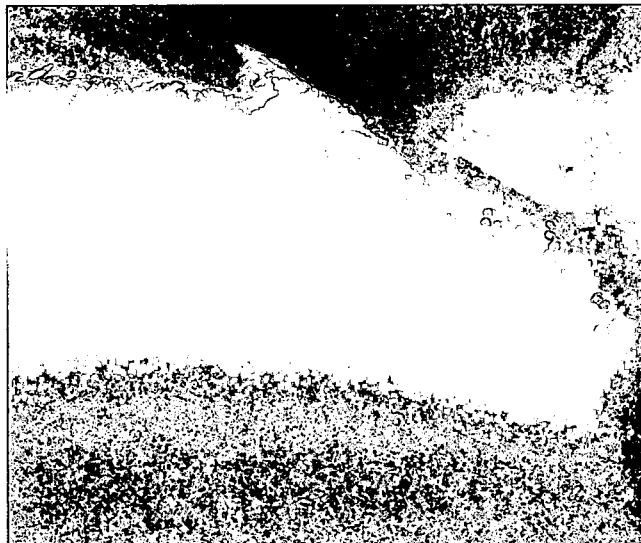
**Figure 39.** (a) Measured and (b) predicted solidified fuel area in the quartz duct after two hours of cooling for JPTS (F3775) at a flow rate of 60 mL/min with  $C^* = 1 \times 10^{10}$ .

Because a  $C^*$  value of  $1 \times 10^{10} \text{ kg/m}^3$  gives the best agreement between the simulations and measurements, therefore, for all the other simulations in this paper, a value of  $C^* = 1 \times 10^{10} \text{ kg/m}^3$  is used for both F3804 and F3775 fuel samples. As described earlier, the effective heat of fusion ( $\Delta H_e$ ) value is used to predict the solidification behavior. Since the effective heat of fusion is nearly the same for both the fuel samples, the same value of  $C^*$  provides similar results.

However, detailed crystal structures of JP-8 and JPTS are also studied here and are found to be significantly different. The solidification of jet fuels involves complex molecular phenomena. The dynamic freezing process of jet fuel can be affected by several factors like crystal shape and size. Separate experiments were performed to study the crystal growth of JPTS (F3775) (Figure 40a) and JP-8 (F3804) (Figure 40b) fuels under forced flow conditions. For this study, the fuel flow rate was 120 mL/min, which is close to actual flow rates observed in aircraft fuel tanks. These images represent the crystal structures that have grown from the bottom surface and extend into the bulk liquid fuel. Figure 40(a) (JPTS) shows long needle-like crystals that are closely grouped, while Figure 40(b) (JP-8) shows solidified crystals in the form of fine plates that appear like a clustered arrangement. At later times, with a further decrease in temperature, jet fuel crystals grow and accumulate to further grow into the bulk. Since solidified jet fuel primarily consists of normal alkanes, the difference between the two crystal structures is believed to be due to differences in the normal alkane distribution (Figure 33). The JPTS sample consists of 27.4% normal alkanes mostly ranging from C<sub>9</sub> to C<sub>14</sub> and centered around C<sub>11</sub>. In contrast, JP-8 fuel sample consists of 23.8% normal alkanes and has a wider distribution that ranges mostly from C<sub>8</sub> to C<sub>15</sub>.



(a)



(b)

**Figure 40.** Crystal structures of fuel samples of (a) JPTS (F3775) and (b) JP-8 (F3804).

Although both JP-8 and JPTS fuel samples vary in their crystal microstructures, they require the same value of  $C^*$ . Same  $C^*$  implies similar morphology and similar

porosity, but JP-8 and JPTS have different morphologies. This indicates that the governing equations used for simulations here have certain limitations and that includes their inability to capture small-scale details of the crystal microstructure. Nevertheless, this limitation is not fatal here, as the focus is on simulating the two-phase coexistence region and calculating the total solid fraction (hold-up) and overall freezing behavior under forced flow conditions.

The region occupied by the solid-liquid fuel matrix grows in time as the temperature decreases. Therefore, it is important to predict the increase in solidification with time and validate the solidified fuel area with measurements. Figure 41 provides further validation of the simulations by comparing them with the measured solidified fuel area using a  $C^*$  value of  $1 \times 10^{10} \text{ kg/m}^3$ . Figures 41(a) and 41(b) show images from the experiments and a calculated contour plot of liquid fraction, respectively. Both figures show the solidified area of JP-8 (F3804) after one hour of cooling for an inlet fuel flow rate of 60 mL/min. Figure 41 also shows the predicted and measured temperatures at two different locations. The temperature at a location near the center of the duct is  $-33^\circ\text{C}$ , which is expectedly higher than the temperature near the bottom surface ( $-53^\circ\text{C}$ ). These figures show good agreement between the measured and predicted temperatures (within  $2^\circ\text{C}$ ). (The uncertainty in the measured temperature is  $\pm 1^\circ\text{C}$ .) As the cooling proceeds, the amount of frozen fuel trapped in the duct increases. Since colder fuel is more dense and tends to reach the bottom surface, the upper surface experiences the flow of relatively warmer fuel. The warm fuel near the upper surface reduces the growth rate of solidified fuel on the top surface. The relatively low temperatures of the horizontal surfaces results in the conduction of heat to the dividing plate. Therefore, for a location near the dividing

plate, the temperature is lower due to increased heat transfer caused by the dividing plate. Because of the lower temperatures there, solidified fuel accumulates around the dividing plate.

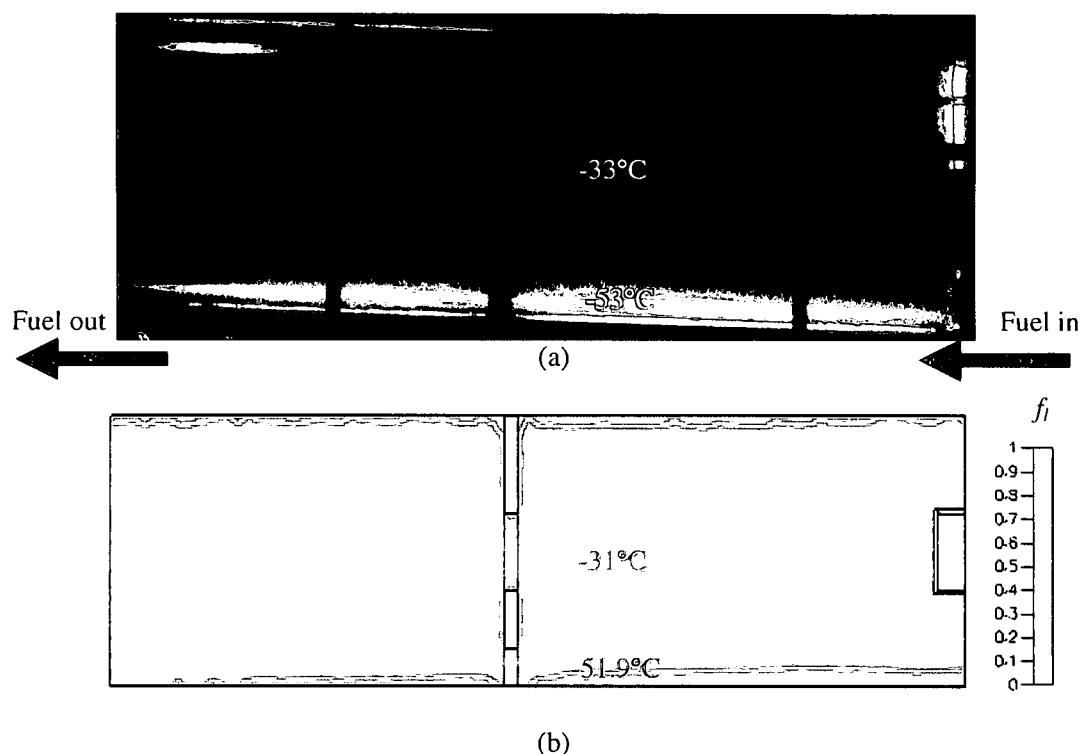
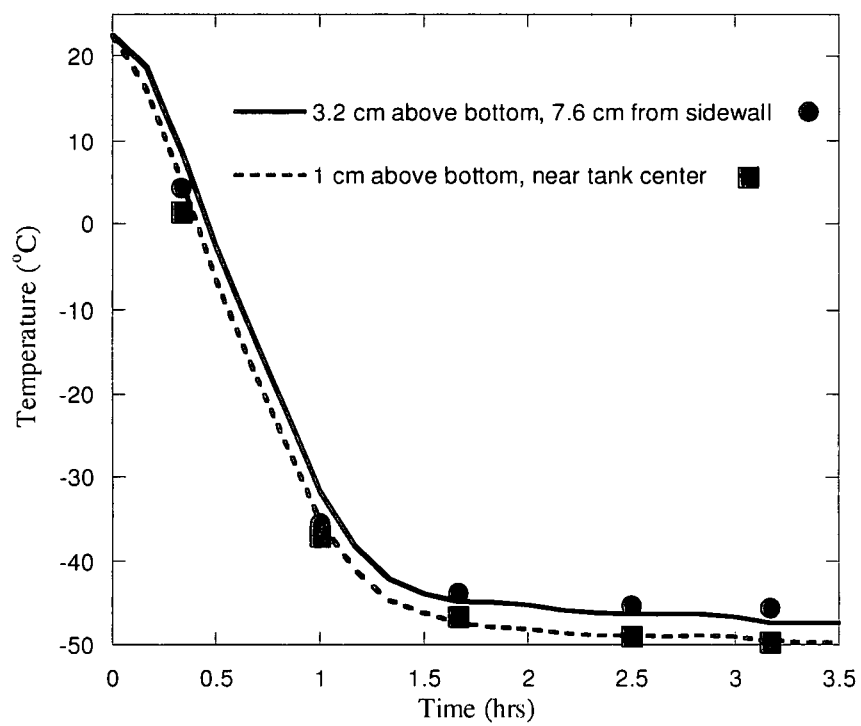


**Figure 41.** Images of JP-8 (F3804) showing (a) measured and (b) calculated liquid fraction after one hour of cooling and a flow rate of 60 mL/min.

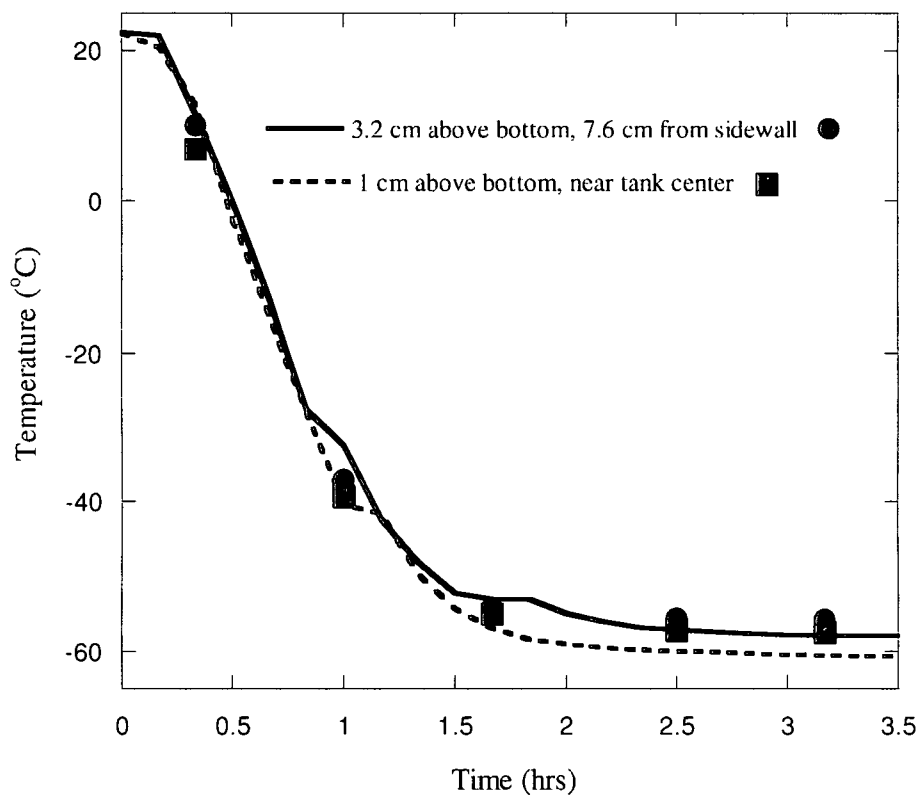
To further validate the simulated temperatures and to study the thermal profile of the cooling fuel within the duct, the simulations are compared with the measurements. Figures 42(a) and (b) compare calculated and measured temperatures for the two fuels – JP-8 (F3804) and JPTS (F3775), respectively using a  $C^*$  value of  $1 \times 10^{10} \text{ kg/m}^3$ . These plots show how the temperature varies with time at two different thermocouple locations. It can be observed that the calculations are in relatively close agreement with the



measurements (within 3°C). Similar agreement was observed at other thermocouple locations in the duct. Calculated contour plots can be useful in representing a complete thermal profile in the duct at any specific time. Figure 43 shows the calculated temperature contours and velocity vectors inside the glass duct after (a) 10 minutes and (b) two hours of cooling. Both figures show relatively large velocity vectors at the inlet due to the expansion of the flow area after the inlet. Since Figure 43(a) represents an earlier time (after 10 minutes of cooling), fuel temperature is relatively high and there is no frozen fuel accumulated in the duct. Due to the absence of frozen fuel, the flow is unobstructed and the velocity vectors are larger and can be observed near the top and bottom surfaces of the duct. Figure 43(b) represents the temperature profile in the duct at a later time (after two hours of cooling), and hence, the temperature of the fuel is lower (below the freeze point). Therefore, solidified fuel accumulates near the horizontal walls and the velocity vectors are not observed near the horizontal surfaces. As a result, the rectangular opening located at the bottom of the dividing plate is obstructed by the solidified fuel and restricts the flow through it. Hence, the fuel flows towards the outlet through the center opening only. Therefore, if the expected fuel temperature in an aircraft fuel tank is below freezing, then an opening near the bottom should be made large enough to allow the fuel to flow through it. Because of the narrow flow passage, the velocity through the duct accelerates and increases by as much as a factor of four.



(a)



(b)

**Figure 42.** Measured and simulated temperatures for the fuel samples of (a) JP-8 (F3804) and (b) JPTS (F3775) at two different thermocouple locations. The symbols represent measured temperatures.

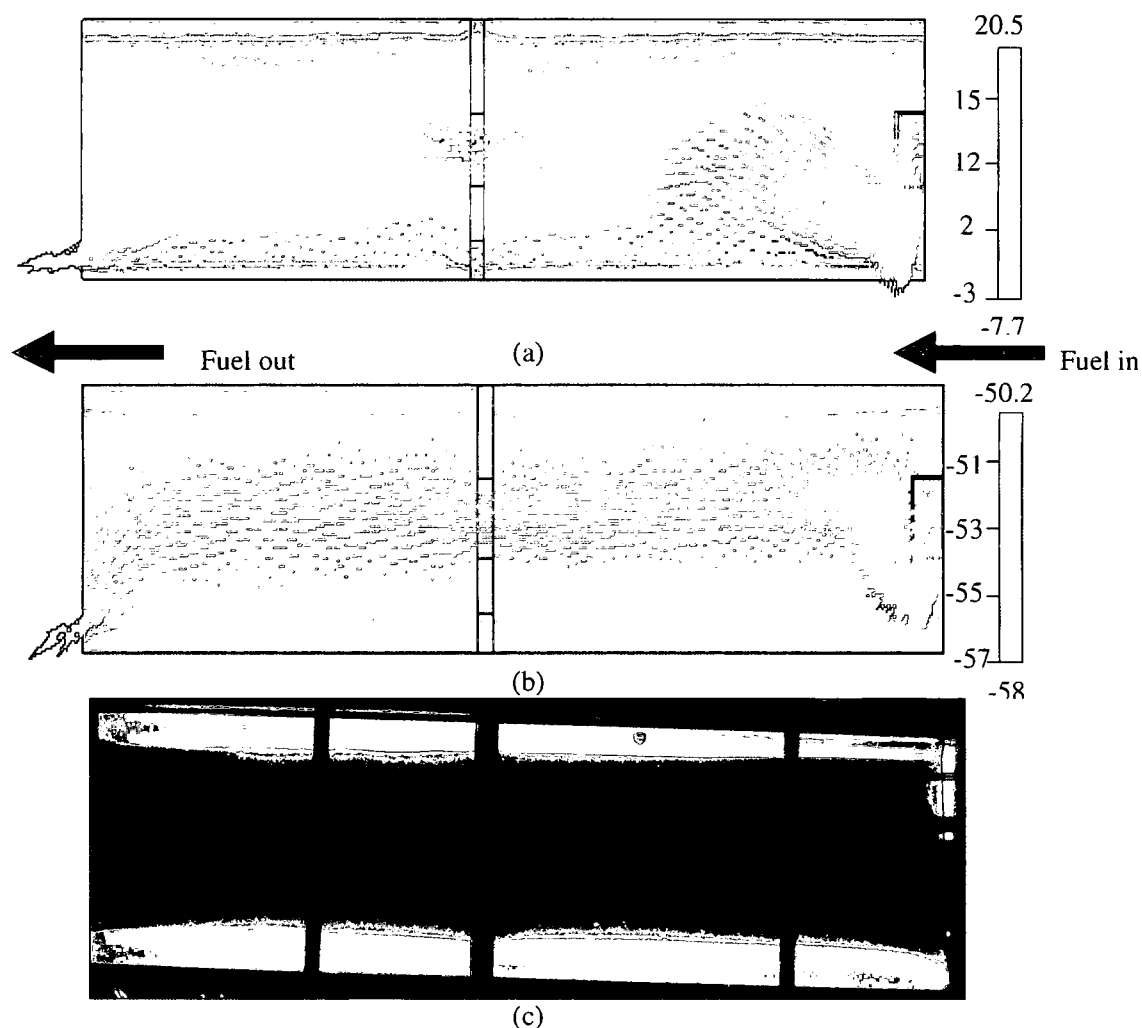


**Figure 43.** Temperature contours and velocity vectors for JP-8 (F3804) in the quartz duct after (a) 10 minutes, and (b) two hours of cooling, and (c) image of frozen fuel after two hours and a flow rate of 60 mL/min.

#### 4.5.2 Effect of fuel flow rate on freezing

To study the effect of fuel flow rate on temperature and solidification profiles inside the duct, simulations were performed in which the inlet flow rate was varied. Four different fuel inlet velocities (0.80 cm/sec, 0.30 cm/sec, 0.15 cm/sec and 0.08 cm/sec) were selected for their influence on fuel solidification. Here, the results with the fuel inlet

velocity of 0.80 cm/sec and 0.08 cm/sec are shown in Figures 44 and 45. The wall temperatures followed the schedule of Figure 37.

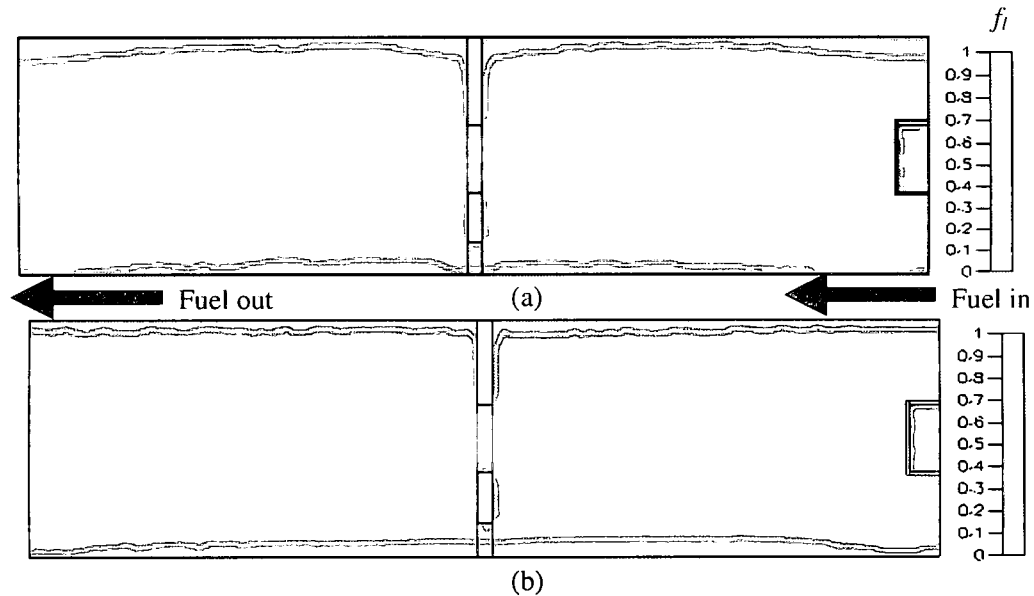


**Figure 44.** Predicted liquid fraction of JPTS (F3775) in the duct after two hours of cooling for an inlet velocity of (a) 0.8 cm/sec and (b) 0.08 cm/sec.

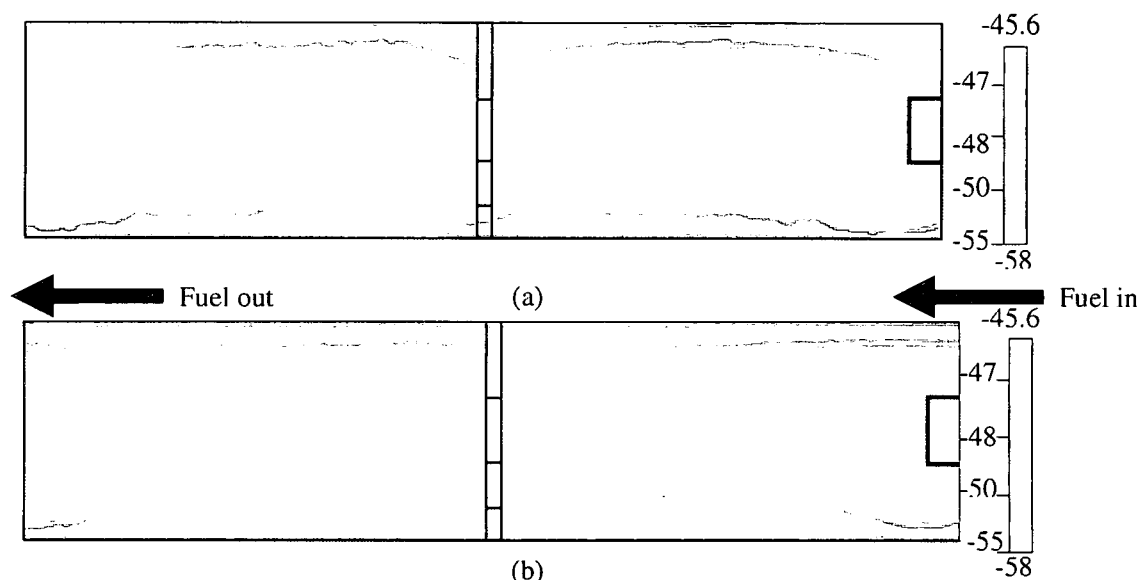


**Figure 45.** Predicted temperature profile of JPTS (F3775) in the duct after two hours of cooling for an inlet velocity of (a) 0.8 cm/sec and (b) 0.08 cm/sec.

Figure 44 shows the calculated contour plots representing the liquid fraction of the jet fuel (F3775) in the duct after two hours of cooling. Figure 44(a) shows that when the inlet velocity is 0.80 cm/sec, the calculated fraction of solidified fuel in the duct is 0.0763. It is observed that the fraction of solidified fuel increased to 0.0896, 0.1054, and 0.130 when the fuel velocity is decreased to 0.30 cm/sec, 0.15 cm/sec and 0.080 cm/sec, respectively. Thus, when the fuel inlet velocity is relatively higher, the total solid fraction in the duct is lower. This result is expected because when the fuel velocity is lower, the fuel remains in the duct for a comparatively longer period and, consequently, is subjected to lower temperatures for a longer residence time. Because higher fuel velocities show a decrease in the accumulation of the solidified fuel, it is beneficial to have higher fuel velocities in the fuel tanks. Figure 44(a) shows that higher velocities result in a more disordered and jagged layer of the solidified fuel along the horizontal surfaces. Also, due

to higher inlet velocity, the bottom surface immediately below the deflector does not show any accumulation of the frozen fuel. Moreover, the rectangular opening at the bottom remains open and high flow rates create an uneven solidified fuel layer near the bottom surface. Therefore, the overall area of solidified fuel near the bottom surface is less than that at the top surface. In contrast, with decreased fuel velocity (0.08 cm/sec), the solidified fuel area near bottom surface becomes smoother (Figure 44b). Also, the rectangular opening near the bottom surface is nearly blocked due to accumulation of the solidified fuel.

Figures 45(a) and (b) show the temperature profiles in the duct when the fuel inlet velocities are 0.80 cm/sec and 0.08 cm/sec, respectively. It is observed that the average fuel temperature inside the duct increases by approximately 3°C when the inlet velocity is 0.08 cm/sec relative to when the inlet velocity is 0.80 cm/sec. However, it was observed in Figure 44 that the amount of frozen fuel is higher when the inlet velocity is lower. This implies that at lower flow rates, although the temperature near the walls is lower, the average temperature in the fuel tank can be higher. But, the temperature is higher only by approximately 3°C which does not affect the temperature profile significantly. Therefore, higher velocities are recommended for fuel flow in aircraft fuel tanks. It can also be observed that the temperature profiles near the top and the bottom surfaces show similarity with the figures showing solidified fuel area (Figure 44). Figure 45(a) shows that higher velocity causes more stratification of fuel in the duct, relative to that observed in Figure 45(b). Also, higher velocities do not allow cold fuel to settle at the bottom surface, resulting in more mixing and an uneven thermal profile near the bottom surface.

In contrast to Figure 45(a), Figure 45(b) shows a smoother or nearly flat temperature contour near the bottom surface, which is due to the lower fuel inlet velocity.



## **CHAPTER 5**

### **Conclusions and Recommendations**

The conclusions here are derived from the three research topics covered in the previous three chapters. In Chapter 2, the flowability and pumpability of jet fuel were studied to determine how changes in fuel properties at low temperature affect jet aircraft fuel system operation. Both experiments and computations were employed to elucidate aspects which affect fuel temperature. Measurements and simulations of cooling of a static tank show complex flow and heat transfer effects. Heat transfer in the tank was found to be significantly increased by the presence of baffle ribs, stringers, and other structural members. The presence of the Z-stringers greatly increases heat transfer and stratification near the tank bottom. The results show that fuel tank temperature sensors need to be located near the tank bottom to reasonably measure low fuel tank temperatures. In addition, the location and geometry of structural members should be considered in the thermal design of a fuel tank.

Calculations were also performed on the effect of ullage level on fuel temperatures and heat transfer. The results show that a relatively small ullage increased fuel temperature stratification, with higher temperatures in the tank center relative to a completely filled tank. A large ullage space may lead to reduced temperatures due to the relatively small fuel volume and high surface to volume ratio.

Evaluation of the effect of temperature on fuel flowability and pumpability was conducted in a wing tank simulator. The results show that flowability and pumpability decrease substantially as temperature is reduced. The measurements show that low freeze point fuels exhibit greater flow reduction than do high freeze point fuels. This indicates that operating fuels near their measured freeze point rather than near the specification freeze point can result in reduced fuel flowability. This needs to be evaluated based on the requirements of individual aircraft fuel systems.

In support of the simulator measurements, viscosity measurements as a function of temperature show that lower freeze point fuels tend to have higher viscosities near their freeze point than do higher freeze point fuels. These higher viscosities result in the lower flow rates observed in the wing tank simulator. The higher viscosity of low freeze point fuels at their freeze point likely results from the fact that the freeze point is a strong function of the larger normal alkanes present, while viscosity reflects the overall normal alkane fuel composition. Large variations (greater than 100%) in the viscosity of different fuel samples were found to be necessary to produce significant effects on the heat transfer within the fuel tank.

In Chapter 3, the flowability and heat transfer behavior of jet fuels was studied with the presence of polyurethane foam. Experiments and CFD calculations were performed to elucidate the factors that may affect the fuel flow and thermal profile. A thermal simulator was used to carry out the low temperature experiments and a two-dimensional numerical grid representing the thermal simulator was used in the calculations. Simulations were validated by comparing them with the experimental results. In addition, real jet fuel properties of JP-8 (F4751) were used in the simulations.

Simulations of draining the fuel tank simulator with foam were compared with those when the foam was not present. The results from both – draining the fuel tank with foam and without foam were nearly identical. Thus, it can be said that the foam does not necessarily affect the fuel flowability at temperatures higher than -37°C. However, it was observed that at low temperatures, heat transfer inside the fuel tank can be affected by the presence of foam. The overall temperature of the fuel is lower when the foam is present relative to when the foam is not present. Also, the porosity of the foam was varied to study its affect on fuel draining. It was found that lower porosities result in lower fuel flow.

In Chapter 4, the low temperature behavior of jet fuels under forced flow conditions was studied using a quartz duct. Experiments and simulations were performed to explore the effect of different flow conditions on jet fuel freezing and the effect of solidification on fuel flow behavior. Two different jet fuel samples (JP-8 and JPTS) were used in the experiments and measured jet fuel properties were used in the simulations. The DSC and GC-MS measurements provided specific heat values and the enthalpy method was used to calculate the hold-up due to freezing. The value of the morphology constant for both the fuel samples was obtained by adjustment until agreement between the measured and calculated area of the solidified fuel was observed.

The values of morphology constant for both fuel samples were found to be the same ( $1 \times 10^{10} \text{ kg/m}^3$ ). However, the observed crystal structures of JP-8 and JPTS were found to be very different. This means that the enthalpy method used here has certain limitations. The enthalpy method depends on the effective heat of fusion ( $\Delta H_e$ ), and because that value is nearly same for both the fuel samples, the calculations predicted the

same value of  $C^*$ . Although this method can be successfully used to simulate the overall flow and heat transfer behavior in solid-liquid region, the enthalpy method cannot predict the details of the crystal structure. This limitation cannot be considered fatal for this study because here the focus is on the overall flow, heat transfer and freezing behavior of jet fuels.

Horizontal walls that were cooled down to the pour point temperature of jet fuel showed significant accumulation of solidified fuel. Due to the increase in solidification at later times, the velocity vectors inside the duct showed that fuel ceased to flow through the rectangular opening at the bottom. Moreover, the dividing plate in the center of the duct acted as a thermal conductor and increased the hold-up of the frozen fuel. Therefore, it is recommended to make larger passages near the bottom walls in the aircraft fuel tank and to optimize the design of fuel tanks such that they have minimum internal structures. Simulations of the effect of varying flow rates showed that lower flow rates resulted in more accumulation of solidified fuel inside the duct. Predicted temperatures and solidified area of fuel inside the duct were found to be reasonably similar to the measurements. Hence, it can be concluded that CFD can be an effective tool to simulate the flow and heat transfer of jet fuels at freezing temperatures under forced flow conditions.

The research presented in this dissertation is very new, and hence, presents a lot of scope for future work. Firstly, instead of a simulator tank, as was used in the present research, an actual aircraft fuel tank can be simulated using CFD to present more reliable and realistic conclusions. Also, since each aircraft has a different tank design, the results presented here cannot be generalized. Therefore, it is more important to design and

simulate individual aircraft fuel tanks. The effect of foam was studied with a two-dimensional grid, hence, there is need to further explore a three-dimensional approach to the problem. The foam used in our studies was coarse polyurethane foam. Future work might include trying different type of foam and using different thermal properties of foam. Moreover, the studies involved only the temperatures above freeze point. The results might significantly change at temperatures below freeze point, where the viscosity of the jet fuel decreases. Therefore, studies with foam must be done at temperatures below freezing. Similarly, for the freezing studies, using a three-dimensional grid is recommended, to present the heat transfer and flow phenomenon better. Moreover, it will be an important contribution if the CFD freezing model can be modified and used for jet fuels with additives.

## **Bibliography**

1. Technical Review, Aviation Fuels, Chevron Products Company.
2. Francis Davidson, Phase Technology, Private Communication, 2001.
3. Aviation Rulemaking Advisory Committee, Fuel Tank Harmonization Working Group, Task Group 4, Foam, July 1998.
4. Coutinho, J. A. P., A Thermodynamic Model for Predicting Wax Formation in Jet and Diesel Fuels, *Energy and Fuels*, Vol. 14, 2000, pp. 625-631.
5. Mehta, H. K., Armstrong, R. S., Detailed Studies of Aviation Fuel Flowability, Boeing Commercial Aircraft Company, NASA CR-174938, 1985.
6. Stockemer, F. J., Experimental Study of Low Temperature Behavior of Aviation Turbine Fuels in a Wing Tank Mode, NASA CR-159615, 1979.
7. McConnell, P. M., Owens, S. F., Kamin, R. A., Prediction of Fuel Freezing in Airplane Fuel Tanks of Arbitrary Geometry – Part 1, *Aircraft Engineering*, Vol. 58, pp. 2-7, 1986.
8. McConnell, P. M., Owens, S. F., Kamin, R. A., Prediction of Fuel Freezing in Airplane Fuel Tanks of Arbitrary Geometry – Part 2, *Aircraft Engineering*, Vol. 58, pp. 20-23, 1986.
9. Zabarnick, S., and Vangness, M., Properties of Jet Fuels at Low Temperature and the Effect of Additives, Preprint- American Chemical Society, Division of Petroleum Chemistry, Vol. 47, 2002, pp. 243-246.
10. CFD Research Corporation, CFD-ACE (U) Users Manual, Huntsville, Alabama, 2002.

11. Hirt, C. W., and Nichols, B. D., Volume of Fluid (VOF) Method for the Dynamics of Free Boundaries, *Journal of Computational Physics*, Vol. 39, 1981, pp. 201-225.
12. Rider, W. J., Kothe, D. B., Mosso, S. J., Cerrutti, J. H., and Hochstein, J. I., Accurate Solution Algorithms for Incompressible Multiphase Fluid Flow, *American Institute of Aeronautics and Astronautics-95-0699*, 1995.
13. Coordinating Research Council, Handbook of Aviation Fuel Properties, Technical Report 530, Atlanta, GA, April 2004.
14. Coutinho, J. A. P., A Thermodynamic Model for Predicting Wax Formation in Jet and Diesel Fuels, *Energy and Fuels*, Vol. 14, 2000, pp. 625-631.
15. Atkins, D. L., Ervin, J. S. and Shafer, L., Experimental Studies of Jet Fuel Viscosity at Low Temperatures, using a Rotational Viscometer and an Optical Cell, *Energy and Fuels*, Vol. 19, 2005, pp. 1935-1947.
16. Assudani, R., Ervin, J. S., Zabarnick, S., Shafer, L., Experimental and Computational Studies of Jet Fuel Flow near the Freeze Point, *Journal of Propulsion and Power*, Vol. 22, No. 3, 2006.
17. Kaviany, M., Principles of Heat Transfer in Porous Media, Second Edition, 1995, pp. 3-6.
18. Atkins, D. L., Ervin, J. S., Saxena, A., Computational Model of the Freezing of Jet Fuel, *Journal of Propulsion and Power*, Vol. 21, pp. 356-367, 2005.
19. Wang, C. Y., Cheng, P., Multiphase Flow and Heat Transfer in Porous Media, *Advances in Heat Transfer*, Vol. 30, pp. 93-196, 1997.

20. Beckermann, C., and Viskanta, R., Mathematical Modeling of Transport Phenomena during Alloy Solidification, *Applied Mechanical Review*, Vol. 46, No. 1, 1993, pp. 1-27.
21. McConnell, P. M., Desmarais, L. A., and Tolle, F. F., Heat Transfer in Airplane Fuel Tanks at Low Temperatures, American Society of Mechanical Engineers, Paper 83-HT-102, 1983.
22. Voller, V. R., and Prakash, C., A Fixed Grid Numerical Modeling Methodology for Convection-Diffusion Mushy Region Phase-Change Problems, *International Journal of Heat and Mass Transfer*, Vol. 30, No. 8, 1987, pp. 1709-1719.
23. D'Arcy, H., *Les Fontaines Publiques de la Ville de Dijon*, Dalmont, Paris 1856.
24. Kozeny, J. S., Ueber Kapillare Leitung des Wassers im Boden, *Akad. Wissen. Wien, math-Naturwissen*, Vol. 136, 1927, pp. 271-306.
25. Moynihan, C. T., Mossadegh, R., and Bruce, A. J., Determination of the Mass Fraction of Crystals in Partly Frozen Hydrocarbon Fuels, *Fuel*, Vol. 63, March 1984, pp. 378-384.



R702033226